In vivo optogenetic interrogation of dendrite-specific synaptic integration during network activity

Inaugural-Dissertation
to obtain the academic degree
Doctor rerum naturalium (Dr. rer. nat.)
Submitted to the Department of Biology, Chemistry and Pharmacy
of Freie Universität Berlin

by

LEIRON FERRARESE

from Rome, Italy

April, 2017

June 2011 – April 2017

Neural Circuits and Behaviour, Group Leader Dr. James Poulet

Max Delbrück Center for Molecular Medicine (MDC)

Neuroscience Research Center (NWFZ)
Charité Universitätsmedizin Berlin
Campus Charité Mitte
Charitéplatz 1, 10117 Berlin

1st Reviewer: Dr. James Poulet

2nd Reviewer: Prof. Dr. Stephan Sigrist

Date of Defence: 23.11.2017

ACKNOWLEDGMENTS

I would like to thank first of all my PhD supervisor **Dr. James Poulet** who gave me the opportunity to work in his laboratory, for believing in me by entrusting me the management of this compelling project and for his persistent and enthusiastic support throughout my PhD with helpful advices and open and interesting scientific discussions.

I am sincerely thankful to **Dr. Jean-Sebastien Jouhanneau** who taught me the technique of *in vivo* electrophysiology, for the enthusiasm he transmitted me in performing these difficult and exciting experiments. Moreover, I am grateful for the experiments he carried out in support of this project.

I wish to thank **Dr. Michiel Remme** for the construction of the neuron model and for the helpful discussions about dendritic integration. I am furthermore grateful to **Dr. Jens Kremkow** for his advices about data analysis, to **Janett König** for her technical help in the laboratory and to **Gergely Katona** for his support with the two-photon system.

I am really thankful to **Dr. Evgeny Bobrov** and **Russel Hodge** for proofreading of this dissertation and writing suggestions, and to **Dr. Philipp Schnepel** for his help in writing the discussion.

Besides, I would like to thank all the past and present members of the Poulet group (in alphabetical order): **Annapoorani**, **Anja**, **Birgit**, **Diana**, **Florian**, **Luc**, **Mikkel**, **Nevena**, **Phill**, **Ricardo, Tobias and Wen-Jie** for the interesting scientific discussions, help, support and enjoyable time spent together during these years.

I thank for funding the **Max Delbrück Center**, a solid institution that believed in me, and the **Neurocure Cluster of Excellence**.

A special thank also to **Jana Droese** and to my friend **Francesco Boccellato** without the support of whom I would had not decided to restart my PhD in the Poulet group.

To conclude I wish to thank all my friends in Berlin and Rome, and thanks to my family to whom this thesis is dedicated, my parents **Francesca** and **Sandro** and my grandparents **Olga** and **Dante**.

Finally, I thank you **Silvia** for your Love and for **Aleandro**, who brightened up the days of writing this dissertation with large smiles and loud “hauah”.

In vivo optogenetic interrogation of dendrite-specific synaptic integration during network activity

SUMMARY

Excitatory cortical pyramidal neurons are the principal output of the neocortex, and have been associated with advanced cognitive functions of the brain. Pyramidal neurons display an anatomical and functional segregation whereby the basal and apical dendrites, that extend to different cortical layers, receive synaptic inputs from different sources. This structure gives them the hypothesized ability to function as an associative link between different streams of information arriving to the cortex to electrotonically distant branches of single neurons. *In vivo* cortical pyramidal neurons are constantly active but it is unclear how network activity impacts on synaptic input integration. The aim of this study is to investigate whether synaptic integration in layer 2/3 pyramidal neurons *in vivo* is determined by input location, moreover I assess the contribution of cortical network activity to dendrite-specific integration.

I used subcellular two-photon stimulation of Channelrhodopsin-2 expressing neurons and *in vivo* whole-cell recordings to show that network activity acts as a location specific modulator of synaptic input strength. Synaptic input to apical dendrites is reduced and compartmentalized in a distant-dependent manner during slow network activity in anesthetize and awake animals. However during active movement in awake mice input from apical dendrites is increased in amplitude. On the other hand, basal synaptic input undergoes a gain modulation during slow network activity whereby small amplitude inputs are amplified and large amplitude inputs are reduced. Activity-dependent gain modulation was also observed for glutamatergic thalamic and local monosynaptic pyramidal cell inputs thought to target basal dendrites. Basal dendritic gain modulation was dependent on a postsynaptic mechanism involving voltage-gated sodium channels.

Thus, I propose that a central functional role of slow cortical network activity is to compartmentalize processing of top-down information thought to target apical dendrites, while amplifying small amplitude bottom-up inputs to basal dendrites. This cell-intrinsic mechanism could serve to bind functionally distinct subthreshold information in single cells.

ZUSAMMENFASSUNG

Erregende Pyramidalzellen stellen die primären Ausgänge des Neokortex dar, und werden mit höheren kognitiven Funktionen des Gehirns in Verbindung gebracht. Pyramidalzellen zeigen eine anatomische und funktionelle Aufteilung, bei der die apikalen und die basalen Dendriten, die sich in verschiedene kortikale Schichten erstrecken, synaptische Eingänge aus verschiedenen Quellen erhalten. Durch diesen Aufbau könnten sie als Verbindung zwischen verschiedenen Informationsströmen fungieren, die an elektrotonisch weit voneinander entfernten Verzweigungen einzelner Neurone im Kortex ankommen. Kortikale Pyramidalzellen sind *in vivo* kontinuierlich aktiv, aber es ist unklar, wie die Netzwerkaktivität die Integration synaptischer Eingänge beeinflusst. Das Ziel dieser Studie ist es, zu untersuchen, ob die synaptische Integration in Pyramidalzellen in Schicht 2/3 *in vivo* durch den Ort des Informationseingangs bestimmt wird. Des Weiteren betrachte ich den Beitrag kortikaler Netzwerkaktivität zur Dendriten-spezifischen Integration.

Ich habe subzelluläre Zwei-Photonen-Stimulation von Channelrhodopsin-2-exprimierenden Neuronen sowie *in vivo* Ganzzellableitungen verwendet, um zu zeigen, dass die Netzwerkaktivität als ortsspezifischer Modulator der synaptischen Eingangsstärke wirkt. Synaptische Eingänge an apikalen Dendriten sind während langsamer Netzwerkaktivität in narkotisierten und wachen Tieren in einer entfernungsabhängigen Weise abgeschwächt und in Abschnitte gegliedert. Während aktiver Bewegungen wacher Mäuse zeigen die Eingänge von apikalen Dendriten jedoch eine größere Amplitude. Synaptische Eingänge basaler Dendriten wiederum zeigen eine Modulation des Verstärkungsfaktors während langsamer Netzwerkaktivität, durch die Eingänge kleiner Amplitude verstärkt und großer Amplitude abgeschwächt werden. Eine aktivitätsabhängige Modulation der Verstärkung wurde auch bei glutamatergen Eingängen vom Thalamus sowie lokalen monosynaptischen Pyramidalzelleingängen beobachtet, die vermutlich an basalen Dendriten ansetzen. Die Modulation der Verstärkung an basalen Dendriten hing von einem postsynaptischen Mechanismus unter Mitwirkung spannungsabhängiger Natriumkanäle ab.

Somit ist es meine Hypothese, dass es eine zentrale funktionelle Rolle langsamer Netzwerkaktivität ist, die Verarbeitung vermutlich an apikalen Dendriten eintreffender Top-

Down-Information aufzugliedern, während Bottom-Up-Eingänge kleiner Amplitude an basalen Dendriten verstärkt werden. Dieser den Zellen intrinsische Mechanismus könnte dazu dienen, funktionell unterschiedliche unterschwellige Informationen in einzelnen Zellen zu verbinden.

TABLE OF CONTENTS

ACKNOWLEDGMENTS 3

SUMMARY 5

ZUSAMMENFASSUNG 6

TABLE OF CONTENTS 8

1 INTRODUCTION 12

1.1 Somatosensory cortex 14

1.1.1 Cortical cell types 14

1.1.2 Laminar connectivity 15

1.1.3 Pyramidal neuron structure and function 16

1.1.4 L2/3 pyramidal neurons 18

1.2 Cortical monosynaptic transmission and integration 19

1.2.1 Synaptic integration in cortical neurons 20

1.3 Spontaneous cortical network activity 22

1.3.1 Network activity effects on neuronal membrane potential 23

1.3.2 Awake rest and active movement 24

1.4 Impact of cortical network activity on synaptic integration 26

1.4.1 Dendrite specific synaptic integration 28

1.5 *In vivo* techniques for dendritic stimulation 30

1.5.1 Currently available techniques 30

1.5.2 *In vivo* two-photon Channelrhodopsin stimulation 31

2 METHODS 34

2.1 Animal surgery 34

2.1.1 Intrinsic optical imaging 34

2.2 Channelrhodopsin-2 transfection 35

2.2.1 Single cell electroporation 35
2.2.2 Cortical viral infections 36
2.2.3 Thalamic viral infections 36

2.3 Craniotomy 37

2.4 Two-photon targeted patch and whole cell recordings 37

2.5 Subcellular two-photon optogenetic stimulation 38

2.6 Paw movement monitoring in awake mice 39

2.7 Histology 39

2.8 Analysis 40
2.8.1 Dataset inclusion parameters 40
2.8.2 Datasets 40
2.8.3 Peristimulus time histograms 40
2.8.4 Selection of Up- and Downstate 41
2.8.5 Amplitude measurements of subthreshold responses 42
2.8.6 Input resistance 42
2.8.7 Isopotential 43
2.8.8 Statistics 44

3 RESULTS 46

3.1 Development of Channelrhodopsin-2 expression and two-photon optogenetic stimulation 46
3.1.1 Single cell electroporation 47
3.1.2 Viral expression of ChR2 48
3.1.3 Testing different channelrhodopsin-2 variants 50

3.2 Targeted two-photon subcellular stimulation 52

3.3 Optostimuli influence on spontaneous spiking activity 55

3.4 Brain states in anesthetized mice 57

3.5 Somatic responses Down- vs. Upstate 58

3.6 Dendritically evoked optogenetic potentials during Downstates 60
3.6.1 The state-dependent modulation of optogenetic potential amplitudes is dendrite-specific 62
3.6.2 State-dependent gain modulation of basal synaptic input 65

3.6.3 Distance-dependent compartmentalization of apical input during active states . 67

3.7 State-dependent gain modulation of synaptic glutamatergic input to basal dendrites 68

3.7.1 Gain control of thalamic synaptic input 68

3.7.2 Gain modulation of local monosynaptic glutamatergic connections 70

3.8 Synaptic gain modulation in awake mice 71

3.8.1 Somatic responses during slow cortical activity in awake resting mice 71

3.8.2 Compartmentalization of apical input during slow network activity 72

3.8.3 Gain modulation of input to basal dendrites 74

3.8.4 Impact of movement on gain modulation 76

3.9 Postsynaptic mechanisms of state-dependent changes in synaptic integration. 79

3.9.1 Somatic modulation can be mimicked by depolarizing current injection 80

3.9.2 The influence of network activity on somatic input resistance 82

3.9.3 Combined effect of driving force and input resistance on the total transmitted charge 85

3.9.4 Synaptic gain modulation of basal inputs is blocked by intracellular applications of voltage-dependent sodium channels using QX-314 87

4 DISCUSSION 92

4.1 *In vivo* ChR2 two-photon subcellular stimulation development 94

4.1.1 ChR2 expression *in vivo* 94

4.1.2 Two-photon scanned stimulation *in vivo* 97

4.2 Spontaneous spiking and subthreshold activity in neocortex 98

4.3 Cortical states in anesthetized and awake mice 99

4.4 Somatic optogenetic stimulation 100

4.5 Dendritically evoked optogenetic potentials 101

4.5.1 Influence of distance from the soma on dendritic OP kinetics 103

4.6 State-dependent modulation of somatic OPs 105

4.7 State-dependent modulation of dendritic OPs 106

4.7.1 Modulation of input to apical dendrites 108

4.7.1.1 Mechanisms mediating the state-dependent modulation of synaptic input to apical dendrites 109

4.7.2 Gain modulation of synaptic input to basal dendrites 111

4.7.2.1 Postsynaptic mechanisms mediating the state-dependent gain modulation of synaptic input to basal dendrites 114

4.8 Functional consequences of dendrite-specific modulations of synaptic input . 118

4.9 Outlook and future experiments 121

Conclusions 123

BIBLIOGRAPHY 124

APPENDIX 136

Abbreviations 136

Index of Figures 138

PUBLICATIONS 140

1 INTRODUCTION

If the brain were simple enough for us to understand it, we would be too simple to understand it.

Ken Hill

The human brain is one of the most sophisticated structures evolution has ever generated. It comprises nearly 100 billion neuronal cells (Azevedo et al., 2009) linked together by more than 100 trillion chemical synapses (Pakkenberg et al., 2003). They form a vast neuronal network that is supported by many other types of cells and contains a large number of specialized subsystems (Meunier et al., 2010). These systems operate partially independently and communicate via massive tracts of fibers (Thivierge and Marcus, 2007). Together they control the homeostasis of organs and systems throughout the body, serve as terminals that collect and organize sensory input for perception, and ultimately coordinate behavior such as voluntary movements. The structure of this system in humans generates thoughts, feelings, and conscious awareness. A long-term aim of the neurological sciences is therefore to identify the neural substrates involved in highly complex mental processes such as perception, learning and memory, decision making and, ultimately, consciousness and relate them to their anatomy.

Under the pressure of evolution, brain functions have shaped cerebral structure and in turn, brain architecture determines the operations that are possible. Likewise, activity and structure are functionally interlinked. These two central aspects of the brain have been typically studied in parallel by implementing separate types of experiments: anatomical studies that define the arrangement of cells in interconnected micro- and macro-circuits, and functional studies investigating the cellular mechanisms of electrochemical activity. However, early relationships between brain regions and functions were established in the 19th century, with the experimental method of introducing lesions in localized regions of animal brains and describing their effects on motor function, sensation and behavior (Pearce, 2009). Relating brain activity to neuronal fibers at a finer resolution required new methods of staining and mapping of neurons, which showed that the nervous system is composed of

a huge number of individual nerve cells that are connected by synaptic terminals positioned throughout anatomically widespread and distributed dendritic structures (Golgi, 1873; Ramón y Cajal, 1904).

Neuronal signals flow through a labyrinth of cerebral synaptic connectivity; they are transmitted through synapses and the convoluted neuronal dendritic arbor leads and shapes the integration of synaptic input in single neurons. The activity of the network is a product of the signals flowing through this complex architecture and the routes they take. This means that a single neuron's activity is tightly connected to the processes taking place in a large network of cells, and it cannot properly be described independently from the structure and activity of this larger environment. In the 20th century, electroencephalography (EEG) provided evidence that neurons interact as a unified network by generating electrical activity waves in the brain (Berger, 1929). Since then EEG has provided a holistic view of a brain that is constantly active and revealed that the amplitude and frequencies of brain waves change as a neuronal network becomes involved in different activities (Destexhe et al., 2003; Sanchez-Vives and McCormick, 2000). A major step toward linking these phenomena to neuronal activity was made using fine glass pipettes to record electric potentials from single neurons (Brock et al., 1952). Whole cell patch clamp recordings of neurons in acute brain slice preparations have permitted precise analyses of the transmission of signals among groups of neurons, making it clear that the dendritic integration of single synaptic inputs plays a major role in a neuron's output (Rall, 1967; Spruston, 2009) and, by extension, ultimately shapes the activities of the network. Constant developments and improvements in electrophysiological, optical and molecular techniques have now made it possible to study neuronal processing in the living, active brain.

While *in vivo* electrophysiology has contributed to our understanding of neuronal activity during sensory perception, questions regarding the integration of dendritic synaptic inputs *in vivo* remain open. Addressing this issue would require the ability to make recordings of single neurons in living animals, as well as to control and monitor synaptic inputs to specific sub-cellular locations. In this study, I focused on how internal brain activity influences the integration of synaptic inputs received from different dendritic locations in single cortical pyramidal neurons *in vivo*, with an overall aim of linking neuronal anatomy to its physiological function.

1.1 Somatosensory cortex

During evolution, the differentiation of *Animalia* from other Kingdoms saw a development of neuronal cell assemblies needed to carry out two main types of tasks: first, the detection of environmental changes and secondly, the control of movement in response. Along with the evolution of sensory organs, animals' perception of the environment became more and more elaborate and could only be computed if they were accompanied by a parallel increase in the complexity of neuronal structures. In the mammalian brain, the area devoted to the perception and integration of sensory input is the sensory neocortex. My thesis focusses on synaptic integration between neocortical neurons of the somatosensory cortex.

1.1.1 Cortical cell types

The somatosensory cortex can be anatomically divided into six layers (Ramón y Cajal, 1899). Each layer has its own particular arrangement of cell populations and pattern of connectivity within the layer, across the other layers and with other brain structures (Douglas and Martin, 2004). The neocortex neuronal population has been classified according to criteria based on anatomical and electrophysiological features, projection targets, genetic labeling and molecular markers. About 75% of cortical neurons are glutamatergic excitatory pyramidal neurons, which are found in all the layers, at a higher proportion in layers 2 and 3 (L2/3), 5 and 6 (Binzegger, 2004; Oberlaender et al., 2012) (Figure 1).

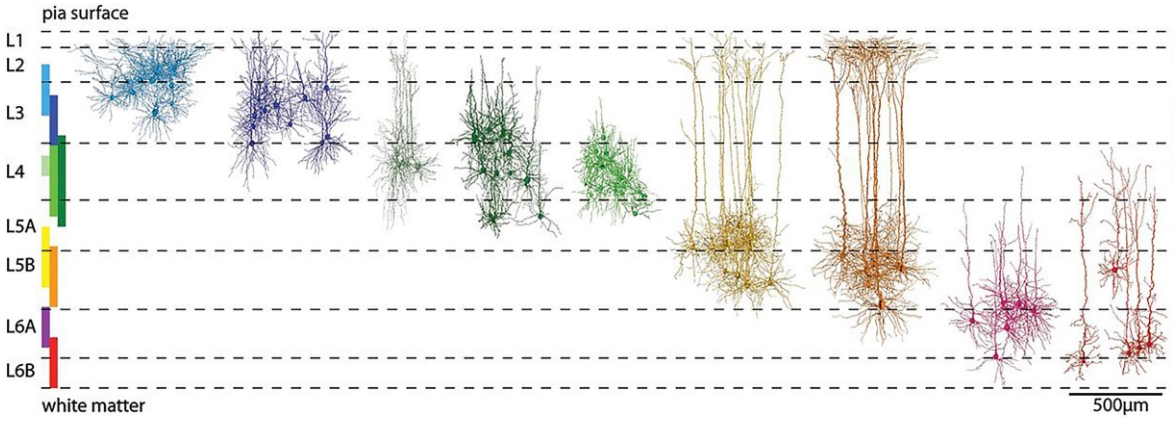

Figure 1. **Definition of excitatory cell types in a barrel column.**
Cluster analysis of morphological features of 9 identified excitatory cell types across L1 to L6b of the somatosensory cortex (Reproduced, with permission, from Oberlaender et al., 2012).

The remaining 15–20% of neurons in the somatosensory cortex are cortical inhibitory interneurons releasing γ-aminobutyric acid (GABA). They belong to three main, non-

overlapping subsets (Lee et al., 2010). 30% are parvalbumin-positive (PV) neurons that form GABAergic synapses around the soma, proximal dendrites and the axon initial segment of pyramidal neurons (Packer and Yuste, 2011) and also innervate other interneurons. PV fire thin action potentials (APs) and sustain tonically very high firing rates, so they are regarded as fast-spiking neurons (Steriade, 2001) and are thought to be rather non-selective in their inhibitory target neurons. The largest population of interneurons (50%) are cells that express vasoactive intestinal peptide (VIP), which mostly inhibit other inhibitory cells (Staiger et al., 2004). The smallest group, representing the remaining 20% of the GABAergic population, consists of somatostatin-expressing (SST) interneurons that mainly inhibit the distal dendrites of pyramidal neurons (Jiang et al., 2013; McGarry, 2010; Wang et al., 2004).

1.1.2 Laminar connectivity

Cortical layers have complex input and output connectivity with long range and local connections (Figure 2). Within the superficial layers of the neocortex, layer 1 is only populated by a scarce number of inhibitory interneurons and the long range excitatory projections entering from other cortical regions, including the motor cortex (M1) and sub cortical regions such as the posteromedial complex of the thalamus (POm), innervating apical dendrites of L2/3 and L5 pyramidal neurons (Veinante and Deschênes, 2003; Wimmer et al., 2010). Dense populations of pyramidal excitatory neurons can be found in Layers 2 and 3; they locally innervate other L2/3 neurons, provide excitation to L5 (Feldmeyer et al., 2006) and also manage long-range communication through axonal projections that stretch to distant cortical areas. In terms of input, L2/3 neurons are innervated by excitatory contacts from L4 and L5 in addition to long-range input from M1, POm and the ventroposteromedial thalamus (VPM) (Feldmeyer et al., 2002; Veinante and Deschênes, 2003; Wimmer et al., 2010). L4 has a population of characteristic excitatory spiny stellate neurons that gives it a granular cytological appearance and represent the main input layer of the cortex. Sub-granular Layer 5 pyramidal neurons provides the largest source of cortical output (Harris and Shepherd, 2015). The pyramidal neurons of deep layers 5 and 6 are very large cells that project their apical dendrites vertically up to layer 1 (L5) or layer 4 (L6) and innervate profusely along the layers and other cortical and non-cortical areas.

The cellular organization and connectivity of the neocortex structures the way sensory information is processed and integrated. Its layered architecture directly influences each

neuron, while the different types of cells play distinct roles in its information processing functions.

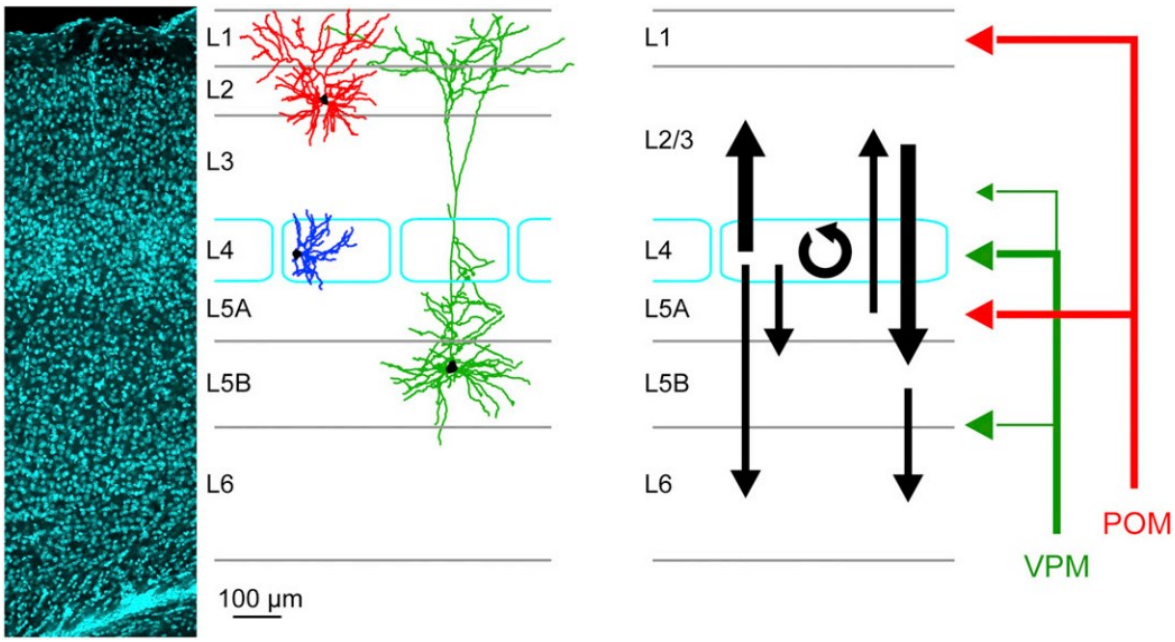

Figure 2. **Excitatory synaptic input-output relationships in the somatosensory barrel cortex.** Left: confocal image of DAPI-stained nuclei (cyan) at a single focal plane through the C2 barrel column. Middle: schematic representation of the cortical layers (barrels within L4 in cyan) with examples of typical dendritic morphologies of excitatory cortical neurons (in red, an L2 neuron; in blue, a spiny stellate L4 cell; in green, an L5B pyramidal neuron). Right: schematic representation of the main excitatory connections between cortical layers within a barrel column (black), as well as the main thalamic inputs to the barrel cortex from the VPM nucleus (green) and the POm nucleus (red) (Reproduced, with permission, from Petersen and Crochet, 2013).

1.1.3 Pyramidal neuron structure and function

Pyramidal neurons are found primarily in forebrain structures such as the cerebral cortex, the hippocampus and the amygdala, areas which have been associated with advanced cognitive functions in the brains of mammals, birds, reptiles and fishes (Elston, 2003; Nieuwenhuys, 1994). Most of the synaptic input pyramidal neurons receive (75-95%) is excitatory. It may originate with other pyramidal neurons in their vicinity, from other cortical areas and direct thalamic input (DeFelipe and Fariñas, 1992). In terms of output, pyramidal neurons of the neocortex form excitatory glutamatergic synapses with local and distant cortical and non-cortical brain areas, including the spinal cord, brainstem, basal ganglia and thalamus (Harris and Shepherd, 2015).

Pyramidal cells have a particular anatomy with an extended dendritic tree that is able to receive thousands of inputs and a lone axon, typically emanating from the base of the soma

and branching profusely, making many synaptic contacts along its length (Spruston, 2008). The soma is characteristically large and pyramidal in shape with a large base. One of the defining anatomical features of pyramidal neurons is their pattern of dendritic branches. While basal dendrites extend laterally from the cell body and mainly receive input from local circuits (Feldmeyer et al., 2006), apical dendrites ascend vertically to other cortical layers, in particular to layer one, where in some pyramidal neurons a prominent dendritic arbor extends in a typical tuft shape (DeFelipe and Fariñas, 1992) (Figure 2, Figure 3). This region predominantly collects information from other cortical and non-cortical brain regions (Shipp, 2007).

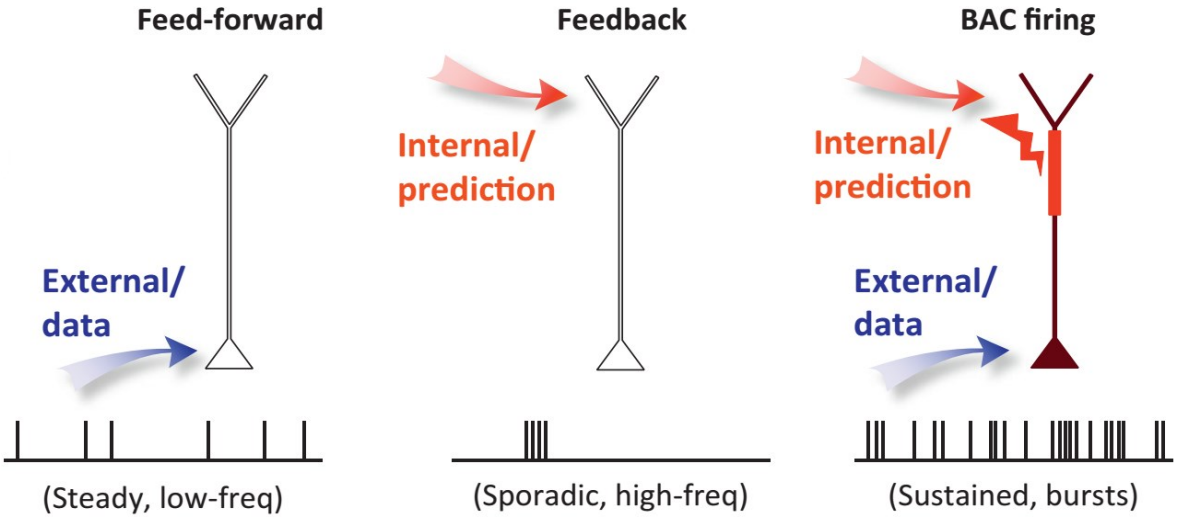

Figure 3. **Conceptual representation of pyramidal neurons functioning as a coincident detector.**
Any given perception is represented internally via a cortical 'engram' of neurons receiving feed-forward (blue) and feedback (red) information. In this hypothesis, the concept of an engram is functionally encapsulated by pyramidal neurons because they are the only cells that project to other areas within and outside the cortex. Neurons receiving predominantly feed-forward information are likely to fire steadily at low rates, whereas feedback input to the distal dendrite should occasionally reach the threshold and produce a short burst of action potentials. The simultaneous combination of the two streams will result in sustained firing and possibly change the mode of firing to bursts (Reproduced, with permission, from Larkum, 2013).

This structure is thought to give pyramidal neurons the ability to function as an associative link between sensory (or feedforward) input from thalamus and associative, centrally generated (or feedback) input which arrives at the upper layer from other cortical areas (Larkum, 2013). In L5 pyramidal neurons these functions are thought to be served by their active dendritic integration capabilities (Major et al., 2013), such as the backpropagation activated calcium channels (BAC) (Larkum et al., 2009) (Figure 3).

Its hypothetical role as a coincident detector makes the pyramidal cell an important component of the cortex's capacity to integrate information. This means that insights into cortical information processing can be gained by studying how pyramidal neurons collect and integrate synaptic input, to generate spiking output.

1.1.4 L2/3 pyramidal neurons

The superficial layers of the neocortex receive information from numerous other neocortical regions and respond by signaling to a similar number of other regions. This positions them at a key point in the network for integration of information across cortical areas (Harris and Shepherd, 2015). Layer 2/3 is an area with the highest number of synapses and pyramidal neurons of this region represent the most abundant population of cells in the cortex (Binzegger, 2004). However, compared to the large layer 5 pyramidal neurons, layer 2/3 pyramidal neuronal subcellular compartments are more poorly defined (Figure 1) and they respond to sensory stimuli more sparsely and less frequently than those of L5. Together meaning that it has been harder to evaluate their functions (Barth and Poulet, 2012; Petersen and Crochet, 2013).

Neurons in superficial layers exhibit a level of spontaneous and evoked activity that is many times lower than that seen in deep layers. The lower firing rates of L2/3 excitatory neurons are partly a result of resting membrane potentials (V_m), which are more hyperpolarized than in L5 pyramidal neurons (Lefort et al., 2009). A subset of layer 2/3 pyramidal neurons robustly fire to sensory input but the vast majority produces only few APs in response to a given sensory stimulus (Hromádka et al., 2008; O'Connor et al., 2010). The sparse firing of L2/3 neurons is modulated by anesthesia and brain state and is not thought to be due to an absence of excitatory input, but rather because their firing is strongly inhibited. Recent studies suggest that L2/3 pyramidal neurons show a certain degree of selectivity for visual (Ohki et al., 2006, 2005), auditory (Bathellier et al., 2012; Rothschild et al., 2010) and somatosensory stimuli (Andermann and Moore, 2006; O'Connor et al., 2010). So there is increasing evidence for high stimulus selectivity as a functional cause of sparse firing in L2/3 excitatory neurons (Barth and Poulet, 2012; Petersen and Crochet, 2013).

The supragranular layers may therefore have a central role in the fine selection and integration of information across the neocortex, with L2/3 pyramidal neurons being main actors in this process. While these neurons receive high levels of excitatory input, the low

firing rates suggests that signals along the dendritic arbor are subjected to a finely tuned process of integration that gives rise to output only in specific situations. These factors make L2/3 pyramidal neurons an interesting model to study the integration of subthreshold signals.

1.2 Cortical monosynaptic transmission and integration

The integration of synaptic inputs in single neurons and the way in which a neuron generates action potential outputs is a critical feature of the computational capacity of the entire cortical network. Pyramidal neurons receive input through ligand gated ionotropic or metabotropic receptors. Both are transmembrane proteins and are activated by the binding of a specific ligand that has been released by the presynaptic bouton. While metabotropic receptors have a slower, modulatory effect on synaptic transmission, ionotropic receptors are fast-opening channels that can be excitatory or inhibitory, depending on the type of ion they are selective for. The majority of inhibitory synapses release GABA, which opens anionic channels selective for chloride ions (Cl^-) and responsible for inhibitory post-synaptic potentials (IPSPs).

The most common excitatory neurotransmitter in the brain is glutamate, which binds to and activates the alpha-amino-3-hydroxy-5-methyl-4-isoxazole propionic acid (AMPA), Kainate and N-methyl-D-aspartate (NMDA) receptors (Auger and Marty, 2000). When opened, these channels allow an electrotonic flow of positive ions such as sodium (Na^+), potassium (K^+) and calcium (Ca^{2+}) (NMDA only), and this ultimately leads to membrane depolarization. The arrival of a single action potential at the excitatory presynaptic terminal triggers a quantal release of glutamate, which can activate one or more synaptic spines that expose ionotropic receptors (Auger and Marty, 2000). The resulting membrane depolarization is defined as the unitary excitatory post-synaptic potential ($_u$EPSP), and it represents the functional unit of neuronal communication.

Neurons are able to receive thousands of almost simultaneous synaptic inputs because of their intricate, extended dendritic arbor. Morphological studies have shown that non-spiny symmetric synapses that form on the soma, perisomatic regions and the initial segment of the axon are predominantly of the inhibitory type, whereas excitatory synapses, which represent 75-95% of the total input, are arranged all along dendritic regions (DeFelipe and Fariñas, 1992; Larkman, 1991). Excitatory synapses are not randomly distributed along the dendritic tree: more than 95% of them form on dendritic spines and are called of the

asymmetric type (Colonnier, 1968), thus the allocation of spines is strongly related to input arrival position.

How an individual EPSP affects the generation of the action potential at the somatic level depends on how it is transmitted from the postsynaptic bouton along the dendrite. Along this path, it will be integrated with other EPSPs and IPSPs, modulated by voltage gated channels and a range of other passive and active processes which occur in dendrites (Larkum and Nevian, 2008; Rall and Rinzel, 1973; Spruston, 2008; Stuart and Spruston, 2015).

1.2.1 Synaptic integration in cortical neurons

The dendritic integration of signals is regulated by passive and active dendritic properties. Passive properties, which are modeled based on cable theory, depend on dendritic structure, size, and branching and are assumed to have properties like conductive cables with leaky membranes immersed in a conductive medium (Rall, 1967). These features impose the rules on the spatial and temporal calculation of the effects of EPSPs and IPSPs and ultimately determine the temporal broadening and amplitude filtering of the signal as it appears at the soma (Cuntz et al., 2014; Spruston, 2009).

The active properties are based on the effects of different voltage-dependent currents as determined by the distribution of channels, which varies across cell types and dendritic regions. Active properties in pyramidal neurons include the effects of regenerative dendritic events such as calcium, NMDA and sodium spikes (Larkum and Nevian, 2008; Major et al., 2013). Such voltage dependent currents are thought to be activated by simultaneous, clustered inputs; they enhance signals and overwhelm the normal attenuation introduced by filtering. Moreover dendritic spikes interact with back-propagating action potentials (bAPs) during cell firing (Larkum and Nevian, 2008). Persistent sodium currents (Na_P) can also increase the synaptic input amplitude at depolarized levels (Stuart and Sakmann, 1995) while sodium-potassium hyperpolarization-activated currents (I_h) can have a normalizing effect on synaptic input amplitude (Magee, 1999). More factors come into play along the route of a single synaptic input toward the soma: as excitatory and inhibitory synapses are activated, it can be boosted or dampened (Lee and Dan, 2012; Spruston, 2009). These currents affect more than just the inputs; they also change the conductance properties of the path along dendrites, which in turn affects the propagation of the signal and the degree of leakiness of the neuronal membrane (Destexhe et al., 2003; Spruston, 2009; Williams, 2004) (Figure 4).

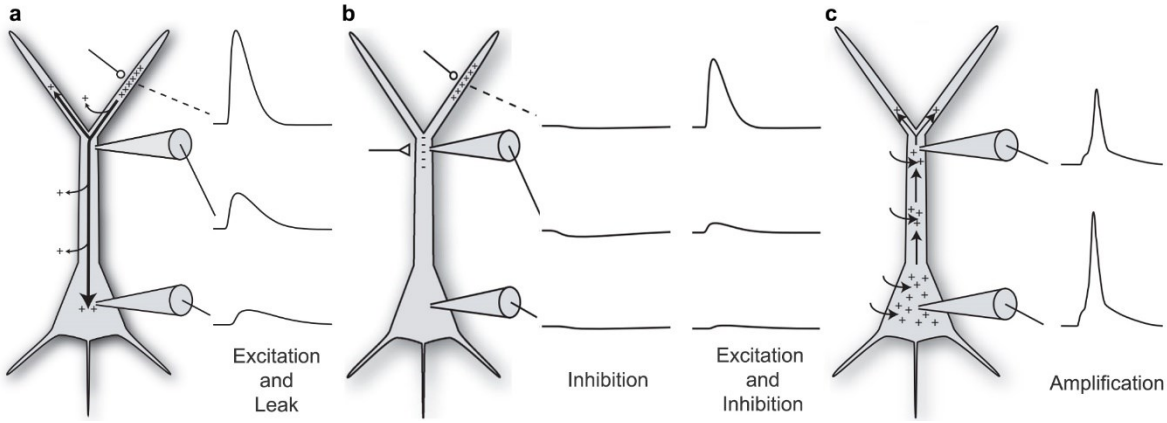

Figure 4. **Dendritic attenuation and filtering of an EPSP.**
A schematic diagram of a pyramidal neuron, indicating the pyramidal soma, apical dendrites (from soma apex), basal dendrites (corners of soma base), and an axon (from center of soma base). **a**. Activation of a synapse on an apical dendrite produces a local EPSP (top) that is larger and faster than the EPSP recorded at more proximal locations (as indicated by recording electrodes). EPSP attenuation is caused by loss of charge between the synapse and other locations, as well as changes in local input impedance. **b**. Synaptic inhibitory input sum up to the potential shunting ultimately the EPSP. **c**. Active dendritic currents, elicited by EPSP depolarization amplify the resulting somatic contribution of EPSPs. (Reproduced, with permission, from Spruston, 2009).

The dendritic integration properties of neocortical pyramidal neurons have been characterized extensively in *in vitro* studies (Larkum and Nevian, 2008; Spruston, 2008). Acutely dissociated neuronal preparations have the advantage of isolating single neurons from their networks, so that an input can be finely tuned and the output can be described unambiguously (Giugliano et al., 2004). Acute brain slice preparations preserve part of the local network in which the neuron is embedded as well as the structure and the original connectivity of that circuit. EPSPs from synaptic connections in cortical slice preparations can be elicited and recorded (Markram et al., 1997) and active dendritic properties can be described in the context of established neuronal models (Major et al., 2008).

In comparison to such *in vitro* techniques, intracellular recordings in intact living animals have presented methodological obstacles, and there have only been minor successes in achieving fine control over synaptic integration by using extracellular drugs. *In vivo* studies, however, are the best way to study neuronal function under unaltered physiological conditions and, besides preserving the entire structure and connectivity of the brain, *in vivo* recordings permit monitoring neuronal computation during spontaneous activity of the network, which is typically lost *in vitro*. This background activity includes the effects of neuromodulatory pathways, which can have a marked influence on cellular properties and network activity *in vivo* (Lee and Dan, 2012). As a result, *in vitro* studies can only provide

a description of possible types of computations that can be performed by dendrites. They are well suited for studies of the physical machinery and integrative capabilities of dendrites, but they cannot resolve which of the many integration mechanisms observed *in vitro* actually come into play in the brain in active networks (Stuart and Spruston, 2015).

1.3 Spontaneous cortical network activity

A brain can be seen as a predictive device whose anticipatory powers emerge from the various rhythms it generates. Nervous systems are active at all times during waking and sleeping but the physiological functions of different brain rhythms vary between a few that are obvious to the impenetrable (Buzsáki, 2006). Examples of the obvious type are breathing or walking, effortless exercises that are made possible by self-sustaining spinal cord oscillators termed central pattern generators (Brown, 1911; Marder and Calabrese, 1996; Wilson, 1961). Centrally generated rhythmic neuronal activity is also fundamental for more complex brain functions such as memory formation in the hippocampus and perception and cognition in the neocortex. Cortical network activity that has been observed since the first EEG recordings made in awake animals and humans. Researchers initially defined five fundamentally different types of cortical "brain waves" (Berger, 1929; Buzsáki, 2006; Clark, 1946; Demos, 2005; Kobayashi and Himwich, 1962; Woolsey et al., 1947). *Gamma* waves (40 to 100 Hz) are involved in higher processing tasks as well as cognitive functions. *Beta* waves (12 to 40 Hz) are known as high-frequency, low-amplitude brain waves and are commonly observed in awake animals. *Alpha* waves (8 to 12 Hz), known to be important for memory consolidation and emerge with relaxation. *Theta* waves (4 to 8 Hz) are involved in restorative sleep and are connected to the experience and feelings evoked by deep emotions. In the hippocampus, the coupling of slow *theta* and *gamma* activity is vital for memory functions such as episodic memory (Buzsáki, 2006; Nyhus and Curran, 2010). Finally, *Delta* waves (< 1 to 4 Hz) are observed during periods of deep sleep. Virtually no nervous system function, be it the simplest motor event or the most complex cognitive act, exists outside of a rhythmic time metric therefore to understand the contributions of specific neurons to complex brain tasks such as perception, motor control, learning and cognition, influences of different brain activities need to be taken into account.

Many functions have been ascribed to cortical network activity including enhanced responsiveness or gain modulation that can improve signal detection in central neurons, a reduction in the variability of responses and a sharpening of temporal processing capabilities

(Hô and Destexhe, 2000; Rudolph and Destexhe, 2003; Stacey and Durand, 2001). During synaptic "noise" neuronal responses have an augmented capacity to follow high-frequency synaptic stimulation and can detect rapid changes of temporal correlation among thousands of input sources (Rudolph and Destexhe, 2003, 2001). In addition, even low-amplitude excitatory inputs can have a small probability of evoking spikes in high-conductance states with consequences at the network level (Chance et al., 2002; London et al., 2010). Moreover, dendritic plateau potentials are correlated with active brain states induced by sensory stimulation and play a role in promoting long-term potentiation in thalamo-cortical connections (Gambino et al., 2014).

1.3.1 Network activity effects on neuronal membrane potential

Network activity is observed in intracellular membrane potential (V_m) recordings *in vivo*. These can be performed in intact brains during different periods of brain activity (Destexhe et al., 2003) (Figure 5 b, c). Even under deep anesthesia, induced through barbiturates, neurons are subject to spontaneous synaptic input, producing slow synchronous waves of activity. Under ketamine-xilazine or urethane anesthesia, neurons fluctuate between periods of high and low synaptic activity to produce a pattern similar to slow-wave sleep (Destexhe et al., 2003). These slow membrane potential fluctuations induce a hyperpolarized, synaptically quiescent Downstate which alternates with a depolarized, active Upstate (Steriade et al., 1993) (Figure 5 b). During active network states, layer 2/3 pyramidal neurons receive a continuous barrage of excitatory and inhibitory synaptic inputs throughout their dendritic tree and soma (Destexhe and Paré, 1999). This intense background activity arises from the thalamo-cortical and intracortical presynaptic neurons, and is thought to be sustained by layer 5 neurons (Beltramo et al., 2013). The thalamo-cortical excitatory connections loop has a key role in controlling and sustaining the alternating cortical state change (Poulet et al., 2012). The modulation of brain states is also influenced by cholinergic, GABAergic and noradrenergic projections from the brainstem and basal forebrain (Lee and Dan, 2012).

Switches from the Down- to the Upstate causes the postsynaptic membrane voltage to fluctuate, resulting in a net depolarization of the somatic V_m and sparse and irregular action potential firing during Upstates (Barth and Poulet, 2012; Destexhe et al., 2003). In contrast, during the quiescent Downstate, the cell receives little or no synaptic input, resulting in a more hyperpolarized V_m, which more closely resembles the *in vitro* situations (Figure 5 a,

b). From Down- to Upstates the biophysical properties of cortical neurons are thought to change substantially and have important consequences for synaptic integration (Bernander et al., 1991). Consequently, observations carried out *in vitro* may not be directly transferrable to *in vivo* situations (Steriade, 2001).

1.3.2 Awake rest and active movement

Recently, intracellular recordings have shown distinct patterns of cortical activity in awake, resting or actively behaving animals. Large amplitude, slow (< 5 Hz) fluctuations of the V_m of cortical neurons are a hallmark of quiet wakefulness in mice (Crochet and Petersen, 2006; Poulet and Petersen, 2008). These V_m fluctuations are similar to the Up- and Downstates induced by anesthesia. Even though the hyperpolarized V_m (V_{hyp}) lasts for a shorter period of time than in a Downstate, it is similar in V_m value, as the depolarized phase (V_{dep}) is similar to an Upstate V_m. On the other hand, during active movement, when the mouse is actively scanning its environment, these slow membrane potential fluctuations are suppressed. The variance in membrane potential is decreased and the remaining fluctuations of the membrane potential become less correlated in nearby neurons. Additionally, excitatory neurons depolarize on average by a few millivolts (Poulet and Petersen, 2008) (Figure 5 c).

The desynchronized cortical state in the primary somatosensory (S1) cortex during movement correlates with an increased firing rate of thalamo-cortical cells, driving important aspects of the cortical state change during movement (Poulet et al., 2012). Neuromodulatory inputs are also likely to play a significant role in generating desynchronized brain states (Constantinople and Bruno, 2013; Lee and Dan, 2012).

Network activity has a profound effect on the synaptic input evoked by somatosensory stimulation (Crochet and Petersen, 2006; Petersen et al., 2003; Polack et al., 2013; Sachdev et al., 2004; Zhao et al., 2016) as well as auditory (Pi et al., 2013; Pinto and Dan, 2015) and visual stimuli (Pinto and Dan, 2015). Importantly, the cortical sensory processing of the same peripheral stimulus differs strongly in comparisons between quiet and active cortical states. The large sensory response evoked during quiet wakefulness might serve to alert the animal, while the smaller and spatially confined response during the active cortical state might enhance fine-level discrimination of sensory input (Crochet and Petersen, 2006).

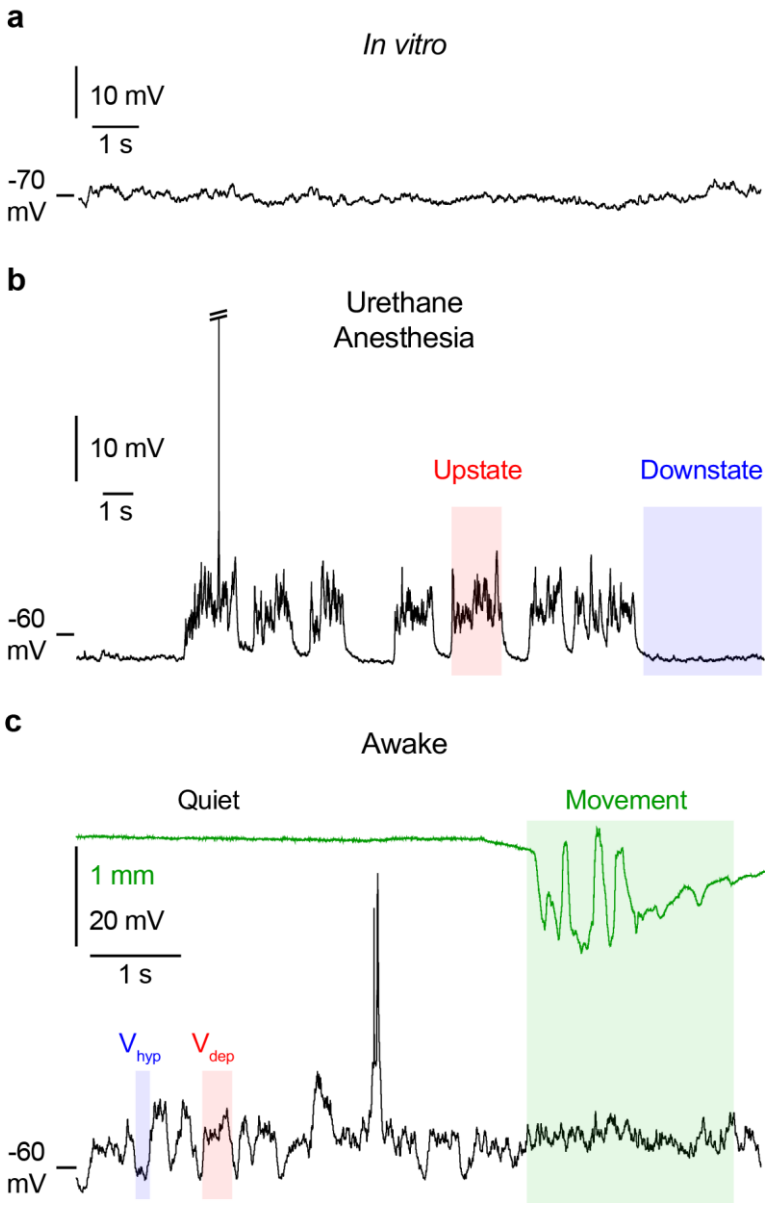

Figure 5. **Intracellular whole-cell recordings during different states of activity.** Comparisons of spontaneous membrane potential oscillations across different cortical states in L2/3 pyramidal neurons. **a**. *In vitro* recordings obtained in cortical slices; in this case, the network activity is minimal, as shown by the quiescent intracellular signal, which shows only discrete synaptic events. **b**. Under urethane anesthesia, the V_m oscillates between two phases: depolarized periods (Upstates) with fast irregular V_m oscillations; and hyperpolarized periods (Downstates) during which activities are absent or strongly reduced. **c**. In the awake mouse, the intracellular recording is characterized by a highly fluctuating membrane potential that is associated with irregular firing. During quiet periods, the V_m oscillate between depolarized (V_{dep}) and hyperpolarized (V_{hyp}) phases. During active movements, oscillations are suppressed, the network is desynchronized and the V_m is moderately depolarized.

Little is known, however, about the impact of network activity on unitary excitatory postsynaptic potentials *in vivo*. The $_u$EPSP is the smallest signal a neuron can receive from another neuron and can thus be regarded as the minimal functional unit of neuronal

communication. Studying how the integration of a single input is affected by different brain activities is pivotal in understanding neuronal computational rules *in vivo*, whereby neurons are subject to numerous simultaneous inputs.

1.4 Impact of cortical network activity on synaptic integration

Neurons evolved a structure of large and elaborate dendritic arbors that collect thousands of inputs. Signals are integrated with many others and the impact of their contribution is combined at the axonal initial segment close to the soma, where the action potential may or may not be triggered. Hence, somatic V_m fluctuations represent the result of the complex integration of thousands different inputs across the whole anatomy of the neuron and the point at which they merge with suprathreshold neuronal activity. The impact of spontaneous network activity on neurons has been characterized mainly from somatic recordings, but fully understanding dendritic integration requires considering how brain activity affects dendritic processing.

Despite the synchronization of dendrites with somatic V_m and with network activity during periods of Up- and Downstates (Larkum et al., 2007; Waters and Helmchen, 2004), the resulting dendritic V_m is only a partial sum compared to the V_m at the soma. The relative impact of a synaptic input to the somatic V_m depends on its distance from the soma: inputs arriving at closer distances contribute more than signals that originate more distantly from the soma, which may not make much of a contribution. The farther a dendrite is from the soma, the more it will be subject to local V_m oscillations (Spruston, 2008; Williams, 2004). Moreover, in comparison to the soma and perisomatic areas, dendrites are thinner and tend to shrink toward the tip. This changes the volume surface ratio and thus increases impedance of the conductive structure (Rall, 1967; Rall and Rinzel, 1973). The high impedance in dendrites affects their responses to synaptic input by increasing the local amplitude of EPSPs by up to two orders of magnitude (Jaffe and Carnevale, 1999; Spruston, 2008), making V_m fluctuations on dendrites sharper, more amplified and turbulent compared to the soma (Larkum et al., 2007; Waters and Helmchen, 2004). On the other hand, such large amplitude dendritic $_u$EPSPs encounter a gradient of decreasing impedance toward the soma that dampens them and can thus filter out most of the distant inputs (Jaffe and Carnevale, 1999; Nevian et al., 2007; Williams and Stuart, 2002).

When networks are active, other factors affect this passive filtering as well. Modeling studies have predicted that $_u$EPSPs arriving during an active state would be reduced in

amplitude due to the lower driving force and shunting effect of increased conductance (Bernander et al., 1991; Destexhe and Paré, 1999). Synaptic noise, however, could also enhance responsiveness to low amplitude inputs due both to mechanisms of stochastic resonance induced by voltage fluctuations, which is an amplification of weak inputs by the assistance of noise in nonlinear systems (Hô and Destexhe, 2000; Rudolph and Destexhe, 2001) and to the activation of active properties of the dendrites (Larkum and Nevian, 2008; Major et al., 2013). Enhanced dendritic responsiveness is more likely to happen in a depolarized active network, when even small stimuli can elicit dendritic spikes that reliably propagate up to the soma (Destexhe et al., 2003).

Another factor influencing integration in active networks states is the presence of voltage-dependent conductances including potassium, sodium, calcium and I_h (sodium-potassium) currents, which may induce different normalizations of synaptic efficacy (Berger et al., 2001; George et al., 2009; Migliore and Shepherd, 2002; Stuart and Sakmann, 1995; Williams and Stuart, 2000). This type of normalization has been found to compensate for the drop in the somatic amplitude of a synaptic input with increasing distance from soma in hippocampal neurons (Magee, 1999). In other series of *in vitro* slice experiments a broadening of the $_u$EPSP and an increase in amplitude was observed during the depolarization of a postsynaptic cortical pyramidal neuron (González-Burgos and Barrionuevo, 2001; Hirsch and Gilbert, 1991; Markram et al., 1997; Stuart and Sakmann, 1995; Thomson et al., 1988).

Most of these studies have focused on either hippocampal or neocortical L5 pyramidal neurons. In L2/3 dendritic integration in active states might be different due to the low expression of I_h channels (Albertson et al., 2013; Larkum et al., 2007) and to a counterintuitive increase in input resistance during Upstates that might trigger an enhancing effect on synaptic inputs (Mateo et al., 2011; Waters and Helmchen, 2006). Experimental testing of these hypotheses *in vivo* is technically difficult, as it requires postsynaptic V_m recordings and a method to control presynaptic spike timing. Paired recordings from different cortical cell types have shown a reduction in $_u$EPSP amplitude (Crochet et al., 2005), while single cell optogenetic stimulation led to no change in the amplitude of $_u$EPSPs to GABAergic inhibitory interneurons (Pala and Petersen, 2015). Prior work using extracellular stimulation has shown a decrease (Crochet et al., 2005; Mateo et al., 2011; Sachdev et al., 2004), an increase (Reig and Sanchez-Vives, 2007) or a rescaling (Reig et al., 2015) of excitatory inputs to pyramidal neurons during active states.

Overall, there are heterogeneous predictions and data about the role of network activity on synaptic integration in cortical neurons. Cortical slice experiments have shown that synaptic plasticity (Froemke et al., 2005; Losonczy et al., 2008; Sandler et al., 2016) as well as passive and active membrane properties (Branco et al., 2010; Major et al., 2013; Williams and Stuart, 2002) are dependent on the location of dendritic inputs. I hypothesize that input location may also be a key determinant of how $_{u}$EPSPs are modulated in layer 2/3 pyramidal neurons during active cortical states.

1.4.1 Dendrite specific synaptic integration

Excitatory inputs to layer 2/3 pyramidal neurons in the primary sensory cortex are anatomically and functionally segregated. The basal dendrites are confined to the same layer as the soma and they mainly collect excitatory input from neighboring 2/3 pyramidal neurons in their local environment (Feldmeyer et al., 2002), L4 spiny stellate neurons (Feldmeyer et al., 2006), L5 pyramids (Lefort et al., 2009) and the thalamic-specific VPM nucleus (Oberlaender et al., 2012). The large apical dendritic trunk and the vertically branching dendrites (DeFelipe and Fariñas, 1992) gather local inhibitory input and are also targeted by axons from other cortical regions, such as primary motor cortex (Veinante and Deschênes, 2003) and higher order thalamic nuclei such as the non-specific POm nucleus (Shipp, 2007; Wimmer et al., 2010) (Figure 2).

Basal dendrites are generally shorter and thinner than their apical counterparts, and are therefore more subject to the effects of the impedance gradient. However their synapses are on average closer to the soma, so they suffer less from spatial compartmentalization and are more susceptible to bAPs. The regenerative dendritic events which occur on basal dendrites are due to NMDA and sodium but not calcium spikes (Larkum and Nevian, 2008; Nevian et al., 2007).

Apical dendrites, on the other hand, are on average larger and longer and rely on the apical dendritic trunk to convey information to the soma. L5 pyramids have an apical dendritic tuft where conductance is compartmentalized (Williams, 2004); this is nevertheless mitigated by I_h currents along the trunk that help to couple the tuft with the soma via bAPs. The tuft processes information independently, relying on NMDA spikes and the exploitation of calcium events in the trunk to deliver current to the soma (Larkum et al., 2009). Dendritic patch clamp studies in quiescent cortical slices have shown that apical and basal dendrites strongly attenuate synaptic input as it propagates to the soma (Larkum et al., 2007; Nevian

et al., 2007; Williams and Stuart, 2002). Furthermore, during simulation of network activity with procedures that allows to control the dendritic conductance with dynamic clamp, the input from apical dendrites resulted further reduced in amplitude due to apical compartmentalization (Williams, 2004). Even though L2/3 pyramids have a shorter apical dendritic trunk, their apical tuft is more electrically compartmentalized than in L5 due to the almost complete absence of I_h. bAPs and calcium spikes still contribute, however, to input integration in L2/3 neurons (Larkum et al., 2007). The simultaneous arrival of robust signals to basal and apical compartments produces overlapping bAPs, and calcium spikes in the apical dendritic trunk that are able to transform the neuron's firing pattern into bursts of high frequency spikes (Larkum et al., 1999) (Figure 3). This bursting behavior is thought to represent the output signal in detecting synchronous top-down and bottom-up input, for which the pyramidal cell might be designed (Larkum, 2013). This also explains the varying numbers of regular spiking and bursting cells found during different brain activity states (Steriade, 2001). Moreover, synaptic input coinciding with cell firing has been linked to localized synaptic plasticity in both basal (Gordon et al., 2006) and apical dendrites (Sandler et al., 2016).

To control and finely tune this putative coincident detection mechanism, there is also a contribution from different GABAergic inhibitory interneurons. In L2/3, PV interneurons from perisomatic inhibitory synapses into pyramidal neurons, are directly excited by the same pyramids and exhibit an increase in spiking during active states. PVs can therefore be seen as a negative feedback control and their inhibition affects both basal and apical signaling (Packer and Yuste, 2011). Martinotti SST interneurons, innervate predominantly tuft apical dendrites of L5 and L2/3 pyramidal neurons in L1 can act to hyperpolarize and lower firing rates during active states (Jiang et al., 2013; McGarry, 2010; Wang et al., 2004). SSTs produce a constant inhibition on the apical dendritic compartment of pyramidal neurons during slow wave fluctuations, which is suppressed in the desynchronized phases during active movement (Gentet et al., 2012). In addition, a different gradient of expression of voltage-dependent channels such as I_h (Berger et al., 2001) potassium (Harnett et al., 2012) and sodium (González-Burgos and Barrionuevo, 2001; Nevian et al., 2007) currents, which may contribute to dendrite specific integration, have been found in basal and apical compartments of L5 pyramidal neurons.

To date there has not yet been a comparative investigation of the way synaptic input from apical and basal dendrites is altered during network activity in L2/3 neurons *in vivo*.

Shedding light on whether there is different modulation to specific dendritic input would help clarify the connection between the anatomy and physiology of L2/3 pyramidal neurons.

1.5 *In vivo* techniques for dendritic stimulation

The aim of this project is to study the contribution of cortical network activity in awake and anesthetized mice on the dendritic integration of $_{u}$EPSPs on neocortical layer 2/3 pyramidal neurons. Moreover, since pyramidal neurons display an anatomical segregation that leads to different inputs to the basal and apical dendritic compartments, I aim to investigate whether the somatic impact of a dendritic input arriving at these two branches is influenced in different ways by the network activity.

To address these goals I needed to record the somatic subthreshold membrane potential of a neuron in a living mouse while measuring unitary EPSPs, and then develop a method to stimulate selectively discreet dendritic branches to compare their somatic potentials as the network carries out different activities under anesthesia or wakefulness.

1.5.1 Currently available techniques

Synaptic integration *in vivo* involves the processing of spatially separated synaptic inputs during network activity. So far synaptic integration has been studied *in vivo* using sensory (Chadderton et al., 2014; Crochet et al., 2011; Longordo et al., 2013), electrical (Reig et al., 2015; Sachdev et al., 2004) or population optogenetic stimulation (Mateo et al., 2011). While these methods permit the activation of real synapses, they lack in anatomical specificity in input location. They are well suited for studying how neurons participate in processing sensory signals but do not bring information on how single EPSPs are integrated during network activity, or whether there is any dendritic-specific computations.

Two-photon glutamate uncaging permits the control of synaptic inputs to specific locations and has helped in the identification of fundamental properties of synaptic connectivity and integration in cortical slice experiments (Branco et al., 2010; Losonczy et al., 2008; Packer and Yuste, 2011). Glutamate uncaging has also been used in silenced networks *in vivo* (Noguchi et al., 2011), but its use in studying active networks is limited because the caged compound acts as an antagonist of GABA transmission and can send cortical networks into epileptic seizures *in vivo* (Maier et al., 2005).

In vivo paired recordings of neighboring neurons is a powerful method that allows recording the subthreshold activity of two connected cells while being able to elicit action

potentials in the first and recording the $_{u}$EPSP on the second. On the other hand, these experiments are very difficult and time-consuming, since the connectivity of L2/3 neighboring neuron is quite low (Jouhanneau et al., 2015). Moreover, pyramid-to-pyramid connections are usually confined to the basal compartment only (Feldmeyer et al., 2006), and the post-hoc confirmation of the dendritic location of a synapse after an *in vivo* double patch lies at the limits of experimental feasibility. This is prohibitive to do in a consistent manner throughout a whole dataset. To address these issues, I developed a new method using *in vivo* two-photon stimulation of an optical activable ion channel – Channelrhodopsin-2.

1.5.2 *In vivo* two-photon Channelrhodopsin stimulation

Channelrhodopsins are a subfamily of retinylidene proteins, or rhodopsins, that function as light-gated ion channels (Nagel et al., 2003, 2002). They serve as sensory photoreceptors in the unicellular green algae *Chlamydomonas reinhardtii*, where they control phototaxis (Sineshchekov et al., 2002). Expressed in cells of other organisms, they permit the use of light to control electrical excitability, intracellular acidity, calcium influx, and other cellular processes.

Channelrhodopsins can be expressed in neurons using a variety of transfection techniques (viral transfection, electroporation, gene gun) in genetically defined cell types, at which point they can be activated by LED, lasers or two-photon lasers (Andrasfalvy et al., 2010; Yizhar et al., 2011). Channelrhodopsin-2 (ChR2) is an ionic channel that is selective for monovalent cations such as lithium, Na^+ and K^+ with a lower permeability for bivalent cation such as Ca^{2+} (Nagel et al., 2003). Upon activation with blue light (~ 470 nm), ChR2 produces a depolarizing potential in neurons with a millisecond time precision that can be regulated in amplitude by adjusting the intensity of the light. Because the cationic permeability and reversal potential (V_{rev}) of ChR2 are similar to glutamate (Berndt et al., 2011; McBain and Mayer, 1994), optogenetically evoked subthreshold potentials (OPs) can be tuned in amplitude and kinetics to mimic EPSPs (Packer et al., 2012; Prakash et al., 2012). Moreover, stronger stimulation can be used for photostimulation of neurons to probe neural circuits by eliciting action potentials (Boyden et al., 2005; Emiliani et al., 2015).

The native ChR2 protein has been mutated for functional expression in mammalian cells, and versions fused with different fluorophores have been engineered to make it identifiable in organic structures (Boyden et al., 2005). Point mutations have been introduced into the native genetic sequence to generate several variants with improvements in terms of their

responsiveness to light, sensitivity to different wavelengths, to deliver a more stable photocurrent or with faster kinetics that can replicate the millisecond time scale of neuronal communication (Berndt et al., 2011). Several transfection systems have been developed and employed to deliver the membrane protein channel to specific neuronal populations or single neurons in the brain: such as the generation of transgenic lines expressing ChR2, transduction with viral vectors (especially lentivirus and AAVs) and transfection via *in utero* or single cell electroporation (Lin, 2012).

Each of these systems has its advantages and disadvantages: transgenic lines can express the protein only in a subset of specific neurons but it requires long time for the line generation. Viruses can be used in wildtype animals, directed to a specific region and can deliver a very strong expression in few weeks (Herzog, 2007; Nathwani et al., 2011). Electroporation can achieve a very specific labeling, down to the single cell in the entire brain but produce a lower expression and throughput rates in comparison to viral vectors (Judkewitz et al., 2009; Kitamura et al., 2008).

Alongside improvements in Channelrhodopsins, light stimulation has also undergone a boost of development to achieve specific goals in terms of neuronal activation. ChR2 stimulation has been achieved with different light sources; LED blue lights deliver a broad and strong activation with a relatively lightweight and low-power system. It is well suited to obtain the synchronous activation of large populations of neurons or axons. Lasers have a narrower wavelength of excitation, thus multiple sources with different wavelengths can be used in combination to trigger different optogenetic tools without an overlap in excitation (Klapoetke et al., 2014). Lasers used in confocal microscopy have higher spatial specificity and can target small regions of the brain, permitting more selective types of stimulation.

ChR2 used in combination with two-photon light stimulation permits the spatiotemporal manipulation of neuronal activity at the single-cell level. In recent years, two-photon laser microscopy has been widely used in live animal imaging for its clear advantages over previous methods using single-photon confocal imaging (Denk et al., 1990; Zipfel et al., 2003). In two-photon microscopy, the Ti-sapphire laser beam is pulsed at femtosecond intervals, generating frequencies up to 10^{15} Hz. Phase-locked photons are convoluted into a flux at the focal plane where two photons, each bearing half the energy required to excite the fluorophore, can act as a single photon of shorter wavelength (Abella, 1962). The probability of a simultaneous two-photon event decreases quadratically with distance, making it nearly impossible a few micrometers away from the focal plane, which dramatically increases the spatial specificity (Denk et al., 1990). This brings also the

advantage of using more penetrating infrared light, which is less harmful and less subject to scattering in comparison to shorter wavelengths (Helmchen and Denk, 2005). Therefore, two-photon laser imaging increases the depth penetration and resolution that is required to visualize structures such as neurons embedded in the opaque tissue of the brain (Zipfel et al., 2003).

The same advantages can be achieved through two-photon light stimulation (Rickgauer and Tank, 2009). Since the beam of light is virtually absent a few μm both laterally and axially from the focus, the stimulation it evokes can be targeted to spatially confined dendritic spots (Packer et al., 2012). Two-photon photostimulation offers therefore, the subcellular resolution required to activate dendritic areas targeted by synapses (Nikolenko et al., 2007). On the other hand, the extreme high power delivered on a very small spot can damage cells but this was recently overcame with fast scanning, temporal focusing or structured light (Andrasfalvy et al., 2010; Gradinaru et al., 2010; Packer et al., 2012; Vaziri and Emiliani, 2012).

Here I developed a method to mimic excitatory synaptic inputs in a specific temporal and spatial manner by performing subcellular two-photon stimulation of ChR2-expressing pyramidal neurons in layer 2/3. The development of this technique has allowed me to simulate $_{u}$EPSPs in a reliable manner, targeted at specific dendritic locations belonging either to the apical or basal compartment of L2/3 pyramidal neurons of the S1 whisker and forepaw cortex. Used in combination with *in vivo* two-photon targeted patch-clamp somatic recordings (Kitamura et al., 2008), I have assessed the contribution made by ongoing cortical activity in anesthetized and awake mice to the synaptic integration of $_{u}$EPSPs.

This study allowed me to identify a dendritic-specific modulation of single synaptic inputs, influenced by the spontaneous network activity, with apical potentials being attenuated and basal inputs undergoing a gain modulation in amplitude during active, depolarized states, in recordings made in mice under anesthesia and while awake.

2 METHODS

2.1 Animal surgery

All experimental procedures were carried out in accordance with national and local Animal Welfare Office regulations. Post-natal day (P) 8−52 C57BL/6J mice of both sexes were used. For thalamic stimulation experiments (Paragraphs 2.2.3 and 3.7.1), fos-GFP mice (Barth, 2004) were used. For monosynaptic connectivity experiments (Paragraph 3.7.2), NEX-cre (Goebbels et al., 2006) × Ai9 (Madisen et al., 2010) and GAD-67 mice (Tamamaki et al., 2003) were used.

Mice were anesthetized with isoflurane (1.5 to 2 % in O_2) or with an intraperitoneal (i.p.) injection of 1.5 mg/kg urethane or a mixture of ketamine (100 mg/kg) and xylazine (5 mg/kg). 30 minutes prior to surgery mice were administered a subcutaneous (s.c.) injection of metamizole (200 mg/kg). During anesthesia, a rectal probe and heating pad were used to maintain mouse core body temperature at 37°C. After surgery, mice were placed on a heating pad at 37°C until their recovery was complete. For 24 hours after surgery, metamizole was added to drinking water (200 mg/ml). In their home cages, mice had access to food and water *ad libitum* and were checked and weighed daily.

2.1.1 Intrinsic optical imaging

For experiments carried out while animals were awake, the forepaw primary somatosensory cortex (S1) was identified through intrinsic optical imaging of the S1 cortex (Figure 6). The body temperature was kept at 37.5 °C and isoflurane anesthesia was carefully adjusted between 1 and 1.5 % until optimal signaling was achieved. The right forepaw was tethered, as described below (Paragraph 2.6) and a train of tactile stimuli (10 Hz, for 8 s) were delivered with a piezo stimulator (Figure 6 a) while monitoring the primary somatosensory cortex with a monochrome CCD camera (QImaging). The intrinsic stimulus response was visualized with red light illumination (630 nm); the center of response was identified (Figure 6 c, d) and superimposed on the blood vessel pattern seen under green illumination (530 nm)

(Figure 6 b). Afterwards a craniotomy was performed as described below (Paragraph 2.3) (Figure 6 e).

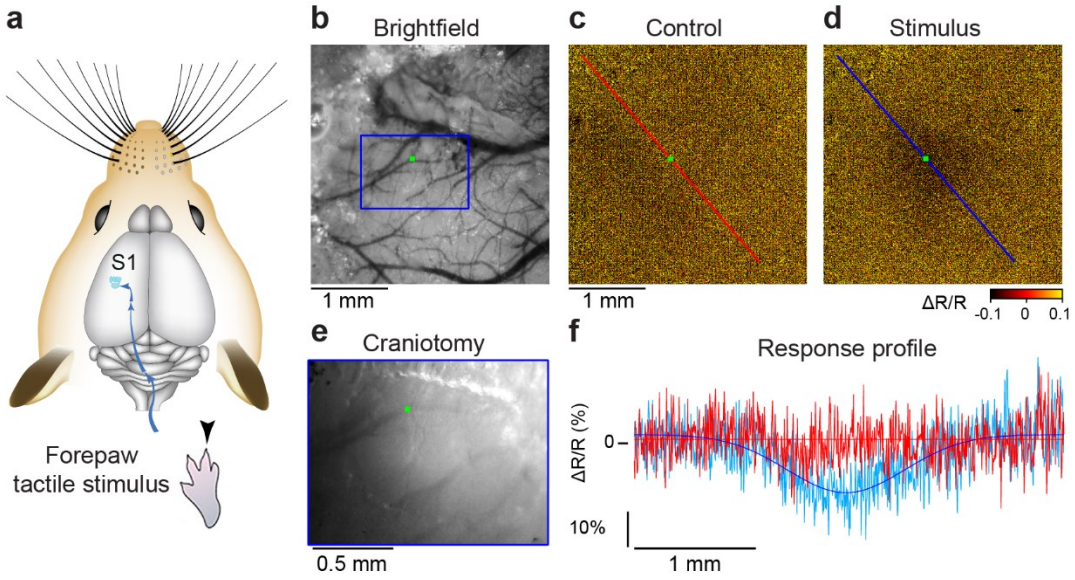

Figure 6. **Intrinsic optical imaging to identify the somatosensory forepaw cortical area.** **a**. Scheme showing the neuronal path from the mouse forepaw to its somatosensory representation in the cortex. **b**. Bright field photo under green light (530 nm) highlighting the layout of veins under the skull. **c**. Averaged intrinsic imaging signal in the forepaw somatosensory cortex during a control with no stimulation. The field of view is the same as in (**b**) but under red light (630 nm). **d**. Same as (**c**) but during the stimulation of the paw, as schematized in (**a**). Darker pixels are linked to an increase in neuronal activity in the area. The green dot represents the center of the response (the point is the same in images **b** to **e**). **e**. Zoom of the same target area in (**b** - **d**) after craniotomy. **f**. Response profile along the diagonal lines shown in (**c**, red, control) vs. (**d**, blue, stimulus).

2.2 Channelrhodopsin-2 transfection

2.2.1 Single cell electroporation

Craniotomies of 0.3–0.5 mm in diameter were performed while keeping the dura intact (Figure 6 e). Visually targeted single cell electroporations were performed under the two-photon microscope (Judkewitz et al., 2009; Marshel et al., 2010). Glass electrodes (12–18 MΩ) were filled with internal solution and a sequence of plasmidic DNA coding for pAAV-CamKIIa-hChR2(HR)-EYFP (Addgene: 26969) or pAAV-CamKII-ChR2(ET/TC)-p2A-EYFP (Berndt et al., 2011). The electrode was pushed up against a single cell, visualized with the shadow method (Kitamura et al., 2008), and then electroporation was performed with the Axoporator 800A (Axon Instruments, Union City, CA, USA). The electroporation consists of the application of a train of negative current pulses of -10 V, for 0.5 ms each,

repeated at 100 Hz, for 1 s, which pushes the negatively charged DNA across the cell membrane while carrying along the dye. This finally leads to the delivery of the dye and plasmid to the interior of the neuron. After an incubation time of 24–48 hours, the dura was removed for two-photon targeted recordings (Figure 10).

2.2.2 Cortical viral infections

P8–12 mice were anesthetized using i.p. injections of a ketamine-xylazine mix and placed in a stereotactic frame (Angle Two, Leica). Stereotaxic coordinates were determined and a craniotomy was performed by drilling over the somatosensory barrel cortex (1.3 mm posterior and 3 mm lateral to Bregma) or the forepaw cortex (0.2 anterior and 2 mm lateral to Bregma). Next, a glass injection pipette (10 µm diameter tip) containing the viral vector solution was connected to an oil piston pressure injection system (MO-10; Narishige) and inserted into layer 2/3 (100–300 µm from pial surface) through the intact dura.

Cortical neurons were infected with channelrhodopsin-2 (ChR2) using an adeno-associated viral vector (AAV2/9) containing pAAV-CaMKIIa-ChR2(T159C)-P2A-EYFP or pAAV-CaMKIIa-ChR2(E123T/T159C)-P2A-EYFP (Berndt et al., 2011; Prakash et al., 2012). 500–1000 nl of virus were injected slowly at 50 nl/min. The injection pipette was removed slowly, the brain covered with petroleum jelly (Vaseline), and the skin resealed. Mice were left in their home cage for 21–28 days while waiting for ChR2-EYFP expression.

2.2.3 Thalamic viral infections

To infect the ventral posteromedial nucleus (VPM) of the thalamus, a lentivirus encoding ChR2-EYFP (VSVG-HIV-Synapsin-ChR2(H134R)-EYFP; Addgene 20945) (Zhang et al., 2007) was injected in P10–12 mice. The procedure was similar to that for cortical infection except that the craniotomy was performed at 1.8 mm posterior and 1.75 mm lateral to Bregma. An injection pipette was inserted to a vertical depth of 3.25 mm. At that point, 500–600 nl of viral solution were injected slowly at a rate of 50 to 100 nl per minute. Mice were left for 1 to 2 weeks while waiting for ChR2 expression (thalamic ChR2 stimulation experiments and analysis was performed by Dr. J-.S. Jouhanneau) then a second craniotomy was made over the hemisphere contralateral to the recording (1.8 mm posterior; 2 mm lateral) for the insertion of an optical fiber (200 µm diameter; Thorlabs) coupled to a 450–480 nm blue light source (473 nm DPSS Laser System; LabSpec) into the somatosensory

thalamus. To optogenetically activate VPM neurons, a 3 ms light pulse (~ 40 mW) was delivered at 0.25 Hz. In some experiments, VPM projections were directly activated by blue light pulses (3 ms, ~ 40 mW) delivered to the surface of the brain that lay over the recording site. Histological sections from every mouse were used to confirm the infection site and ensure that the L5b and L4 axonal projection pattern of VPM axons was typical (Figure 23 a) (Jouhanneau et al., 2014).

2.3 Craniotomy

P21–50 C57BL/6 mice were anesthetized using isoflurane (1–2%) during the implantation of a lightweight metal head holder glued to the skull with cyanoacrylate glue (Loctite 401). The mouse body temperature was maintained at 37˚C with a heating blanket. A recording chamber was then made from dental cement (Paladure, Heraeus Kulzer). The skull was covered with Ringer's solution (in mM): 135 NaCl, 5 KCl, 5 HEPES, 1.8 $CaCl_2$, 1 $MgCl_2$. A small craniotomy (< 1 mm) was made over the barrel cortex (posterior 1–2 mm, lateral 2–3 mm from Bregma) or forepaw S1 (posterior 0 mm, lateral 1.5–2.5 mm from Bregma) (Figure 6 e), after which the dura was carefully removed with a needle. A drop of 1.8% agarose in Ringer's solution was placed on top of the craniotomy to stabilize the brain. All recordings made under anesthesia used exclusively urethane. For awake experiments (Figure 21 and Figure 26), mice were head-restrained and paw-tethered (Paragraph 2.6), as previously described (Milenkovic et al., 2014; Zhao et al., 2016).

2.4 Two-photon targeted patch and whole cell recordings

A Femto2D *in vivo* two-photon laser-scanning microscope (Femtonics) was used to visualize cells in combination with 920 nm, for EYFP identification or 820 nm, for Alexa 594 (Invitrogen) identification light from a Chameleon Ultra II (Coherent) Ti-sapphire pulsed laser light source via a 40x 0.8 NA water immersion objective (Olympus). Two high-sensitivity photomultipliers (PMT) were used to detect fluorescent signals. Imaging was controlled with MES software (Femtonics) running in MATLAB (MathWorks). To reduce the level of optical stimulation of ChR2-expressing neurons during the visualization of the EYFP signal, a few, low-power (~ 5 mW) raster scan images were made at 920 nm. Once a neuron was identified as expressing the protein, the shadowpatch method (Kitamura et al.,

2008) was employed using 820 nm light to identify the shadows of cell somata and perform the final targeting steps with the recording pipette.

Whole-cell patch clamp recordings were made with 2 mm borosilicate glass electrodes (Hilgenberg) with a resistance of 5-7 MΩ. Pipettes were filled with intracellular solution containing (in mM): 135 potassium gluconate, 4 KCl, 10 HEPES, 10 phosphocreatine, 4 MgATP, 0.3 Na3GTP (adjusted to pH 7.3 with KOH) and 2mg/ml biocytin for anatomical reconstructions and Alexa Fluor® 594 dye (Thermo Fisher). In a subset of experiments (Figure 32 and Figure 33), 1 mM QX-314 bromide (Tocris) was added. Recordings were made using an Axon Multiclamp 700b amplifier (Molecular Devices) in current clamp mode with an Ag/AgCl ground electrode in the recording chamber.

Using motorized micromanipulators (Luigs & Neumann) the pipettes were inserted into the brain under visual control at an angle of 34° applying positive pressure of 130–180 mbar. While lowering pipettes into the tissue until about 120 µm depth, pressure was gradually reduced to 50–80 mbar. Cells were approached at low positive pressure (30 mbar), contact with a neuron was validated by live two-photon images, and changes in resistance were visualized on an oscilloscope (Tektronix TDS2024C). Upon contact, negative pressure was applied to form a gigaseal and subsequently break in and enter the whole-cell recording configuration. Recordings were filtered at 10 kHz and digitized at 20 kHz via an ITC18 (Heka) analogue-to-digital converter connected to a computer under the control of IGOR-Pro (Wavemetrics).

For the monosynaptic connectivity experiments, performed by Dr. J-.S. Jouhanneau (Paragraph 3.7.2, Figure 24), up to 4 recording pipettes were inserted into the brain and two to four pyramidal neurons were targeted as previously described (Jouhanneau et al., 2015). To evoke single action potentials, square current pulses (10–20 ms, 100–400 pA) were injected into each cell at a rate of 1 or 0.5 Hz. Z-stack images (2 µm/slice) were made after the completion of the recordings to confirm cell identity.

2.5 Subcellular two-photon optogenetic stimulation

Two-photon optogenetic stimulation was performed using the imaging laser source (at 920 nm wavelength) opened for 10 ms to deliver 10–25 mW (measured below the objective). Somatic stimulations were performed with a spiral scan line (diameter: 8 µm, thread pitch: 0.45 µm). The spiral scan line was scanned two times at a constant speed (19 µm/ms) during

this stimulation epoch. The cell was filled with red Alexa-594 during whole-cell recordings and the dendrites were imaged at 820 nm.

At the beginning of each recording, at least 30 somatic stimuli were applied and the amplitude of an average Downstate response was evaluated online as a measure of the neuronal responsiveness to light; the power of further subcellular stimulations could then be tuned accordingly. Next, dendritic stimulations were targeted to thin apical or basal dendrites using the red Alexa signal in the dendrites for *in vivo* guidance. Apical dendrites were identified by following the branching of the apical dendritic trunk emerging from the top of the pyramidal cell body and moving toward the pial surface. In contrast, basal dendrites were identified by following the branching of laterally emerging dendrites moving around the soma focal plane. I then used a zigzag scan line (side length: 1 µm, displacement: 0.1 µm) to activate individual dendritic regions at the same speed as somatic stimulations, resulting in 10 epochs in 10 ms. Cells were stimulated 250 times in one run at 3 Hz; following each run, the stimulation positions were checked and readjusted if necessary. 3 to 6 runs were performed per cell. Optical stimulation was controlled using MES software (Femtonics) running in MATLAB (MathWorks).

2.6 Paw movement monitoring in awake mice

For awake recordings, mice were first habituated to head-fixation over a 3-day period. The right forepaw was tethered to the holding platform so that it hung over the edge of the platform. A force-feedback movement sensor arm (Aurora Scientific, Dual-Mode Lever Arm Systems 300-C) was positioned underneath the paw. Contact was maintained between the sensor arm and the paw with a constant pressure throughout the recordings to provide an online monitor of movement. Paw movements were recorded and delivered alongside neuronal recordings at 20 kHz via an ITC18 board (Heka) under the command of IGOR-Pro (Wavemetrics) software (Zhao et al., 2016).

2.7 Histology

Mice were deeply anesthetized through an i.p. injection of urethane and transcardially perfused with 4 % paraformaldehyde (PFA). The brain was fixed in 4%-PFA overnight and stored in phosphate buffer. A VT1000 S vibrating microtome (Leica) was used to make 100 µm-thick coronal or tangential slices that were subsequently stained for cytochrome oxidase

and biocytin with a standard ABC kit (Vectastain) with DAB enhancement. Slices were mounted in Moviol and stored at 4°C until the stained neurons were reconstructed using NeuroLucida software (MicroBrightField). Putative GABAergic inhibitory interneurons were excluded from the dataset.

2.8 Analysis

2.8.1 Dataset inclusion parameters

Recorded neurons were included in the dataset only when they met specific parameters related to the health of the neuron and quality of the patch. If the average Downstate V_m was below -50 mV, the patch was considered not well sealed or the cell was considered unhealthy and excluded. At the beginning of each recording, a firing pattern was assessed by injecting 0.5 ms steps of current (-200, -100, +50, +100, +150, +200, +250 and +300 pA). Neurons which did not respond with action potentials (APs) to at least the +300-pA stimulus or whose APs reached peak amplitudes below -10 mV were excluded. Finally, only recordings with an access resistance below 60 MΩ were included in the dataset.

2.8.2 Datasets

Subcellular ChR2 stimulation results included data from the primary whisker and primary forepaw somatosensory cortexes. Because both regions produced similar results, the datasets were combined (Figure 17, Figure 19,Figure 20,Figure 21, and Figure 33). All experiments using awake mice were obtained from the primary somatosensory forepaw cortex. Part of the VPM stimulation dataset (Figure 23) has already been published (Jouhanneau et al., 2014); however, comparisons between Up- and Downstate responses have not been previously reported. Likewise, a subset of the monosynaptic connections used in the analysis shown in Figure 24 (a - c) was included in a previous analysis (Jouhanneau et al., 2015); however, the comparison of Down- and Upstate $_u$EPSPs has not been previously reported.

2.8.3 Peristimulus time histograms

Peristimulus time histograms (PSTHs) were computed in relation to the timing of spontaneous or evoked spikes from a cell in a window of -50 to 100 ms from the onset of the stimulus (at 0 ms). The bin width was 10 ms and AP counts per bin were displayed as

firing rates in action potentials per second (AP/s). A pre-stimulus window of 30 ms before the stimulus onset was taken as the value for baseline activity, and was compared to a post-stimulus window of the same length, which was interpreted as evoked activity.

2.8.4 Selection of Up- and Downstate

Subcellular responses were separated into responses during depolarized (Upstate) or hyperpolarized (Downstate) phases based on the pre-stimulus V_m. Typically, a histogram of the V_m was generated and the point equidistant from the two normally distributed curves over Down- and Upstates was taken as a reference to split the states. Sweeps falling into a ± 2 to ± 5 mV window surrounding the divide, or those sweeps with a standard deviation > 1.5 mV (as measured between the two windows -50 to -1 ms and +50 to +100 ms), were considered transition states and were removed from further analysis (Figure 7). In cases in which the V_m did not achieve clear bimodal distributions and in awake data, Down- or V_{hyp} and Upstate or V_{dep} thresholds were defined at a set distance from the most hyperpolarized value obtained in the sweep. All data were visually inspected to confirm the automatic sorting procedure. Those segments with spontaneously occurring APs were removed from further analysis.

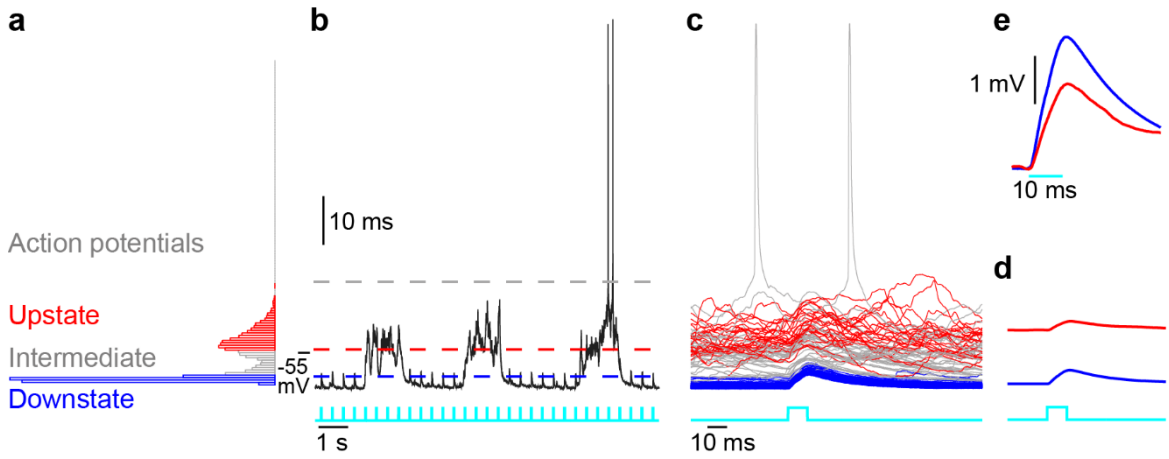

Figure 7. **Up- and Downstate selection and analysis.**
a. Histogram of spontaneous V_m distributions in a neuron recorded under urethane anesthesia (from **b**) and subdivided in Up- and Downstates according to the bimodal distribution; APs and intermediate states were excluded. **b**. Segment of the whole cell recording from which (**a**) was generated. Dashed lines extending from (**a**) show the Up/Down selection. Optogenetic stimuli were delivered (10 ms, 3 Hz) continuously during V_m oscillations. **c**. Segments cut around each of the optogenetic stimuli in (**b**) and overlapped along the time axis. Each of the segments is labeled as Up (red), Down (blue) or discarded (grey) according to (**a**). **d**. Averages of labeled Up and Down segments in (**c**). **e**. The same averages that appear in (**d**) overlapped on the V_m axis at stimulus onset, highlighting differences in response kinetics.

2.8.5 Amplitude measurements of subthreshold responses

The amplitudes of optogenetic potentials (OPs) were measured from the averaged response. The amplitude of a response was measured as the difference between the average V_m ± 0.5 ms centered on the peak time response and the 1 ms average of the V_m baseline (-1 to -2 ms before stimulus onset). Noise was calculated by randomly selecting a time point before the onset of the stimulus and measuring the V_m difference between the 1 ms average around each time point and the amplitude of the response. The latency of the stimulus was defined as the point at which two linear fits crossed: the first from -15 ms to -5 ms prior to the onset of the laser pulse, the second between time points corresponding to 20 to 80 % of the peak V_m response amplitude. The half width was calculated as the difference in time between 50 % of the rising phase and 50 % of the decay phase of the evoked response.

The signal to noise ratio was calculated by measuring the variance of OP amplitude and the background V_m variance -30 to -10 ms prior to the stimulus onset on each individual trial. Next the mean variance was calculated and the OP variance (signal) was divided by the background variance (noise). Response significance was assessed by bootstrapping analysis: individual trials comprising signal and noise values were randomly resampled with replacement up to 10,000 times; signal and noise normal distributions were compared and when distributions overlapped < 5 % the signal was considered significantly different from noise. Recordings whereby both Up- and Downstate responses were not significantly different from noise were excluded from the dataset.

2.8.6 Input resistance

-100 pA, 80 ms current pulses were injected via the recording pipette at 5.55 Hz. The V_m responses to the current pulses were then split into Up- and Downstates, as discussed above, then averaged. The access resistance was subtracted offline using an exponential fit of the V_m from a 2 ms period following the start of the injection of current (Zhao et al., 2016). The difference in V_m between the baseline and the time point at which the fit crossed the onset time of the injection of the current was taken as the access resistance. The input resistance was calculated from the difference in mV between the response to the injection of current, corrected for access resistance and the pre-stimulus V_m (Figure 8). Tau was calculated from the exponential fit of the relaxation phase of the V_m from 2 ms after the end of the hyperpolarizing pulse.

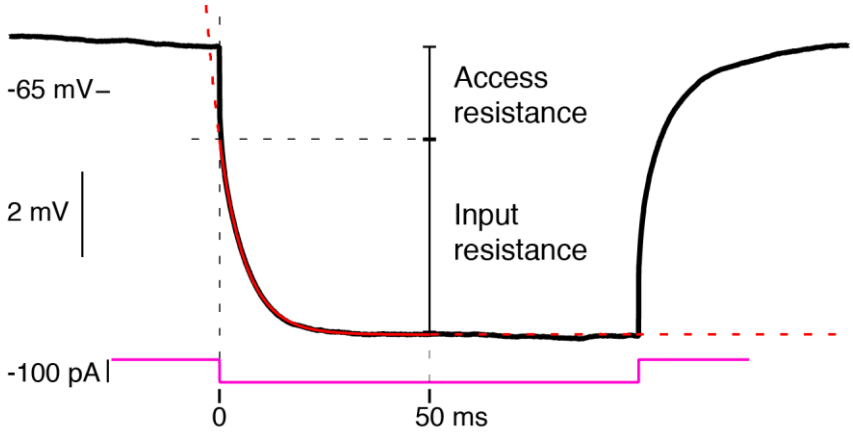

Figure 8. **Offline access resistance subtraction and input resistance calculation.**
In black: an average trace in Downstate of a train of negative current steps (magenta). In red: a single exponential fit between 2 and 50 ms. The point where the fit extrapolation (red dashed line) meets the onset line at 0 ms (black dashed) is taken as the reference to split the contributions of access and input resistance. The input resistance contribution to the V_m change is then converted in Ω following Ohm's law.

2.8.7 Isopotential

Trains of three positive current pulses lasting 500 ms were applied at five different intensities of current (+300 to +700 pA, ~0.5 Hz) to generate bursts of action potentials at similarly high frequencies (30 to 50 Hz) (Figure 9 a).

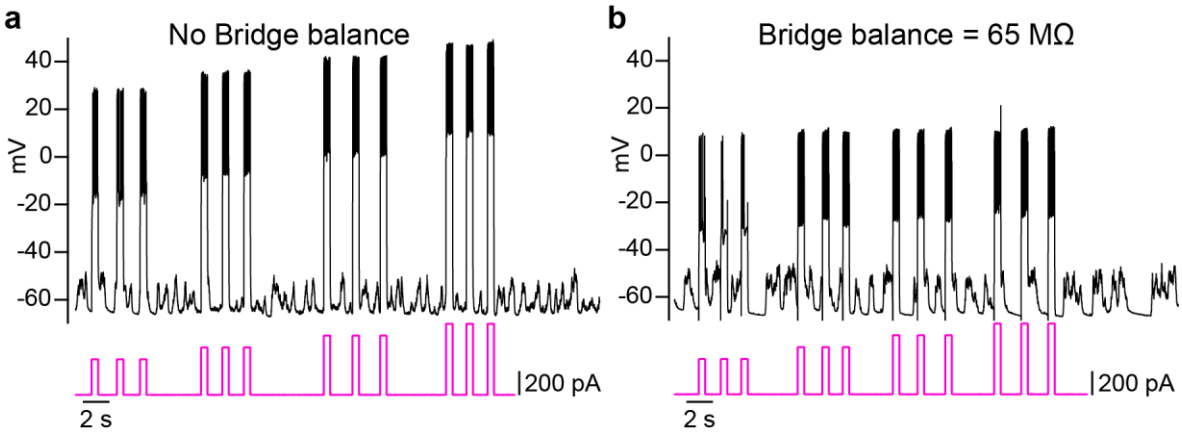

Figure 9. **Online access resistance assessment and correction with bridge balance.**
a. Trains of four different positive current pulses (magenta trace) produce similar action potential bursts but different V_m peak values due to access resistance. **b**. Pulse intensities identical to those in (**a**) but applying a bridge-balancing of 65 MΩ to correct for the access resistance effect. Access resistance was calculated from the difference in V_m peak values found in (**a**).

Peak action potential averages from the different current intensities were compared and any differences in peak V_m were considered to be caused only by the access resistance. Thus, the access resistance was calculated and the bridge balance was applied. The trains of pulses

were repeated until all averaged peak V_m rose and leveled off at the same value (Figure 9 b). Bridge-balanced positive currents were applied in steps of 3 s until the depolarization induced in the Downstate came closest to the mean Upstate V_m (Isopotential currents ranged from +150 to +300 pA).

2.8.8 Statistics

Custom-written scripts in IGOR-Pro (Wavemetrics) were used to analyze all data. Correlations between Downstate amplitudes and the ratio of Up:Down response amplitudes were made on the $\log_{10}$ of the Downstate amplitudes with Pearson's linear correlation. Correlations between ratios of Up:Down response amplitudes and stimulation site distances from the soma were calculated using Pearson's linear correlation.

The number of stimuli delivered in Upstates were 195 ± 113 soma anesthetized, 192 ± 105 basal anesthetized, 114 ± 52 basal awake, 204 ± 143 apical anesthetized, 106 ± 75 apical awake, 45 ± 12 VPM, 154 ± 93 basal QX-314.

Expected amplitude values in Upstates were calculated based on the change in pre-stimulus V_m, assuming a reversal potential of 0 mV for OPs and EPSPs based on the equation:

Equation 1. **Expected amplitude based on driving force difference due to V_m difference.**

$$\frac{(\text{Up Vm} - \text{Vrev})}{(\text{Down Vm} - \text{Vrev})} = \frac{\text{Up amplitude}}{\text{Down amplitude}}$$

Therefore:

$$\text{Expected Up amplitude} = \text{Down amplitude} \times \left(\frac{(\text{Up Vm} - \text{Vrev})}{(\text{Down Vm} - \text{Vrev})}\right)$$

For statistical analyses, were used two-tailed non-parametric tests. Paired data were tested using the Wilcoxon signed rank test and unpaired data using the Wilcoxon rank sum test. Normality was assessed with a Kolmogorov-Smirnov test. The data presented in the results and in figures show the mean ± standard deviation (S.D.)

3 RESULTS

The aim of this project is to study the integration of unitary excitatory post-synaptic potentials ($_u$EPSPs) in neocortical layer 2/3 pyramidal neurons *in vivo*. Since pyramidal neurons display an anatomical segregation, through which the basal and apical dendritic compartments receive different inputs, I wanted to examine whether a dendritic input arriving at the soma via the two branches is integrated in the same ways. Because *in vivo* neurons are constantly active, I investigate the contribution that cortical network activity in the brains of awake or anesthetized mammals makes to the dendrite-specific integration.

To address these goals I first needed to develop a method to stimulate discrete dendritic branches selectively and record the somatic subthreshold membrane potential *in vivo*. To achieve this, I combined the expression of Channelrhodopsin-2 (ChR2) in layer 2/3 pyramidal neurons (Berndt et al., 2011; Boyden et al., 2005; Nagel et al., 2003) with *in vivo* two-photon targeted recordings and two-photon laser scanned stimulations (Nikolenko et al., 2007; Packer et al., 2012; Prakash et al., 2012). This allowed me to generate spatially restricted inputs during different period of network activity.

3.1 Development of Channelrhodopsin-2 expression and two-photon optogenetic stimulation

To develop a method for the two-photon light stimulation of subcellular structures of neurons *in vivo*, the first step was to achieve a specific, strong expression of ChR2 in pyramidal layer 2/3 cortical neurons in the primary somatosensory cortex of juvenile (P20-P50) C57bl/6 mice.

Different neuron transfection techniques were tested at the start of the project, including viral infection and *in vivo* single cell electroporation. I additionally used several variants of the light-gated channel: ChR2(H134R), (E123T-T159C), (T159C) and C1V1(tt). To target expression to excitatory pyramidal neurons, I used CamKII$_\alpha$ as a gene promoter (Jones et al., 1994; Liu and Jones, 1996).

3.1.1 Single cell electroporation

In vivo two-photon guided single cell electroporation is a technique that permits high labeling specificity via targeting a single neuron for gene expression (Judkewitz et al., 2009). Animals can be used more easily in their desired age for recordings, since expression occurs within 1 to 3 days. Because there is no background noise from EYFP emission from other cells, this facilitates the two-photon targeted patch method (Figure 10), and two-photon subcellular stimulation is more specific.

Single cell electroporation consists of two steps: in the first, the mouse is prepared as for *in vivo* recordings but without a durectomy (Paragraphs 2.2.1, 2.3). The *in vivo* shadowpatch (Paragraph 2.4) is used to target neurons and the plasmidic vector is delivered via a short electrical stimulus. In most cases I electroporated 2 to 20 neurons. The proteins are left for 1 to 3 days to attain sufficient levels of expression meanwhile an agarose layer protects the craniotomy. In the second step, the durectomy is performed and neurons expressing the protein can be re-approached for recordings and optostimulation (Judkewitz et al., 2009). In successful experiments, 1 to 7 neurons were labeled with ChR2-EYFP and targeted one after the other until one successful patch was achieved. The identification of neurons was straightforward and the dendritic projections easy to attribute to their somatic origin. In isolated neurons, the specificity of stimulation was guaranteed.

93 electroporated neurons were successfully patched in 160 animals with the plasmids pAAV-CamKII-ChR2(HR)-EYFP and pAAV-CamKII-ChR2(ET/TC)-p2A-EYFP. Transfected cells showed pyramidal physiological features even though very frequently neurons displayed slightly depolarized resting potentials, with an average Downstate V_m below -50 mV. The range of responses to the two-photon stimuli on the soma was 0.5–2 mV, while responses from proximal dendritic compartments were below 0.2 mV and absent when stimulating distal branches, even at the highest laser powers.

During the time between electroporation and patching, a large craniotomy has to hold up without major tissue reactions for two days. Depending on the deviation from perfect conditions, the physiology of the neurons will be accordingly unhealthy. Single cell electroporation surgery often led to an inflamed dura and difficulties in patching infected neurons. This made the completion of the experiment extremely difficult and thus the technique inappropriate to produce the large dataset required for this project. Another problem was weak ChR2 expression in dendrites, which did not permit an elicitation of depolarizing potentials from distal dendrites. Moreover, often after the second day of

expression clusters of protein started to form blebs on the dendrites which probably interfered with the physiological propagation of dendritic synaptic input.

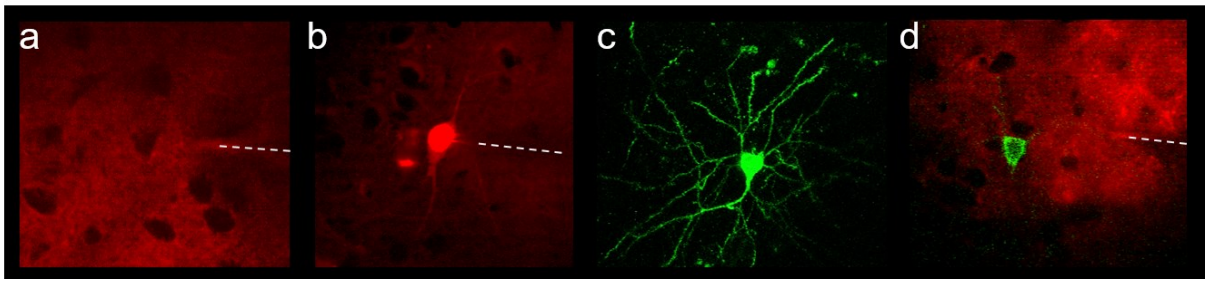

Figure 10. ***In vivo* two-photon guided single cell electroporation.**
The four steps of single cell electroporation are illustrated. **a**. Approach of the cell to be electroporated, visualized with the shadowpatch method with the *dura mater* still present. **b**. The same neuron just after electroporation. **c**. The same neuron 48 hours later and after durectomy, visualized in the green channel to show the ChR2-EYFP expression. **d**. The same neuron during approach, just before patch clamp. The dashed line indicates the pipette.

3.1.2 Viral expression of ChR2

In contrast to transfection by electroporation, viral transduction exploits the viral machinery to enter the cell and bring the coding sequence into the nucleus. This reduces the transfection shock, thus increasing the survival rates and health of neurons. With electroporation, the DNA plasmids are delivered into the neural cytoplasm, and over time they are destroyed by the cell, causing the expression curve to be highest after 2–3 days and then to decrease after one week (Kitamura et al., 2008). Viral vectors incorporate the sequence into the cell genome as lentiviruses do (Naldini et al., 1996) or bring the plasmid into the nucleus, as adeno-associated viruses (AAV) do, preventing plasmid destruction. This causes a rise in expression and the protein accumulates in cells, reaching its peak concentration up to 4–6 weeks after infection, after which it virtually never declines (Herzog, 2007; Nathwani et al., 2011). AAVs, moreover, produce neither toxicity effects nor an immune response (Nathwani et al., 2011).

Viral infections with a simple promoter, on the other hand, do not produce sparse labeling and, in the region of highest expression, nearly all pyramidal neurons are labeled. ChR2-EYFP is a membrane fusion protein; since the soma of the neuron is the region with the lowest surface-to-volume ratio, it is also the region with the lowest relative apparent expression. This makes the neuronal soma, which is the target to approach and patch, almost impossible to visualize when surrounded by the membranous and thus much brighter neuronal projections from neighboring cells (Figure 11 a). To overcome this issue, I moved

away from using the ChR2-EYFP fusion membrane protein to a monocistronic construct that exploits the 9-amino-acid picornavirus p2A motif. This acts as a ribosome-skipping site that produces two separate proteins with a single promoter (Gradinaru et al., 2010; Osborn et al., 2005; Prakash et al., 2012). The result is to express ChR2 as a membrane protein and EYFP in its soluble cytoplasmic version. This has a triple advantage: it makes the more voluminous cell soma brighter, so that it can be approached more easily under the two-photon (Figure 11 c); the not-fused ChR2 is more effective; and neurons do not have to deal with this protein cluster, which preserves their health (Prakash et al., 2012).

AAVs proved capable of delivering stronger and more reliable expression levels than lentiviruses. The larger area of AAV spread (Figure 11 d) ensured that the target region in the somatosensory cortex, which was identified by an intrinsic imaging sensory signal (Paragraph 2.1.1, Figure 6), always expressed ChR2, thereby increasing the throughput rate of experiments. I tested AAV2/2, AAV2/5 and AAV2/9; the latter, as suggested by the literature (Aschauer et al., 2013), produced the best results in neocortical infections. AAV2/9 was used as the ChR2 transfection vector for the rest of the project.

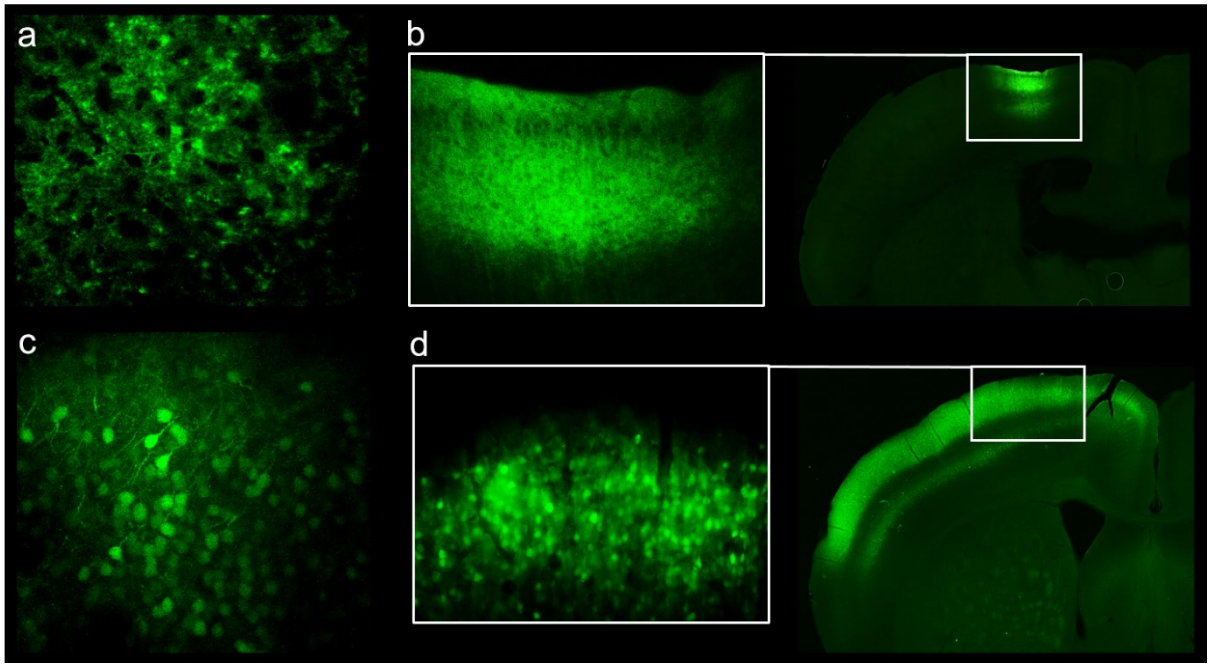

Figure 11. **Cortical viral infections of ChR2-EYFP.**
a. *In vivo* Z-stack of layer 2/3 in mouse infected (Paragraph 2.2.2) with lentivirus carrying the fusion ChR2-EYFP; somas are indistinguishable from the background. **b**. Same animal as in (**a**) but coronal slice, highlighting the small infection region of Lentivirus. **c**. As in (**a**) but in a mouse infected with AAV2/9, carrying the ChR2-p2A-EYFP spliced version; cytoplasmic EYFP expression brightens the soma against the background. **d**. Same as in **b** but for mouse depicted in **c**; AAV infectivity is higher and the area of spread is much larger than for the lentivirus.

3.1.3 Testing different channelrhodopsin-2 variants

The first ChR2 variant I tested was ChR2(H134R), used in the lentivirus construct pLenti-CamKIIa-ChR2(HR)-GFP. Protein expression from the lentiviral vector was dissatisfying and the area of spread was too small (Figure 11 b). As a result, specific cells had to be selected based on ChR2 expression rather than their position in the target somatosensory area. Moreover, even strongly expressing neurons did not respond well enough to two-photon stimuli. The same ChR2 variant in the AAV2/5 vector pAAV-CamKIIa-ChR2(H134R)-EYFP showed stronger expression and larger infected area. Nevertheless, the visibility issues shown in Figure 11 a made it unusable for *in vivo* patch clamps.

Of the p2A constructs in AAV2/9 I first tried the ChR2 variant E123T-T159C (ET-TC) and C1V1(tt). Of the two, ET-TC produced the best responses. Even though other labs (Packer et al., 2012; Prakash et al., 2012) had better results with C1V1, because of its longer wavelength of excitation (1040 nm), we were using a Chameleon Ultra II (Coherent) that did not generate enough power at wavelengths longer than 1000 nm, so I could produce only weak stimulations. The ET-TC variant expressed with AAV2/9 was the first with which I was able to produce responses that differed significantly enough from noise (average depolarization > 0.2 mV) even in distal thin dendrites, using powers at 25 mW or lower, which were necessary to avoid damaging the neurons.

A good predictor of dendritic response to light stimulations is the somatic responsivity (Paragraph 2.5). When average responses to spiral two-photon somatic stimulations delivered at 25 mW are smaller than 1.5 mV, then distal (> 30 μm from soma) dendritic stimulation is probably not achievable (Figure 12 a). Since expression from viral transduction increases with time, the animals start to be usable in the 3rd week after infection (Figure 12 a). Unfortunately, a negative side effect emerged from high levels of expression of the ET-TC variant. In fact, I noted a positive correlation between the expression time and the resting membrane potential of neurons (Figure 12 b), as neurons expressed for longer they became more depolarized.

This could be explained either through a protein accumulation effect, which changes the properties of the neuronal membrane (Zimmermann et al., 2008), or with the opening of channels, which occurred also without light stimulation. In fact, shining light on ChR2 only increases the probability that the protein moves from a closed to open configuration during in its photocycle (Nikolic et al., 2009). Nevertheless, even in the dark, a fraction of channels

stochastically switches configurations for a short time, and with high expression levels, this might lead to a constant depolarization of the resting V_m.

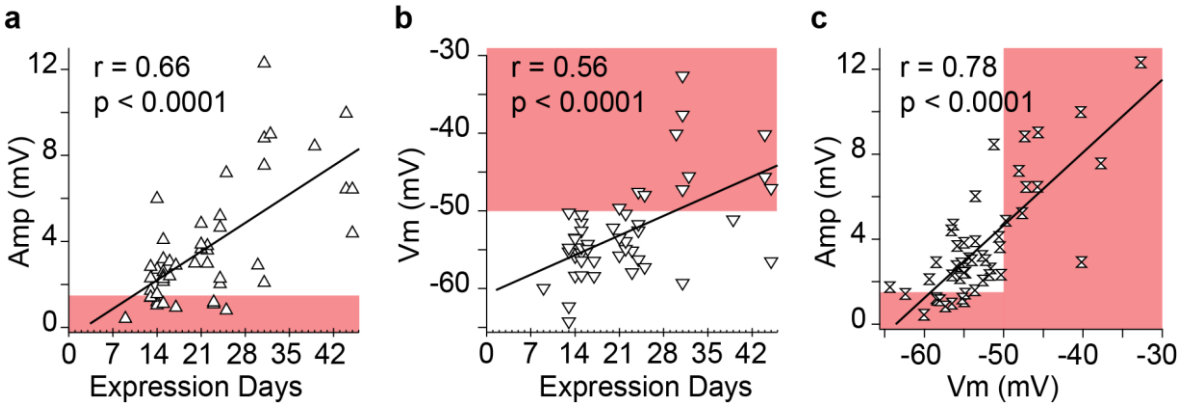

Figure 12. **Channelrhodopsin2 (ET-TC) expression effect on neuronal physiology.** **a**. Graph plotting days of expression versus amplitude of response to two-photon somatic stimulation at maximum usable power (25 mW). Cells responding too weakly to be usable: < 1.5 mV in amplitude (in red area). **b**. The same neurons but plotted against the average resting downstate V_m. Neurons too depolarized to be included > -50 mV in Downstate are represented in the red area. **c**. Same data as in (**a** and **b**) but now showing the response amplitude versus the resting V_m, highlighting the correlation between the two. Neurons excluded for weak response or depolarization appear in the red area. On each graph "r" is the value of the Pearson's linear correlation, also expressed as a linear regression fit (black line).

Either way, the depolarization correlates very strongly with the response levels (Figure 12 c), and neurons with a resting V_m in Downstate > -50 mV are probably in an unphysiological state and were thus excluded from this study (Paragraph 2.8.1). Consequently, the need for high expression to achieve good responses conflicted with the need to keep neurons healthy. This made the success rate of experiments dependent on a narrowed window of usable neurons (Figure 12 c).

Fortunately, another variant (T159C), here termed ChR2(TC), did not exhibit this side effect. Even with very high levels of expression six weeks after the infection, I did not observe any correlation with the depolarized resting V_m (data not shown). Moreover, among the variants tested here, ChR2(TC) has been reported to produce larger currents and to have a reversing potential closer to 0 mV (Berndt et al., 2011), thus making it similar to glutamate reversal (McBain and Mayer, 1994). The T159C variant has a voltage-dependent response (Berndt et al., 2011). However, this did not compromise its use, as it showed similar state dependent modulation as a voltage-independent variant ET/TC (Figure 18).

Almost all the following data reported in this project (~ 89.5 %) were collected with neurons infected with AAV2/9-CamKIIa-ChR2(TC)-p2A-EYFP (102 cells), with only a few

neurons expressing the ET-TC variant (12 cells). Recordings were performed 3 to 5 weeks after infection.

3.2 Targeted two-photon subcellular stimulation

The goal of this project was to mimic EPSPs by eliciting a brief membrane depolarization generated with a photocurrent on a controlled dendritic spot, while simultaneously making recordings at the soma (Paragraphs 2.4, 2.5). The fast scanning system used to deliver photostimulation and the software to control it (MES written in Matlab) was developed by Femtonics and embedded in their two-photon setup. I adjusted several features of the system to bring the stimulation parameters to the optimal characteristics they need with the goal of mimicking EPSPs.

The path followed by the scan during the stimulation can be completely customized in shape and movement velocity: spirals, X-shaped and squared zigzags can be of any size and line spacing. To be consistent with stimulations across cells, I finally decided on a spiral path of 8 μm diagonal and 0.5 μm spacing for somatic stimulations and a squared zigzag of 1 μm side and 0.1 spacing for any dendritic target. Even though dendrites' diameters are highly variable, I always chose to use the same 1 × 1 μm path to maintain a consistent stimulation parameter across the dataset. Since the lateral span of the two-photon beam is around 1 μm (Denk et al., 1990; Rickgauer and Tank, 2009), the main purpose of the zigzag fast movement was to reduce photodamage to the dendrite.

I kept the dwell time the same across these two stimulation parameters with a constant speed of 19 μm/ms, which proved to deliver a good photocurrent without introducing photo damage. For single cell electroporation, I delivered stimulations of 15 ms each, but after moving to AAVs, I reduced it to 10 ms to elicit potentials with shorter kinetics that more closely resembled $_{u}$EPSPs. 5 ms stimulations did not improve the kinetics any further; therefore, I stayed with 10 ms stimulations, with which I was able to obtain responses at higher distances from the soma.

I tested the two-photon scanned stimulations for their specificity in eliciting a brief depolarization, or optogenetic potential (OP), on the subcellular target. To be certain that I was measuring the response of ChR2 and not neuronal or tissue responses to intense light, I first stimulated non-expressing neurons *in vivo*. As expected, somatic stimulations on wild type (WT) (Figure 13 a, b) and EYFP- only expressing neurons (Figure 13 c, d) did not elicit a depolarizing response.

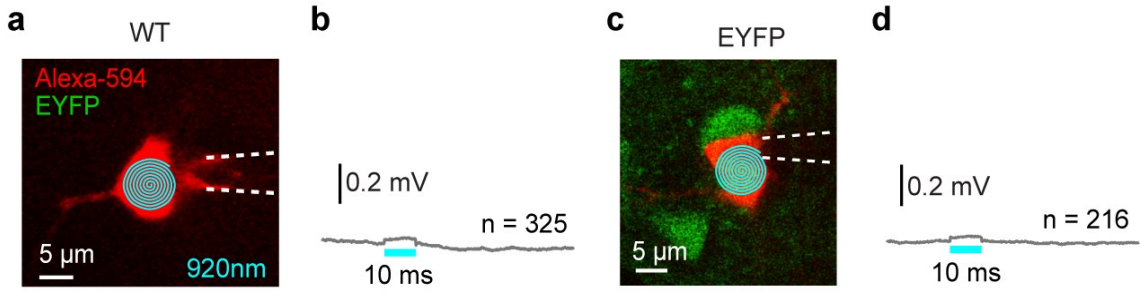

Figure 13. **Two-photon stimulation of ChR2-non expressing neocortical pyramidal neurons *in vivo*.**
a. Two-photon image of somatic laser scanned stimulation during recording of a WT layer 2/3 pyramidal neuron. **b**. The corresponding averaged somatic response, showing no OP in Downstates. **c**. and **d.** Same procedure as for (**a** and **b**), but for a cortical neuron expressing EYFP without ChR2. (n) number of sweeps. Dashed lines indicate the pipette.

The two-photon scanned stimulation has already been proven to be spatially specific (Packer et al., 2012; Prakash et al., 2012; Rickgauer and Tank, 2009) and suitable for subcellular stimulations *in vivo*. To examine this under my experimental conditions I recorded somatic or dendritic responses while moving the center of the stimulation in 10 and 5 µm steps respectively away from the On target (Figure 14 a, e).

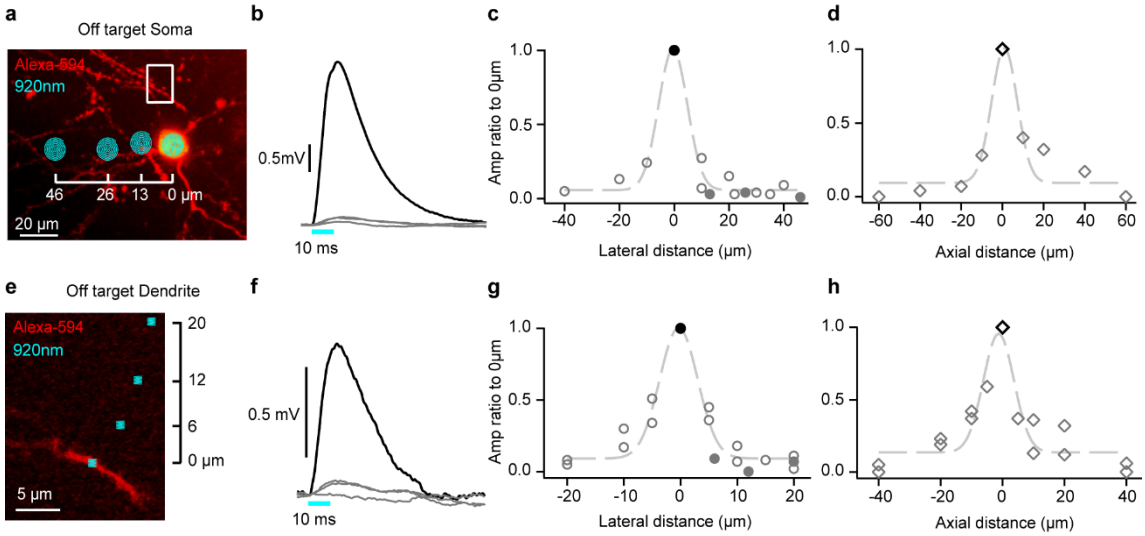

Figure 14. **Off target two-photon stimulation of ChR2 expressing neurons.**
a. *In vivo* image showing On and Off target somatic stimulation spots at the same axial depth but different lateral distances from the soma. **b**. The corresponding somatic averaged OP from the neuron shown in (**a**), with responses to On (black) and Off (greys) target stimuli. **c**. Plot of the OP amplitude normalized to the amplitude over the soma (0 µm, black filled circle); closed circles show examples shown in **b**; open circles show examples from off target stimulation in 3 other neurons. **d**. same as (**c**) but keeping the same lateral position and varying the axial distance. **e.** - **h.** Same as (**a** - **d**) but for dendritic stimulation.

The ratios of Off:On responses showed a steep decrease already at 5–10 µm distance from the center, either moving laterally or axially (Figure 14 b - d, f - h). Overall, the two-photon laser proved to have a spatial specificity in line with similar studies (Prakash et al., 2012).

Since in cortical layer 2/3 the neuronal density is quite high, this result ensured that OPs recorded were not the result of EPSPs from indirect activation of neighboring neurons. In addition, it was important to define the distances from the recording site and the anatomical features of the target subcellular spot under stimulation.

After assessing the location specificity of stimulation, I tested the stimulation temporal parameters. The wavelength of single-photon light stimulation known to generate the largest current flow through ChR2 is around 470–490 nm (Berndt et al., 2011; Rickgauer and Tank, 2009), nevertheless the two-photon effect changes the wavelengths of stimulation in a nonlinear way. The most suitable wavelength of stimulation according to various studies (Andrasfalvy et al., 2010; Rickgauer and Tank, 2009) may vary between 880 and 940 nm depending on the ChR2 variant and laser type. I tested the response across wavelengths between 740 and 1000 nm in 2 cells, maintaining the same power of 12 mW beyond the objective (Figure 15 a, b) and found the most suitable wavelength to be 920 nm. All of the subsequent stimulations in this work were delivered at 920 nm.

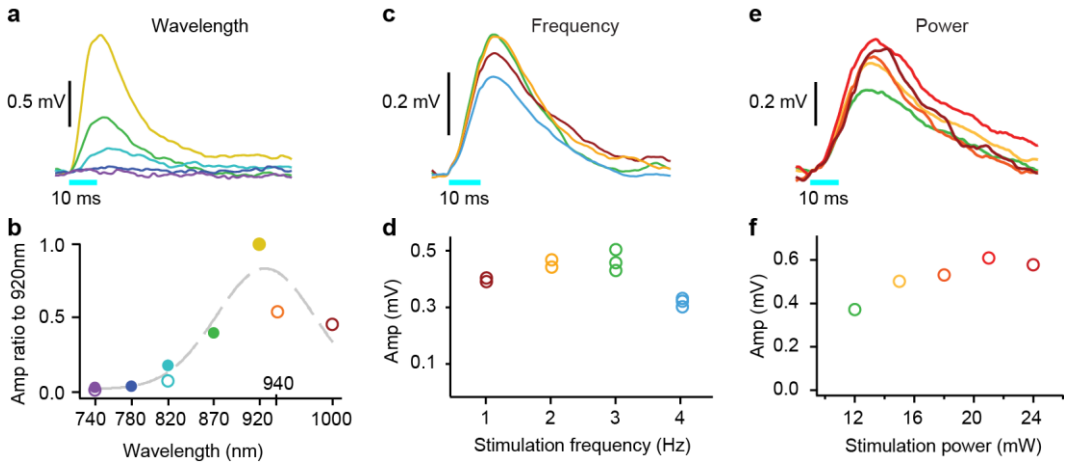

Figure 15. **Two-photon stimulation parameters of ChR2-expressing neocortical pyramidal neurons *in vivo*.**
a. Mean membrane potential (V_m) response to 10 ms somatic spiral optogenetic stimulation (cyan bar) at different excitation wavelengths from a sample neuron; colors correspond to closed circles in (**b**). **b**. The ratio of the measured OP amplitude relative to the response at 920 nm from the same neuron; open circles represent OPs from the neuron not shown in (**a**). **c**. Same procedure as (**a**) using different frequencies of stimulation; colors correspond to frequencies used in (**d**). **d**. Mean OP amplitudes at frequencies from 1 to 4 Hz from a sample neuron; open circles show the mean from different intermingled trials with a randomized order of frequencies in the same neuron. **e**.

Same as (**a**) but using different laser powers for stimulation; Colors correspond to powers used in (**f**). **f**. Mean OP amplitudes at powers from 12 to 24 mW from a sample neuron.

Whole-cell recordings in awake animals are frequently difficult to maintain for long periods. Furthermore, the longer the neuron is in contact with the artificial intracellular solution, the less physiological its activity will be. To obtain significant mean responses during periods of synaptic background activity, I needed to repeat the stimuli on the same subcellular spot as many times as possible, but without causing the response itself to adapt. I compared the average response to stimuli delivered with frequencies from 1 to 4 Hz in the same cell (Figure 15 c, d) and found 3 Hz to be the highest frequency that was non-susceptible to adaptation. I maintained the stimulation at 3 Hz for the rest of the experiments.

Because cells and subcellular targets lie at different depths and different tissue densities lie between the spot and the objective, I could not precisely determine the laser power delivered on each target spot I stimulated. Thus, I used the power directly below the objective as an approximation reference. Depending on the response size, which dependeds on both ChR2 expression and the visibility of the target, I adjusted the power of the stimulations to a range between 12 and 25 mW (Figure 15 e, f). For each target, the stimulation power was held constant.

3.3 Optostimuli influence on spontaneous spiking activity

Since I wanted to study the integration of subthreshold inputs, I first had to ensure the OPs do not elicit action potentials in any of the subcellular regions of stimulation.

Visually targeted recordings were made from pyramidal neurons at a depth of 114.5 ± 22.9 μm, n = 114, using whole-cell pipettes filled with intracellular solution and Alexa 594. I took care to search for cells with reduced laser power (Paragraph 2.4) and observed a normal mean resting membrane potential of (-58.65 ± 4.67 mV, n = 114). *In vivo* images and post-hoc biocytin stainings (in a subset of cells) confirmed that the recordings were made from excitatory pyramidal neurons. I used the intracellular Alexa-594 stain to target two-photon subcellular optogenetic stimulation to three cellular compartments: the soma and apical and basal dendrites. I replicated this dataset in animals anesthetized with urethane and awake resting mice.

Across all the datasets that were analyzed (123 targeted subcellular spots in 96 cells, Figure 16), the OP influenced the spontaneous suprathreshold activity only in 5 recordings. In these cases there was a significant difference between pre- and post-stimulus activity; in

3 cases I observed an increase and in 2 a diminishment. On a population level, only basal stimulations made in awake animals showed a significant increase (Figure 16 l); but on individual cells level, only one out of 11 neurons increased significantly. I can therefore rule out that the two-photon stimulations elicited action potentials. At this point, I decided hence to focus exclusively on subthreshold activity, and excluded suprathreshold activity from analysis (Figure 7).

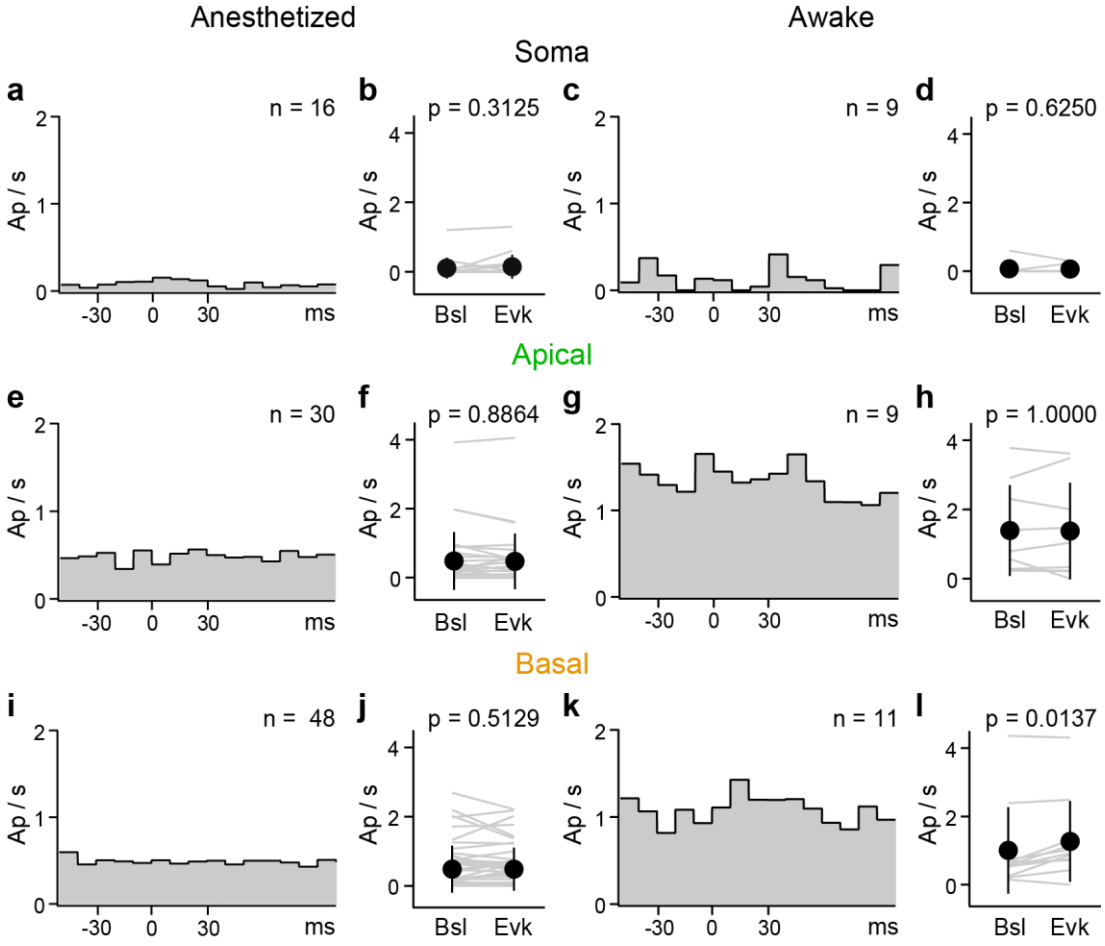

Figure 16. **Two-photon optogenetic stimulation did not trigger action potentials.**
a. Averaged peristimulus time histogram (PSTH) (Paragraph 2.8.3) of somatic two-photon stimulations in anesthetized mice. Action potentials per second (Ap/s) in 10 ms bins. **b**. Averaged action potential baseline (Bsl), calculated by averaging responses within 30 ms prior stimulation and evoked (Evk), 30 ms after, as highlighted in (**a**). **c**., **d**. Same as (**a**, **b**) but on awake recordings. **e. - h.** Same as (**a - d**) but for apical stimulations. **i. - l.** Same as (**a - d**) but for basal stimulations. OPs did not increase the spiking activity; as for (**k**) there were significant differences in population data but differences in only 1 out of 11 of the single examples. Grey lines show data from individual cells; the filled circles with bars represent the mean ± S.D..

3.4 Brain states in anesthetized mice

The first part of the work was carried out on urethane-anesthetized animals. Urethane anesthesia has been reported to produce its effects by potentiating the functions of neuronal nicotinic acetylcholine, $GABA_A$ and glycine receptors and inhibiting NMDA and AMPA receptors (Hara and Harris, 2002). Urethane alters neither excitatory nor inhibitory synaptic transmission and only minimally disrupts signal transmission in the neocortex (Sceniak, 2006). Under urethane anesthesia, the V_m of cortical neurons undergoes a bimodal distribution (Figure 7 a, b) that closely resembles natural slow-wave sleep oscillations (Clement et al., 2008). These slow cortically synchronized oscillations alternate between two periods of network activity called Down- and Upstate (Steriade et al., 1993).

Downstates are silent periods of low synaptic input that display a hyperpolarized stable V_m with low variability, very closely resembling the silent network situation that can be found in *in vitro* preparations, such as acute brain slices. Inversely, Upstates are periods of synchronized neuronal activity in which neurons receive a high amount of excitatory and inhibitory synaptic input. The V_m displays high variability and is more depolarized and neurons can fire spontaneous action potentials. The Upstates resemble, on the contrary, the brain activity that occurs in intact brains of living animals during periods of wakefulness (Paragraphs 1.3.1, 1.3.2, Figure 5). Hence, in *in vivo* anesthetized recordings, the spontaneous alternation of the two states provides an opportunity to measure how the same controlled stimulus will be computed under these different conditions.

The V_m distribution presented some variance of basic parameters such as subthreshold oscillation frequencies and amplitude and suprathreshold firing frequencies as a function of several conditions: the level of anesthesia, whether the recording was performed early or late after the onset of anesthetization, the quality of the recording and the recording period. Under deeper anesthesia neurons tended to be more hyperpolarized, with shorter and less frequent Upstate periods, and APs were generated very rarely. The same parameters increased, however, under lower levels of anesthesia. Soon after the patch clamp, the neurons were also more hyperpolarized, with shorter and less frequent Upstates and low firing rates which tended to increase later in the recording. This was most likely due to changes in the level of anesthetization. The quality of the patch influenced the mean V_m and the amplitude of sub- and suprathreshold oscillations, with well sealed patches displaying a lower access resistance and a more hyperpolarized mean V_m, as well as ampler oscillations and lower firing rates. I took care to include neurons with stable and high quality intrinsic parameters in the dataset.

3.5 Somatic responses Down- vs. Upstate

After a successful patch was achieved in urethane-anesthetized mice, I observed a normal resting membrane potential of neurons (-58.59 ± 4.89 mV, n = 76). I then stimulated the soma of ChR2-expressing pyramidal neurons with brief (10 ms) spiral stimuli (Figure 17 b) delivered at 3 Hz (Figure 17 c, Paragraph 2.5). The somatic responses ($_{soma}$OP) provided not only a first readout of the responsiveness of a ChR2-expressing cell to light stimuli, but a baseline from the response kinetics, which was important to consider when studying the network activity effect on neuronal ChR2 activation.

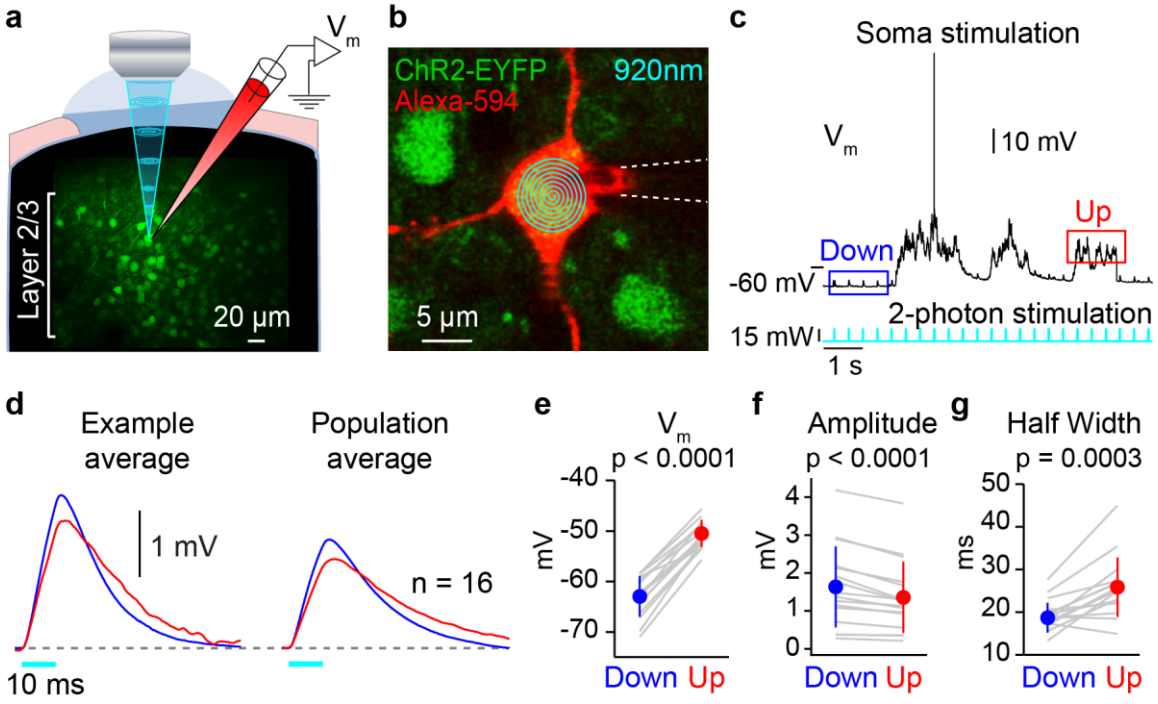

Figure 17. **Modulation of somatic two-photon evoked response amplitude in ChR2 expressing layer 2/3 pyramidal neurons**.
a. Cartoon showing two-photon laser stimulation of ChR2-EYFP expressing neurons. **b**. Example *in vivo* image showing the path of two-photon stimulation (cyan) on the soma of a ChR2-expressing neuron during a whole-cell recording. **c**. Sample membrane potential (V_m) recording of a layer 2/3 cortical neuron under urethane anesthesia, showing small depolarizations (optogenetic potentials, OPs) in response to the laser stimulation (cyan) during hyperpolarized Downstates (blue) and depolarized Upstates (red). **d**. Overlaid, average OPs to somatic stimulation from an example neuron (left) and from the entire population (right) of n = 16 neurons, during Downstate (blue) and Upstate (red). **e**. Somatic V_m increases as neurons go from Down- to Up-state. Grey lines show data from individual cells; the filled circles with bars show the mean ± S.D.. **f**. $_{Soma}$OP amplitude is significantly lower in Upstates than during Downstates. **g**. The half width is significantly prolonged in Upstates in comparison to Downstates.

Somatic stimulation reliably triggered depolarizing optogenetic potentials with a Downstate onset latency of 0.63 ± 0.23 ms. This indicated a direct response to the optical

stimulation, and a rise time of 5.36 ± 0.59 ms, a peak time of 11.97 ± 0.92 ms, half width 19.31 ± 3.49 ms and decay time 18.38 ± 4.27 ms.

I next split and averaged the $_{soma}$OPs into Up- and Downstate responses based on their pre-stimulus V_m (Paragraph 2.8.4, Figure 7) (Down -62.94 ± 4.02 mV vs. Up -51.01 ± 2.69 mV, n = 16, $p < 0.0001$). The $_{soma}$OP amplitude was significantly smaller in Up- than Downstate (Down 1.62 ± 1.02 mV vs. Up 1.34 ± 0.93 mV, n = 16, $p < 0.0001$) (Figure 17 d - f), as expected from the reduction in driving force during depolarized Upstates (Up 1.34 ± 0.93 mV vs. Expected 1.33 ± 0.88, n = 16, p = 0.4637).

The driving force represents the flow of ions passing through open channels and is directly proportional to the difference between the V_m and the V_{rev} of the channel that is involved. ChR2 is a non-selective cation channel with a V_{rev} close to 0 mV. Since in Upstate the average V_m is relatively closer to 0 mV than the average Downstate V_m, the amplitude of OPs is proportionally attenuated by the difference in driving force between the states. Thus, in this study the expected amplitude reduction refers to this driving force effect, calculated as detailed (Paragraph 2.8.8, Equation 1).

However, I observed that the half width of the $_{soma}$OP was significantly longer in Upstates than in Downstates, indicating a slower decay of the OP during network activity (Down 19.31 ± 3.49 ms vs. Up 25.85 ± 6.96 ms, n = 16, p = 0.0003) (Figure 17 d, g) and suggesting an increase in the input resistance of neurons during Upstates.

Although Upstates are regarded as high-conductance states (Destexhe et al., 2003), an increase in input resistance has been reported in L2/3 pyramidal neurons during Upstates (Mateo et al., 2011; Waters and Helmchen, 2006). Such increase reduces transmembrane conductance and prolongs the membrane time constant, which likely directly affects the kinetics of potentials.

Control somatic stimulations of pyramidal neurons expressing the ChR2 subtype ET-TC, which has been reported to have no voltage dependent change in kinetics (Berndt et al., 2011), showed a similar reduction in amplitude and broadening during Upstates (Figure 18).

Because there is no voltage-dependent difference between the responses of the two variants, and the voltage-independent variant also showed a prolongation of kinetics during Upstates, this confirms that the kinetics prolongation is indeed due to changes in the neuronal membrane properties and not to intrinsic features of ChR2(TC) itself.

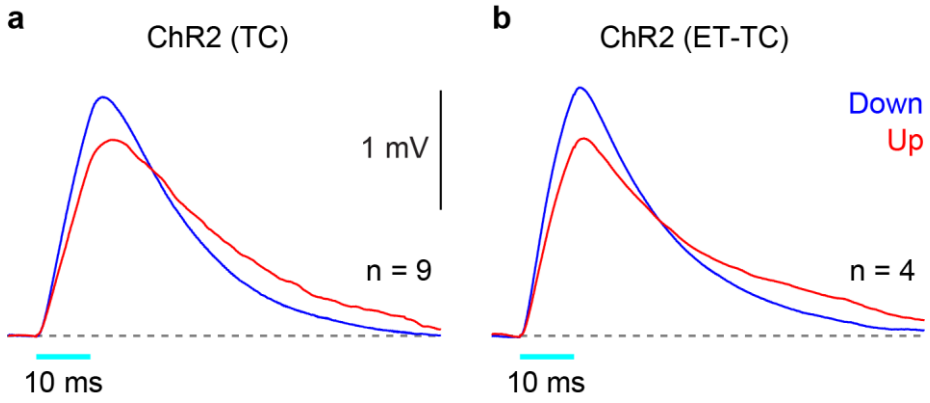

Figure 18. **Slower kinetics in Upstates in two different ChR2 variants.**
a. Overlaid, average light-evoked OPs to somatic stimulation from a population of (n = 9) neurons during Downstates (blue) and Upstates (red) expressing the ChR2 variant T159C (TC) that was mostly used in this work. **b**. Same as (**a**) but from a population of (n = 4) neurons expressing the ChR2 variant E123T-T159C (ET-TC). The variants present similar reductions of $_{soma}$OP amplitude and prolonged kinetics during Upstates.

3.6 Dendritically evoked optogenetic potentials during Downstates

Pyramidal neurons receive EPSPs through an activation of glutamatergic receptors expressed predominantly on dendritic spines (Colonnier, 1968) (Paragraph 1.2). The distribution of spiny excitatory synapses is non-random and spines are arranged all along dendritic regions with a distinct distribution profile. Spines are not present on soma, axon and perisomatic regions (DeFelipe and Fariñas, 1992; Larkman, 1991). Since the aim of this study was to simulate EPSPs, I took care in choosing stimulation sites that would conform to locations associated with excitatory inputs. I therefore generated optical stimuli with a small diameter laser spot (1 µm^2) on apical and basal dendritic branches between 15 and 135 µm from the soma (apical 72.36 ± 35.55 µm n = 30, basal 45.58 ± 21.38 µm n = 48, Figure 19), using the Alexa594 signal to target the stimulation site.

In the somatosensory cortex, pyramidal neurons of layer 2/3 express AMPA and NMDA glutamatergic receptors on their postsynaptic excitatory terminals. AMPA and NMDA are both selective for Na^+ and K^+; NMDA is also selective to Ca^{2+}. Upon glutamate activation, the receptors produce a depolarization with a similar reversal potential tending to 0 mV. Since NMDA is less abundant and its activation also depends on voltage (McBain and Mayer, 1994), an average EPSP releases a Na^+–K^+ flow with a small Ca^{2+} component, responsible for a depolarization with a particularly fast inactivation (Markram et al., 1997). Ultimately, this produces a depolarizing potential curve with specific features in terms of time and amplitude (Jouhanneau et al., 2015; Markram et al., 1997). Even though ChR2

belongs to a completely different family of proteins, it is a cationic selective channel, for Na^+, K^+ and to a minor extent Ca^{2+} (Nagel et al., 2003) (Paragraph 1.5.2). Upon light stimulation, it generates a depolarization with a reversal potential close to 0 mV (Berndt et al., 2011) and kinetics that are slightly slower than those of AMPA receptors but otherwise similar.

The stimulation of apical and basal dendrites evoked OPs ($_{apical}$OPs and $_{basal}$OP) with similar kinetics in Downstates (Apical rise time 6.32 ± 2.14 ms, basal 5.32 ± 0.83 ms; apical peak time 14.50 ± 2.96 ms, basal 13.48 ± 2.39 ms; apical half width 21.97 ± 6.61 ms, basal 19.67 ± 3.94 ms and apical decay time 23.57 ± 15.96 ms, basal 23.70 ± 12.46 ms). The latency of stimulation (Apical 1.74 ± 0.65 ms, basal 1.58 ± 0.67 ms) was correlated with the distance from the soma in both apical and basal dendritic stimulation (Figure 19 c, d). With an averaged propagation velocity of 61.5 ± 14.7 µm × ms^{-1} for apical inputs and 44.9 ± 10.2 µm × ms^{-1} for basal inputs, which is in the range of conduction velocities reported in the literature (Agmon-Snir and Segev, 1993; Nevian et al., 2007).

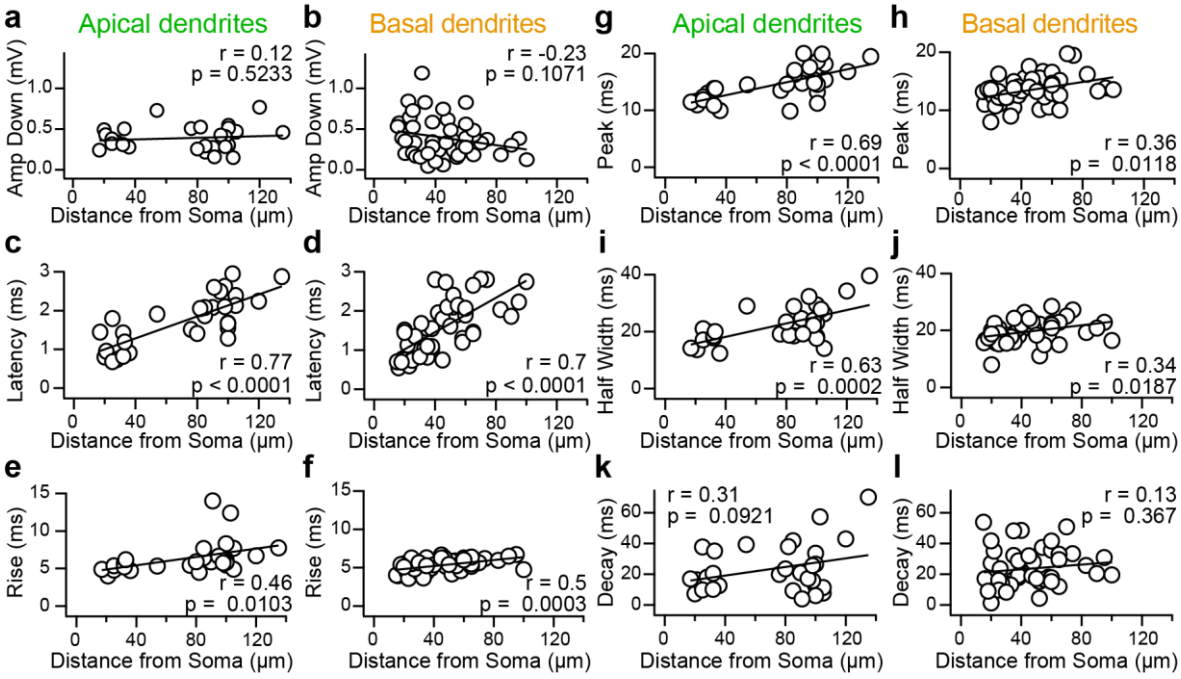

Figure 19. **Dendritically evoked OP kinetics during Downstates are correlated to the distance of stimulation site from soma.**

a. Downstate somatic response amplitude to apical dendrite stimulation as a function of the distance from the soma from entire dataset, open circles represents the mean response from one dendrite, black line shows linear fit of data. **b**. Same as (**a**) but for basal dendrites. **c**. ,**d**. Same as (**a**, **b**) but for onset latency time. **e**., **f**. Same as (**a**, **b**) but for rise time. **g**., **h**. Same as (**a**, **b**) but for peak time. **i**., **j**. Same as (**a**, **b**) but for half width. **k**., **l**. Same as (**a**, **b**) but for decay time.

Moving the stimulation site away from the soma did not change the OP amplitude (Figure 19 a, b). This result is in agreement with a filtering effect of dendritic synaptic input recorded at the soma, which normalizes EPSP amplitudes at medium-short distances (30–150 μm) in a distance-dependent manner (Nevian et al., 2007). However, more distally evoked OPs showed longer latencies and slower kinetics, with all of the kinetics except for decay time exhibiting a significant correlation between kinetic prolongation and the distance of the stimulation site from the soma (Figure 19 c - l). This result was also expected since distant dendrites have smaller diameters with longer time constants, making the local potential larger and longer (Spruston, 2009, 2008; Williams, 2004). Hence, prolonged kinetics is a footprint of large local potentials generated in distant dendrites (Redman and Walmsley, 1983; Williams, 2004).

Overall Downstate dendritic OPs resemble data from cortical slice studies in terms of the range and distance dependency of amplitudes and kinetics (Larkum et al., 2007; Nevian et al., 2007; Williams and Stuart, 2002).

3.6.1 The state-dependent modulation of optogenetic potential amplitudes is dendrite-specific

Layer 2/3 pyramidal neurons project their dendritic trees across different cortical layers (Binzegger, 2004) (Paragraph 1.1.4, Figure 1, Figure 2). The basal dendritic compartment stretches along the same layer 2/3 (Figure 20 f), receives excitatory input mainly from other neighboring pyramidal cells (Feldmeyer et al., 2006) and from layer 4 stellate neurons (Feldmeyer et al., 2002). On the other hand, the apical tuft compartment extends into layer 1 (Figure 20 a), where it collects feedback input mostly from areas outside the local circuit (Larkum, 2013). Therefore, since pyramidal neurons partially compute input from different sources in different compartments, the integration of these inputs may also be compartment-specific (Larkum and Nevian, 2008; Major et al., 2013). Moreover, in comparison to their apical counterparts, basal dendrites are shorter, thinner and express different active and passive dendritic properties (Larkum and Nevian, 2008). Can network activity therefore influence the compartment-specific integration of synaptic input in different ways?

Dendritic stimulations were targeted to apical or basal dendrites using the red Alexa signal in the dendrites for *in vivo* guidance. Apical dendrites were identified by following the branching of the apical dendritic trunk emerging from the top of the pyramidal cell body and moving toward the pial surface. On the contrary, basal dendrites were identified by following

the branching of laterally emerging dendrites around the soma focal plane. In a subset of cells, stimulation spots were subsequently confirmed to be in apical or basal compartments, respectively in layers 1 or 2, by post-hoc analysis carried out by reconstructing the neurons in coronal brain slices (Paragraph 2.7).

As neurons went from Down- to Upstates, $_{apical}$OPs showed a significant reduction in amplitude (Down 0.39 ± 0.15 mV vs. Up 0.24 ± 0.15 mV, n = 30, $p < 0.0001$) (Figure 20 a - d). This change was significantly larger than expected (Up 0.24 ± 0.15 mV vs. Exp. 0.31 ± 0.12, n = 30, p = 0.0128) (Equation 1). Despite the reduction in amplitude, there was no change in the half width (Down 21.97 ± 6.61 ms vs. Up 21.59 ± 13.24 ms, n = 30, p = 0.7151) (Figure 20 b, e). However, normalizing the Upstate $_{apical}$OP to the Down- $_{apical}$OP amplitude resulted in a larger half width in Upstates (Down 21.97 ± 6.61 ms vs. Normalized Up 38.23 ± 25.32 ms, n = 30, $p < 0.0001$). This suggests that the prolonged kinetics in Upstates are maintained in apical dendrites, but since there is an enhancement of amplitude reduction beyond the driving force effect, the potential as a whole is reduced.

In contrast, $_{basal}$OPs, evoked from the stimulation of basal dendrites, showed no overall change in amplitude (Down 0.39 ± 0.24 mV vs. Up 0.39 ± 0.19 mV, n = 48, p = 0.9150) despite the increase in V_m (Figure 20 f - i) and the expected reduction (Up 0.39 ± 0.19 mV vs. Exp. 0.31 ± 0.18, n = 48, p = 0.0001) (Equation 1). In a manner similar to $_{soma}$OPs, $_{basal}$OPs showed a significant increase in half width in Upstates (Down 19.67 ± 3.94 ms vs. Up 26.19 ± 11.08 ms, n = 48, p = 0.0004) (Figure 20 g, j).

Thus while the half width in all compartments increases in Upstates, the amplitude of input to somatic, apical and basal dendrites is modulated to different extents by network activity. OP amplitudes in both the apical and basal compartments diverge from the driving force attenuating effect showed by the somatic stimulations (Figure 17 d), with $_{apical}$OP being more reduced, while $_{basal}$OP are not affected at all. On the contrary, the kinetics seem to scale up or down according to the amplitude, suggesting that the membrane time constant increase observed in Upstates exerts a persistent effect on the kinetics of the potential across compartments.

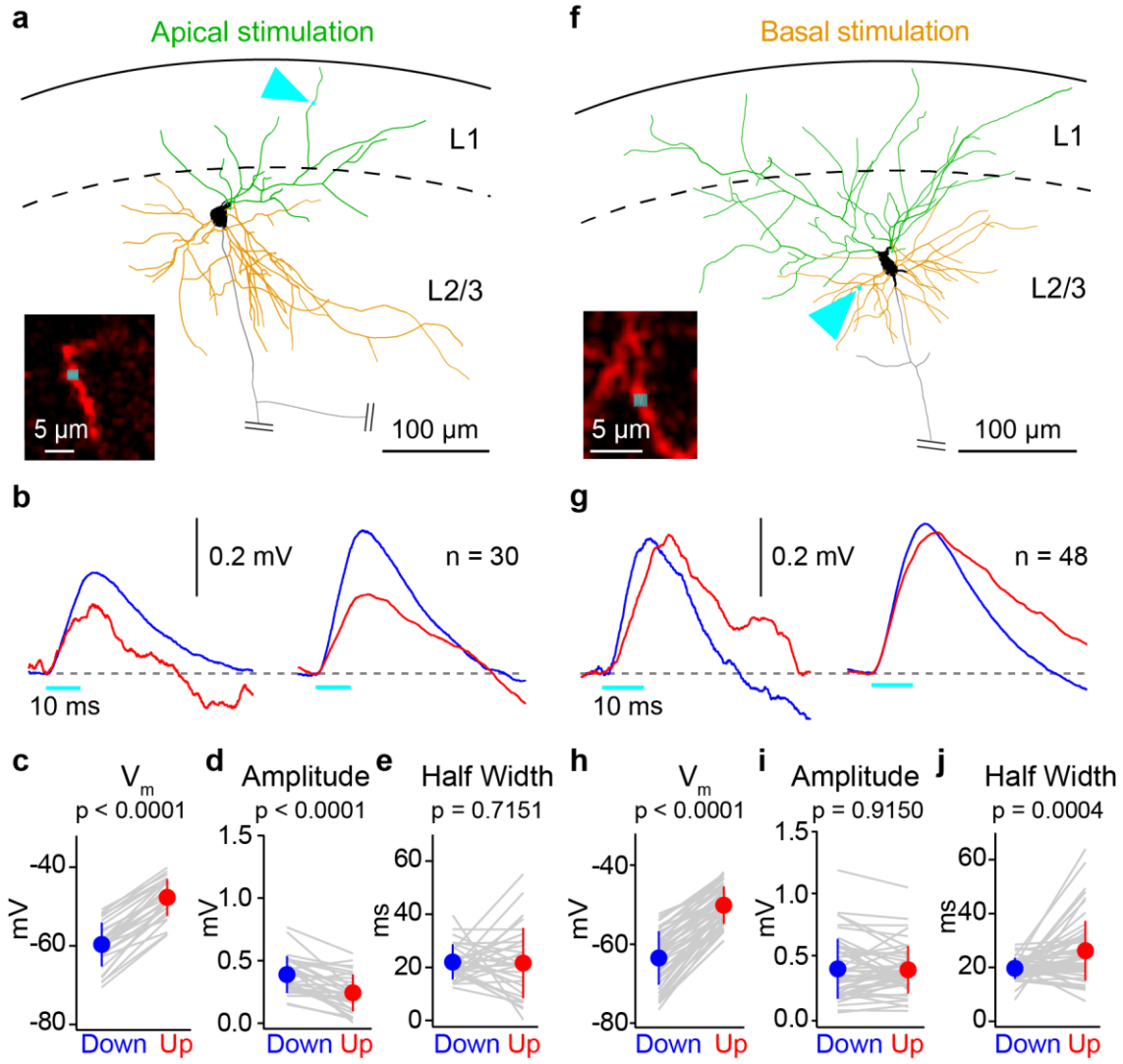

Figure 20. **Dendrite-specific modulation of subcellular two-photon evoked response amplitude and kinetics.**

a. Reconstruction of a representative layer 2/3 pyramidal neuron showing the soma in black, apical dendrites in green and basal dendrites in orange with the two-photon stimulation spot on the apical dendrite highlighted with a cyan arrowhead. Inset shows an *in vivo* image of an Alexa-594-filled dendrite in red and the optogenetic stimulation site in cyan**. b**. Overlaid example (left) and population mean (right) responses to the stimulation of an apical dendrite ($_{apical}$OP) show a reduction in amplitude during Upstates. **c**. The V_m increases as neurons go from Down- to Up-state. Grey lines show data from individual cells; the filled circles with bars indicate the mean ± S.D.. **d**. Amplitude of $_{apical}$OP is lower in Upstates compared to Downstates. **e**. Half width is not significantly different between the states. **f**. Reconstruction of example cell as in (**a**) but for basal dendrite stimulations. **g**. Neither the overlaid sample $_{basal}$OP (left) nor the population average (right) show a reduction in amplitude when Down- are compared to Upstates. **h**. Same as (**c**) but for basal stimulation experiments. **i**. Amplitude of $_{basal}$OP in Up- and Down-states is not significantly different. **j**. Half width is significantly larger in Upstates than Downstates.

3.6.2 State-dependent gain modulation of basal synaptic input

Excitatory connections between layer 2/3 pyramidal neurons generated $_{u}$EPSPs with a range of amplitudes from around 0.1 to 3 mV (Figure 24 e, f) (Jouhanneau et al., 2015). To mimic the natural distribution of the amplitudes I took advantage of the exposure light / ion current relationship of ChR2 (Berndt et al., 2011) by adjusting the two-photon laser power for each stimulation spot. I obtained a spread of amplitudes in Downstates similar to those observed in real $_{u}$EPSPs (compare Figure 20 d, i, and Figure 21 e, h, to Figure 24 e, f).

How does the network activity affect the integration of inputs with different amplitudes? Various models have been proposed to account for the way spontaneous network activity influences different types of modulation of dendritic inputs affecting amplitude and kinetics of EPSPs (Paragraph 1.4). Some models predict a reduction of inputs during active states (Bernander et al., 1991; Destexhe and Paré, 1999) and others an amplification (Hô and Destexhe, 2000; Rudolph and Destexhe, 2003; Waters and Helmchen, 2006); yet others predict an amplification of small or distant inputs that results in a normalization of amplitude distribution in Upstates, depending on the input strength or synaptic location (Berger et al., 2001; George et al., 2009; Magee, 1999; Migliore and Shepherd, 2002).

To examine the state-dependent modulation of OPs with different amplitudes, I plotted the ratio of the Up- to Downstate OP amplitude (Up:Down) as a function of the Downstate amplitude. $_{Soma}$OPs (Figure 21 a - c) and $_{apical}$OP (Figure 21 d - f) showed a similar reduction in amplitude during Upstates at all amplitudes. This resulted in similar Up:Down ratios for soma inputs (Amplitude < 0.4 mV in Downstate, Up:Down 0.88 ± 0.11, n = 3 vs. Amplitude > 0.4 mV in Downstate, Up:Down 0.82 ± 0.07, n = 13, p = 0.2964) (Figure 21 c) and for apical inputs (Amplitude < 0.4 mV in Downstate, Up:Down 0.65 ± 0.34, n = 14 vs. Amplitude > 0.4 mV in Downstate, Up:Down 0.60 ± 0.31, n = 16, p = 0.7587) (Figure 21 f).

Unexpectedly, however, smaller inputs from basal dendrites exhibited a significant increase in amplitude in Upstates ($_{basal}$OP for amplitude < 0.4 mV in Downstate, Down 0.24 ± 0.10 mV vs. Up 0.32 ± 0.14 mV, n = 30, p = 0.0002) despite the expected reduction (Up 0.32 ± 0.14 mV vs. Exp. 0.19 ± 0.08, n = 30, p < 0.0001). Larger amplitude $_{basal}$OP responses decreased (Amplitude > 0.4 mV, Down 0.64 ± 0.19 mV vs. Up 0.50 ± 0.22 mV, n = 18, p = 0.0003) (Figure 21 h, i) as expected (Up 0.50 ± 0.22 mV vs. Exp. 0.49 ± 0.14, n = 18, p = 0.8650). Up:Down ratios exhibited significant differences as well, depending on the size of their amplitude (For amplitude < 0.4 mV in Downstate, Up:Down 1.41 ± 0.54, n = 30 vs. inputs > 0.4 mV in Downstate, Up:Down 0.77 ± 0.23, n = 18, p < 0.0001) (Figure 21 i).

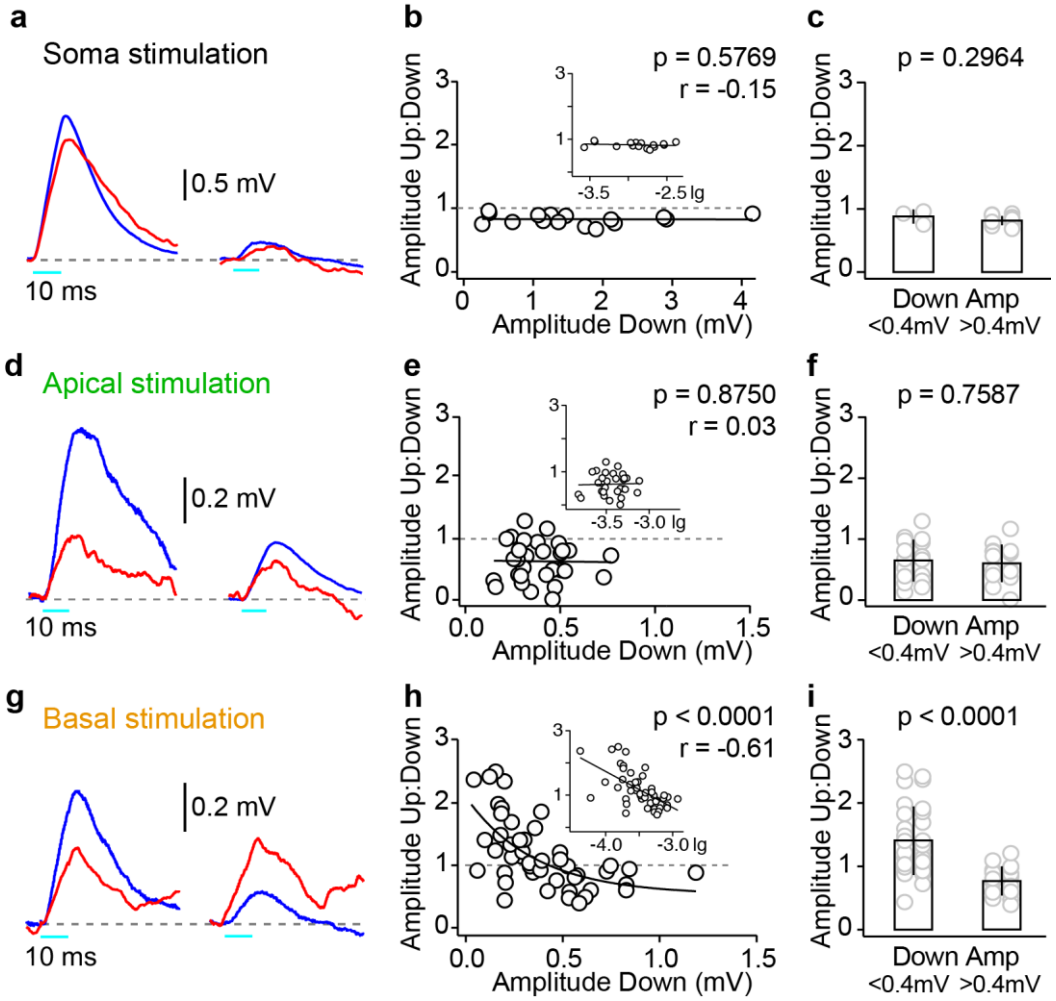

Figure 21. **Cortical state-dependent gain modulation of basal dendritic inputs in anesthetized mice.**

a. Two example mean, overlaid $_{soma}$OPs with different Downstate (blue) amplitudes that both show a small reduction in Upstate (red) response amplitude. **b**. No significant correlation between the ratio of $_{soma}$OP Up:Down amplitude and Downstate $_{soma}$OP amplitude. Inset, linear correlation between Up:Down and the lg of Downstate amplitude. **c**. No significant difference in the same data as in (**b**) but divided in two groups by Downstate OP amplitude. **d**. Same as (**a**), but for $_{apical}$OPs. **e**, No significant correlation between the ratio of $_{apical}$OP Up:Down amplitude and the lg of Downstate $_{apical}$OP amplitude. Inset as in (**b**). **f**. same as in (**c**) but for data in (**e**), no significant correlation. **g**. Overlaid, sample mean $_{basal}$OP with larger amplitude in Downstate shows a reduction in Upstates, whereas smaller amplitude sample $_{basal}$OP shows an increase. **h**. A negative correlation between the ratio Up:Down $_{basal}$OP amplitude and Downstate $_{basal}$OP amplitude results in smaller amplitude inputs increasing and larger amplitude inputs decreasing in amplitude during Upstates. Inset, linear correlation between Up:Down and the lg of Downstate amplitude. **i**. Splitting data from (**h**) as in (**c**) shows a significant difference between small and large $_{basal}$OP responses. Black lines are single exponential (basal) or linear (apical, soma and insets) fits. Apical and somatic data are fit with a line to highlight that there is no exponential correlation, as reported by the lack of linear correlation in the log scale of the same data (insets).

This resulted in a negative relationship between the degree of state-modulation and $_{basal}$OP amplitude, with a significant linear correlation between the Up:Down amplitude ratio and

the logarithm base 10 (lg) of the Downstate amplitude (r = -0.61, p = < 0.0001) (Figure 21 h).

0.4 mV was chosen as a divide point between large and small amplitudes because when plotting the amplitude of $_{basal}$OP responses in Down- versus Upstate a significant linear regression crossed the Up:Down amplitude ratio unity (ratio = 1) at this V_m value.

As can be seen in (Figure 21 g - i), inputs to the basal dendritic compartment undergo a gain modulation of the amplitudes in Upstates. This results in a single exponential relationship that narrows the distribution of amplitudes during active states which induces a normalization. This effect is not present in potentials elicited in apical dendrites or the soma.

3.6.3 Distance-dependent compartmentalization of apical input during active states

Direct dendritic patch studies have shown how dendritic integration can have a filtering effect on synaptic input amplitudes, in a manner that is directly related to the distance of the input from the soma (Larkum et al., 2007; Major et al., 2008; Nevian et al., 2007; Williams and Stuart, 2002). Such a distance-dependent attenuation might be corrected or reversed during active network states (Nevian et al., 2007; Rudolph and Destexhe, 2003).

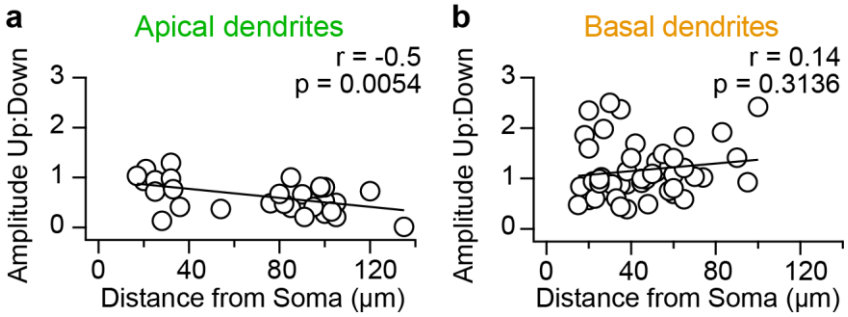

Figure 22. **OP amplitude Up:Down ratio as a function of the distance of dendritic optogenetic stimulation from the soma.**
a. Up:Down ratio of somatic recorded amplitude in response to apical dendrite stimulation as a function of the distance from the soma for the entire dataset. Open circles represents the mean response ratio from one dendrite; the black line shows the linear fit of data. Significant negative correlation between ratio of Up:Down $_{apical}$OP amplitude and the stimulation dendritic site distance from the soma. **b**. Same as (**a**) but for basal dendrites. Ratio of Up:Down $_{basal}$OP amplitude is not correlated to the distance of the stimulation dendritic site from the soma.

$_{Apical}$OP inputs more distant from the soma showed a larger reduction in amplitude during Upstates than inputs from branches nearer the soma (r = -0.5, p = 0.0054) (Figure 22 a), supporting a compartmentalization of processing in apical dendrites during network activity (Williams, 2004). In contrast to $_{apical}$OPs, there was no correlation between the modulation

strength of $_{basal}$OPs and distance from the soma (r = 0.14, p = 0.3136) (Figure 22 b), in line with a model of basal dendritic filtering that is independent of distance up to 150 µm from the soma (Nevian et al., 2007).

3.7 State-dependent gain modulation of synaptic glutamatergic input to basal dendrites

A gain modulation of synaptic input amplitude by network activity has been reported before (Reig et al., 2015) but the effect was attributed to network mechanisms rather than a postsynaptic process of dendritic integration, as our data suggest. ChR2 is a non-specific cation channel with a reversal potential of around 0 mV (Berndt et al., 2011). Thus, the increase in $_{basal}$OP amplitude in Upstates goes against the reduction in driving forces associated with a more depolarized V_m. To exclude the possibility that the effect might be due to an unphysiological depolarization of dendrites during ChR2 stimulation, I next examined whether a boosting of small-amplitude basal inputs is also observed with glutamatergic inputs.

3.7.1 Gain control of thalamic synaptic input

I took advantage of the distinct pattern of axonal projections of thalamic ventral posteromedial nucleus (VPM) neurons (Figure 23 a). VPM axons mostly target layer 4 neurons that subsequently project to the basal dendrites of layer 2/3 neurons (Feldmeyer et al., 2002), but they also have axonal collaterals near the border of layer 4 and 2/3 that may directly come into contact with the basal dendrites of layer 2/3 neurons (Figure 23 b). I infected VPM neurons with ChR2, and Dr. Jouhanneau optogenetically activated their cell bodies or cortical axons during visually-targeted whole-cell recordings from layer 2/3 pyramidal neurons (Figure 23 b) (Jouhanneau et al., 2014). VPM stimulation evoked a depolarizing input with a short latency followed by a hyperpolarization which was likely due to inhibition from local cortical GABAergic neurons. Measurements of the early depolarizing response did not show an overall change in amplitude when comparing Down- to Upstates (Down 1.23 ± 1.00 mV vs. Up 0.77 ± 0.55 mV, n = 11, p = 0.2060). Plotting the Up:Downstate amplitude of the depolarizing response as a function of the Downstate amplitude revealed a significant negative correlation and a state-dependent modulation similar to that observed with OPs evoked in basal dendrites (Figure 23 b - f). Thus, these

data show that a gain modulation also occurs in the case of glutamatergic inputs directed to basal dendrites of layer 2/3 pyramidal neurons, evoked by VPM stimulation and suggest that weak sensory-evoked glutamatergic inputs may also be amplified during active network states (Reig et al., 2015).

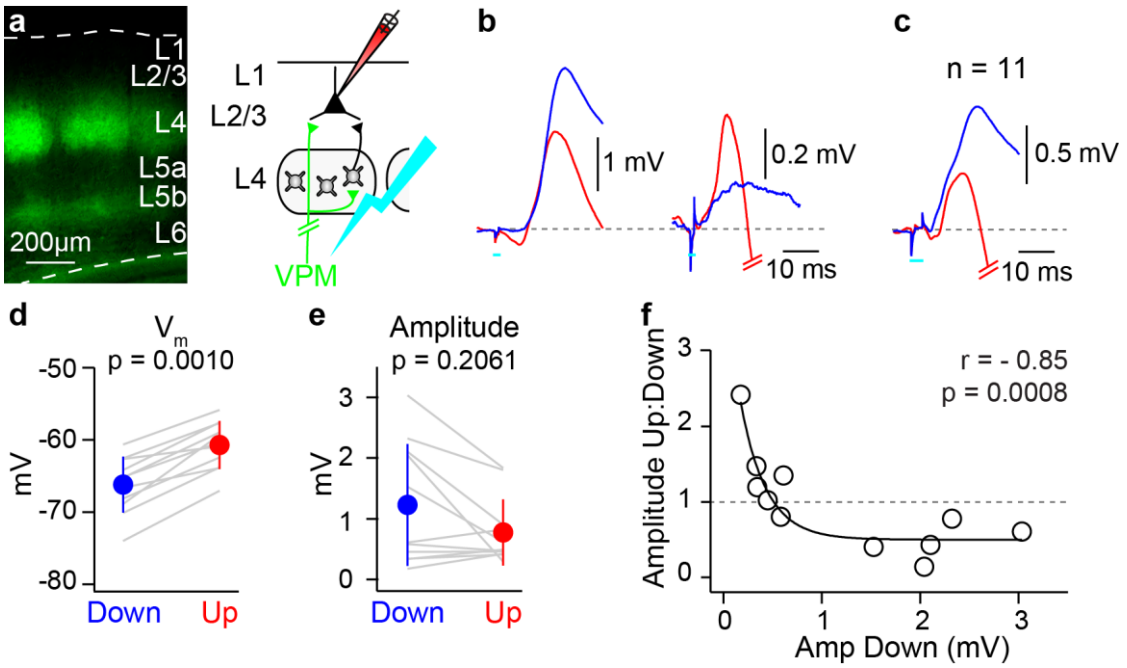

Figure 23. **Glutamatergic inputs to layer 2/3 neurons from ventral posteromedial thalamic nucleus show state dependent gain modulation.**
a. Example of a cortical coronal slice showing a somatosensory barrel cortex innervation pattern of ventral posteromedial (VPM) thalamic axons which express ChR2-EYFP. Dashed white lines show pial surface and border with white matter. Cartoon shows the recording and stimulation scheme. **b**. Two average, overlaid responses from cortical layer 2/3 whole-cell recordings upon VPM stimulation during Down- (blue) and Upstates (red) show an example of a larger amplitude that decreases in Upstates and an example of a smaller amplitude that increase in Upstates. **c**. As in (**b**) but the population average response. **d**. Significant increase of V_m from Down- to Upstates. Grey lines show data from individual cells; the filled circles with bars show the mean ± S.D.. **e**. Across the population there were no significant differences in the amplitudes of responses to VPM stimulation in Up- compared to Downstates. **f**. A significant negative correlation between the ratio of the Up:Down amplitude and the lg of Downstate response amplitude, showing the amplification of small amplitude VPM responses during Upstates. Open circles represent the mean response from a single cell; the black line is a single exponential fit.

Data reported here and in Figure 23 were collected in collaboration with Dr. J.-S. Jouhanneau. The dataset is extracted from previously published collaborative work (Jouhanneau et al., 2014) and reanalyzed by Dr. Jouhanneau for the purpose of this study.

3.7.2 Gain modulation of local monosynaptic glutamatergic connections

Optogenetic VPM stimulation activates a large population of presynaptic neurons. To measure whether unitary glutamatergic EPSPs ($_u$EPSP) also undergo state-dependent gain modulation, we next performed multiple (2 to 4) targeted whole-cell recordings from monosynaptically connected layer 2/3 pyramidal neurons *in vivo* (Jouhanneau et al., 2015). The vast majority of the synaptic contacts of these cells target the basal dendrites of neighboring excitatory neurons (Feldmeyer et al., 2006).

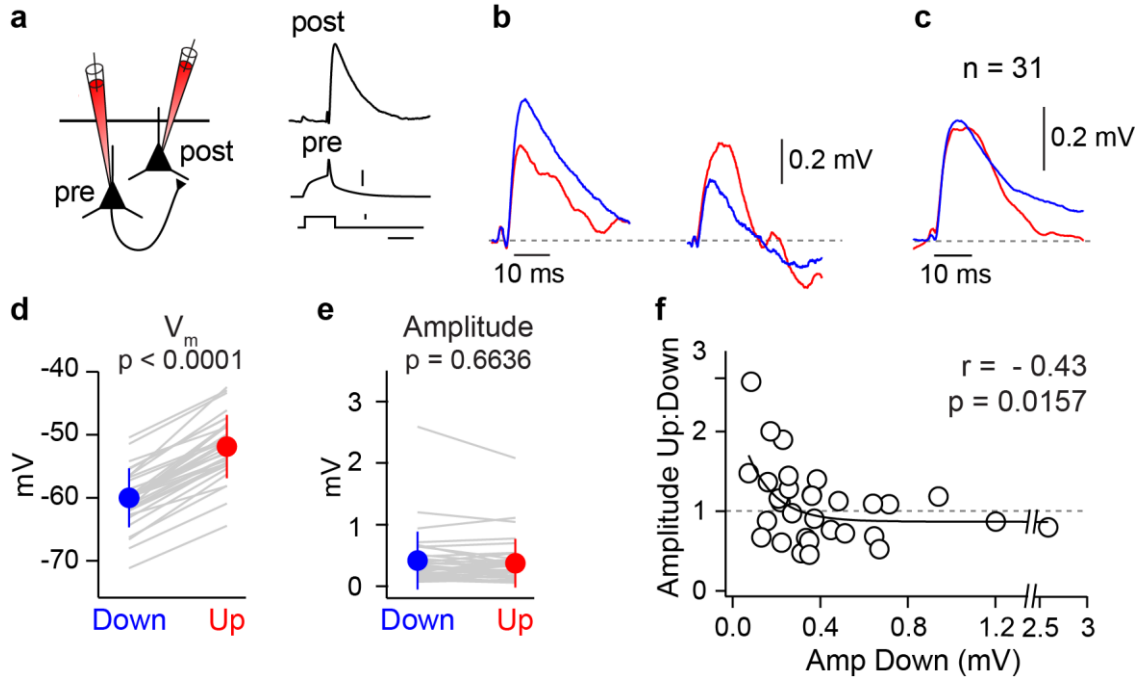

Figure 24. **Local cortical monosynaptic glutamatergic connections show state dependent gain modulation.**
a. Schematic of experimental setup used to test for monosynaptic connectivity *in vivo* and an example connection, current scale bar shows 200 pA; the V_m scale bar is 40 mV for the presynaptic and 0.1 mV for the postsynaptic neuron. **b.** Two representative averaged $_u$EPSPs with different Downstate amplitudes. The larger response (left) is decreased in Upstates whereas the smaller is increased (right). **c**. Overlaid population averages, of $_u$EPSP in Down- and Upstates. **d**. Significant increase of V_m from Down- to Upstates. **e.** $_U$EPSP experienced no change in amplitude in the Upstate compared to Downstate across the entire population. **f**. Significant correlation between lg of the Downstate amplitude of $_u$EPSPs and the ratio of amplitude Up:Down, highlighting the amplification of small amplitude $_u$EPSPs during Upstates. Open circles represent mean response from a single cell, black line is a single exponential fit.

We then evoked single action potentials using brief, depolarizing injections of current and measured the postsynaptic response in neighboring neurons to identify specific connections and compare $_u$EPSP amplitudes between Down- and Upstates (Figure 24 a, b). Across 31 connections with a depolarizing $_u$EPSP in Upstates, the mean amplitude during Upstates was

not significantly different from the Downstate amplitude (Down 0.45 ± 0.47 mV vs. Up 0.43 ± 0.39 mV, n = 31 connections, p = 0.6636) (Figure 24 c, e). Notably, however, smaller amplitude $_{u}$EPSPs increased in amplitude in Upstates, while larger amplitude $_{u}$EPSPs decreased (Figure 24 b), resulting in a significant negative correlation between the ratio of the $_{u}$EPSP amplitude in Up:Down and the lg of Downstate amplitude (Figure 24 f). Thus, a state-dependent gain modulation is a fundamental feature of the integration of glutamatergic local monosynaptic inputs *in vivo*.

Data reported in this paragraph and in Figure 24 were collected by Dr. J.-S. Jouhanneau and partly published in (Jouhanneau et al., 2015).

3.8 Synaptic gain modulation in awake mice

While Up- and Downstates are a hallmark of anesthesia and slow wave sleep, cortical neurons in awake resting mice also oscillate between brief, hyperpolarized periods (V_{hyp}) and depolarized (V_{dep}) V_m values (Poulet and Petersen, 2008; Zhao et al., 2016). Therefore, I next performed stimulations of somatic, apical and basal dendrites in awake resting mice (Figure 25, Figure 26).

All awake recordings were performed on neurons in the right forepaw primary somatosensory cortex, which was identified using intrinsic optical imaging (Paragraph 2.1.1, Figure 6). Patched neurons displayed a normal resting V_m (-57.13 ± 3.25 mV, n = 20). During recording in the left forepaw S1, the right forepaw was tethered and spontaneous movements were recorded (Paragraph 2.6). By matching paw movement and neuronal V_m recordings, movement and quiet resting periods were separated in the analysis (Figure 28 a); quiet periods were subdivided in hyperpolarized V_{hyp} and depolarized V_{dep} periods (Figure 25 b).

3.8.1 Somatic responses during slow cortical activity in awake resting mice

Somatic stimulations in awake mice triggered $_{soma}$OPs during quiet resting periods with onset latencies of 0.67 ± 0.70 ms, indicating a direct response to the optical stimulation. The rise time was 4.51 ± 0.61 ms, the peak time 11.96 ± 1.34 ms, the half width 20.21 ± 7.91 ms and the decay time 21.41 ± 13.73 ms, with an overall $_{soma}$OP amplitude of 1.07 ± 0.58 mV (n = 9).

I next split and the averaged $_{soma}$OPs into V_{dep} and V_{hyp} state responses based on their pre-stimulus V_m (Paragraph 2.8.4 and Figure 25 b) (V_{hyp} -62.31 ± 2.96 mV vs. V_{dep} -54.26 ± 2.62 mV, n = 9, p = 0.0039). The $_{soma}$OP amplitude was significantly smaller in V_{dep} than V_{hyp}

state (V_{hyp} 1.29 ± 0.58 mV vs. V_{dep} 1.02 ± 0.61 mV, n = 9, p = 0.0078) (Figure 25 c - e), as expected from the reduction in driving force during V_{dep} (V_{dep} 1.02 ± 0.61 mV vs. Expected 1.12 ± 0.50, n = 9, p = 0.3594) (Equation 1).

Therefore, awake slow V_m oscillations affect somatic modulations in the same way as Up- and Downstates in urethane anesthetized mice (Paragraph 3.5).

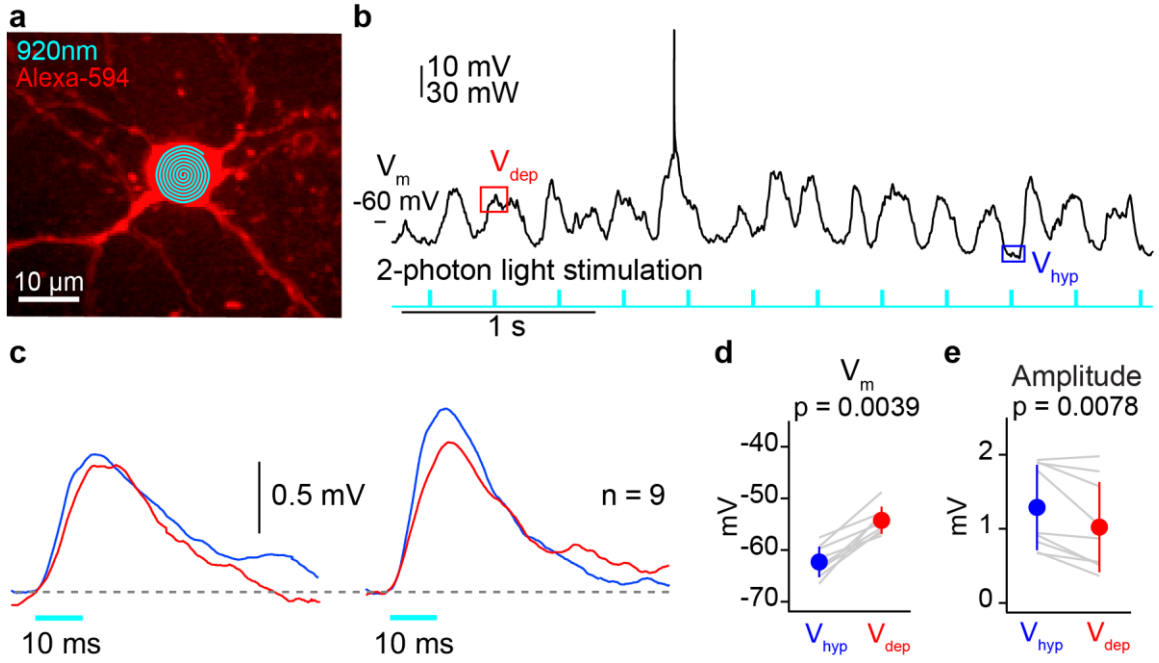

Figure 25. **Somatic optogenetic stimulation during slow cortical activity in awake, resting mice.**
a. Example *in vivo* image showing the path of two-photon stimulation (cyan) on the soma of a ChR2-expressing neuron during whole-cell recording in an awake resting mouse. **b**. Whole-cell recording of neuron in (**a**) during slow cortical fluctuations with epochs of hyperpolarized (V_{hyp}) and depolarized (V_{dep}) membrane potential. Cyan ticks show optogenetic stimulation times. **c**. Averaged light evoked $_{soma}$OPs to soma stimulation from an example neuron (left) and the population average (right) with V_{hyp} (blue) and V_{dep} (red) responses overlaid. **d**. V_m difference between V_{hyp} and V_{dep} phases of slow oscillation. **e**. $_{Soma}$OP V_{dep} amplitude is significantly lower than during V_{hyp}.

3.8.2 Compartmentalization of apical input during slow network activity

Next, I examined dendritic inputs during slow oscillations in awake mice. I stimulated apical and basal dendrites between 21 and 115 µm from the soma (Apical 76.78 ± 25.94 µm, n = 9, basal 55.18 ± 29.69 µm, n = 11) during periods of hyperpolarization (V_{hyp}) and depolarization (V_{dep}) in resting mice.

Stimulations of apical and basal dendrites evoked $_{apical}$OPs and $_{basal}$OPs whose kinetics were similar in hyperpolarized (V_{hyp}) periods (Apical rise time 5.50 ± 1.83 ms, basal 5.48 ±

1.48 ms; apical peak time 14.75 ± 3.93 ms, basal 16.05 ± 2.29 ms; apical half width 19.09 ± 9.79 ms, basal 26.02 ± 8.10 ms and apical decay time 20.18 ± 19.97 ms, basal 31.46 ± 26.15 ms). The latency of OP (Apical 1.71 ± 0.61 ms, basal 1.48 ± 0.67 ms) correlated to the distance from the soma in stimulations of both apical ($r = 0.87$, $p = 0.0020$) and basal ($r = 0.90$, $p = 0.0001$) dendrites.

Splitting the data between V_{hyp} and V_{dep} phases of the slow activity revealed a modulation of OP amplitudes that was similar to our data from anesthetized mice. As neurons went from V_{hyp} to V_{dep} (Apical V_m V_{hyp} -60.16 ± 4.93 mV vs. V_{dep} -49.61 ± 2.08 mV, $n = 9$, $p = 0.0039$) (Figure 26 c), $_{apical}$OPs showed a significant reduction in amplitude (apical amplitude V_{hyp} 0.84 ± 0.58 mV vs. V_{dep} 0.39 ± 0.46 mV, $n = 9$, $p = 0.0039$) (Figure 26 b - d) that was significantly larger than expected (V_{dep} 0.39 ± 0.46 mV vs. Exp. 0.69 ± 0.46, $n = 9$, $p = 0.0078$) (Equation 1). Moreover, the reduction was more pronounced than in anesthetized experiments (Paragraph 3.6.1, Figure 20 b, d).

In contrast, $_{basal}$OPs showed no overall change in amplitude (Basal amplitude V_{hyp} 0.70 ± 0.42 mV vs. V_{dep} 0.46 ± 0.30 mV, $n = 11$, $p = 0.0674$) despite the increase in V_m (Basal V_m V_{hyp} -56.63 ± 3.63 mV vs. V_{dep} -45.75 ± 3.85 mV, $n = 11$, $p = 0.0010$) (Figure 26 f-h) and the expected reduction in amplitude based on the reduction in driving force (Basal amplitude V_{dep} 0.46 ± 0.30 mV vs. Exp. 0.57 ± 0.35, $n = 11$, $p = 0.4648$) (Equation 1). This result is similar to that shown by basal stimulations in anesthetized experiments (Paragraph 3.6.1, Figure 20 g, i).

Thus, the reduction in amplitude of apical input in periods of V_{dep} during slow wave oscillations in quiet resting awake mice, is even stronger than that seen during Upstates in anesthetized animals. On the other hand, network activity in awake mice seems to affect basal stimulations in the same way as Upstates under anesthesia. Even though there was a trend toward an average basal amplitude that was smaller in V_{dep} versus V_{hyp}, contrary to anesthetized recordings where there was no state-related difference – although this distinction did not reach a level of significance (compare Figure 26 f to Figure 20 g). This can be explained through the observation that in awake recordings, small basal inputs are underrepresented (Figure 26 h and Figure 27 c, d); indeed in magnitude-dependent modulations, the grand average is representative of a population only if the range of amplitudes is distributed equally across the dataset. In this case a lack of small inputs, which were increased in Upstates, creates a bias toward a smaller averaged Upstate response. If different amplitudes were equally represented, this discrepancy between awake and anesthetized responses would probably vanish.

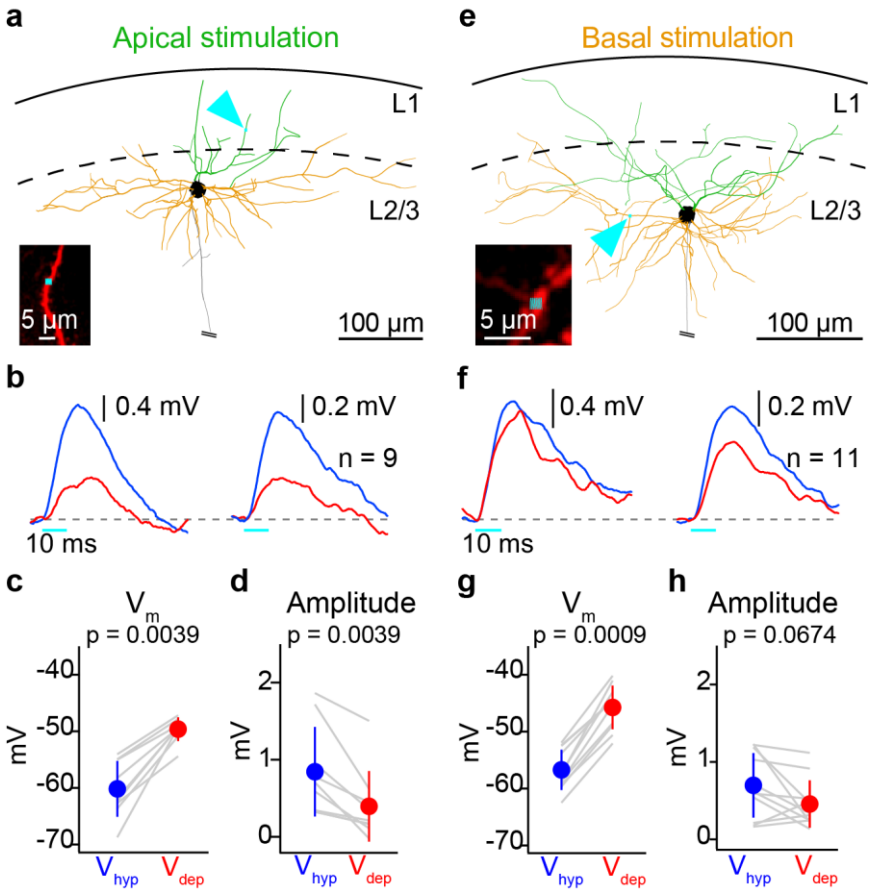

Figure 26. **Basal and apical dendrite optogenetic stimulation during slow cortical activity in awake, resting mice.**
a. Reconstruction of example neuron showing apical dendrites in green and basal dendrites in orange, with the two-photon stimulation spot of the apical dendrite highlighted by cyan arrowhead. Inset shows an *in vivo* image of an Alexa-594 filled dendrite in red and optogenetic stimulation site in cyan. **b**. Averaged light-evoked $_{apical}$OP from a representative neuron (left) and the population average (right) with V_{hyp} (blue) and V_{dep} (red) responses overlaid. **c**. V_m differences between the V_{hyp} and V_{dep} phases of slow oscillations. **d**. $_{Apical}$OP V_{dep} amplitude is significantly lower than during V_{hyp}. **e**. Reconstruction of example cell as in (**a**) but for basal dendrite stimulation. **f**. Example $_{basal}$OP (left) and the population average (right) both showing no reduction in amplitude comparing V_{hyp} to V_{dep}. **g**. V_m increases as neurons go from V_{hyp} to V_{dep} phases of slow cortical oscillation. **h**. Amplitude of $_{basal}$OP in V_{hyp} and V_{dep} is not significantly different.

3.8.3 Gain modulation of input to basal dendrites

I next plotted the ratio of the V_{dep}:V_{hyp} OP amplitude as a function of the V_{hyp} OP amplitude. The $_{apical}$OPs showed similar V_{dep}:V_{hyp} amplitude ratio reductions at all V_{hyp} amplitudes (Apical inputs < 0.4 mV in V_{hyp}, V_{dep}:V_{hyp} 0.55 ± 0.05, n = 3 vs. inputs > 0.4 mV in V_{hyp}, V_{dep}:V_{hyp} 0.38 ± 0.29, n = 6, p = 0.3809) (Figure 27 b). In contrast, smaller amplitude $_{basal}$OP inputs exhibited significant increases in amplitude ratios during V_{dep}, while larger amplitude responses decreased (For basal inputs < 0.4 mV in V_{hyp}, V_{dep}:V_{hyp} 1.89 ± 0.70, n = 3 vs.

inputs > 0.4 mV in V_{hyp}, V_{dep}:V_{hyp} 0.55 ± 0.30, n = 8, p = 0.0121) (Figure 27 d). This resulted in a negative relationship between the degree of state-modulation and the $_{basal}$OP amplitude, with a significant linear correlation between the amplitude ratio V_{dep}:V_{hyp} and the logarithm of the V_{hyp} amplitude (r = -0.76, p = 0.0062) (Figure 27 c).

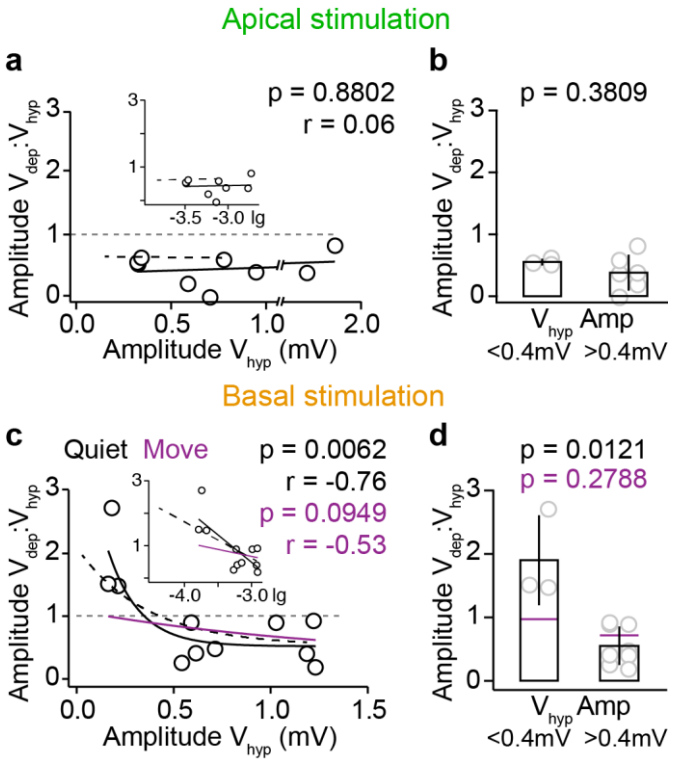

Figure 27. **Cortical state dependent gain modulation of basal dendritic input in awake mice during quiet or active movement.**
a. No significant correlation was observed between the ratio of V_{dep}:V_{hyp} $_{apical}$OP amplitude and V_{hyp} $_{apical}$OP amplitude. Inset, linear correlation between V_{dep}:V_{hyp} and the lg of V_{hyp} amplitude. **b**. Here the same data was divided into two groups of amplitude according to V_{hyp} OP amplitude; no significant difference was observed. **c**. A negative correlation between the V_{dep}:V_{hyp} ratio in $_{basal}$OP amplitudes and V_{hyp} $_{basal}$OP amplitude led to increases in the amplitudes in smaller inputs and decreases in the amplitudes of larger inputs during V_{dep}. Inset, linear correlation between V_{dep}:V_{hyp} and the lg of V_{hyp} amplitude. **d**. Splitting data from (**c**) as in (**b**) shows a significant difference between small and large $_{basal}$OP responses. Black lines are single exponential (basal) or linear (apical and insets) fits. Purple fits, values (**c**) and averages (**d**) represent the same values but calculated for Move:V_{hyp} ratio, in basal only. Dashed black lines are the corresponding fits for data from anesthetized mice (from Figure 21 e, h) highlighting the similarities. Apical data are fit with a line to highlight the lack of an exponential correlation, as shown by the lack of a linear correlation in the log scale of the same data (inset).

A state-dependent gain modulation of basal inputs is therefore seen in awake resting mice during slow network activity, as well as in anesthetized mice (Paragraph 3.6.2). This suggests that the gain modulation has a function in the signal integration during the

processing of meaningful network activity and it is not an artifact due to the side effects of anesthesia side.

3.8.4 Impact of movement on gain modulation

While large-amplitude, slow fluctuations are highly correlated between neighboring layer 2/3 neurons in resting animals, they are abolished during movement, resulting in a desynchronized or ‘‘active’’ cortical state (Poulet and Petersen, 2008). The active state has been linked to a modulation of sensory responsiveness (Crochet and Petersen, 2006; Polack et al., 2013; Zhou et al., 2014). This situation led me to examine whether soma, basal and apical inputs are modulated differently during different network and behavioral states. By monitoring spontaneous forepaw movements during recordings and optostimulations, I could identify and analyze inputs to the soma, apical and basal dendrites as presented above (Paragraphs 3.8.1, 3.8.2) and examine their integration in comparison to the active movement state (Move) (Figure 28).

Overall, the V_m during Move periods was less variable than that of quiet periods, without a clear bimodal distribution (Figure 28 a). The V_m of Move periods lay, on average, between the V_m values established for V_{hyp} and V_{dep} during quiet periods. While they were closer to V_{dep} values, they were significantly different from both (For soma, Move V_m -56.56 ± 3.75 mV vs. V_{hyp} -62.31 ± 2.96 mV n = 9, p = 0.0039; Move vs. V_{dep} -54.26 ± 2.62 mV, n = 9, p = 0.0039) (Figure 28 c).

Likewise, $_{soma}$OP amplitudes during Move lay between those for V_{hyp} and V_{dep} (Figure 28 b) during quiet periods, yet once again significantly differed from both (soma Move amplitude 1.10 ± 0.64 mV vs. V_{hyp} 1.29 ± 0.58 mV, n = 9, p = 0.0391; Move vs. V_{dep} 1.02 ± 0.61 mV, n = 9, p = 0.0117) (Figure 28 d). The Move amplitude was reduced as much as expected by the driving force reduction between Move and V_{hyp} (Soma Move amplitude, 1.10 ± 0.64 vs. Expected 1.16 ± 0.51, n =9, p = 0.4961) (Equation 1). Thus, somatic input seems to be modulated only by the difference in driving force, as directly determined by the difference in V_m between these three “states” in awake mice.

Measurements from apical inputs, however, showed an unexpected trend. In quiet periods $_{apical}$OP amplitudes undergo a massive reduction during V_{dep} (Paragraph 3.8.2, Figure 26 b, d), but during the active Move state they were not reduced (Apical Move amplitude 0.76 ± 0.54 mV vs. V_{hyp} 0.84 ± 0.58 mV, n = 9, p = 0.3594; Move vs. V_{dep} 0.39 ± 0.46 mV, n = 9, p = 0.0039) (Figure 28 e, g). Even though the average Move V_m was closer to V_{dep}, it still

differed significantly from both quiet states (Apical Move V_m -53.11 ± 2.31 vs. V_{hyp} -60.16 ± 4.93 mV, n = 9, p = 0039; Move vs. V_{dep} -49.61 ± 2.08 mV, n = 9, p = 0.0039) (Figure 28 f). The Move amplitude reduction was in line with the V_m difference between Move and V_{hyp} (Apical Move amplitude 0.76 ± 0.54 mV vs. Expected Move amplitude 0.74 ± 0.50 mV, n = 9, p = 0.9101) (Equation 1).

In contrast, the effects of movement on inputs from basal dendrites were similar to those observed during V_{dep} in quiet periods. This means that the average $_{basal}$OP amplitude during Move did not differ from the V_{dep} amplitude; both were significantly reduced in comparison to V_{hyp} (Basal Move amplitude 0.49 ± 0.28 mV vs. V_{hyp} 0.70 ± 0.42 mV, n = 11, p= 0.0185; Move vs. V_{dep} 0.46 ± 0.30 mV, n = 11, p = 0.9658) (Figure 28 j). Despite the fact that the average Move V_m lay between those for V_{hyp} and V_{dep}, it differed significantly from both (Basal Move V_m -49.23 ± 4.32 vs. V_{hyp} -56.63 ± 3.63 mV, n = 11, p = 0.0010; Move vs. V_{dep} -45.75 ± 3.85 mV, n = 11, p = 0.0010) (Figure 28 i). Finally, V_m depolarization reduced the basal Move amplitude in comparison to V_{hyp} as expected (Basal Move amplitude 0.49 ± 0.28 mV vs. Expected 0.61 ± 0.37 mV, n = 11, p = 0.1230) (Equation 1).

In summary, active movement impacts the state-dependent modulation of stimuli to basal and apical dendrites in different ways. On apical dendrites, movement seems to counteract the attenuating compartmentalization along the branches, completely canceling it out and restoring a linear modulation in line with the driving force, or even enhancing the signal to a V_{hyp} level. This suggests that the apical compartmentalization during depolarized states may be due to a constant inhibition mechanism, which would be released during a top-down feedback signal through layer 1 that occurs during active movement (Paragraph 1.4.1).

In basal dendrites, however, active movement does not seem to interact with the normal driving force effect on the amplitude, but it might downregulate the amplitude-dependent gain modulation to restore a linear correlation. Indeed, plotting the amplitude ratio Move:V_{hyp} as a function of the V_{hyp} amplitude does not result in an exponential fit or in a significant linear correlation with the logarithm of V_{hyp} amplitude (r = -0.53, p = 0.0949) (Figure 27 c purple). Similarly, splitting the dataset at 0.4 mV, as the V_{hyp} amplitude divide, does not result in a significant difference between small and large $_{basal}$OP responses (for basal amplitudes < 0.4 mV in V_{hyp}, Move:V_{hyp} 0.97 ± 0.30, n = 3 vs. amplitudes > 0.4 mV in V_{hyp}, Move:V_{hyp} 0.71 ± 0.25, n = 8, p = 0.2788) (Figure 27 d purple). However, more data are required to confirm this movement-dependent modulation.

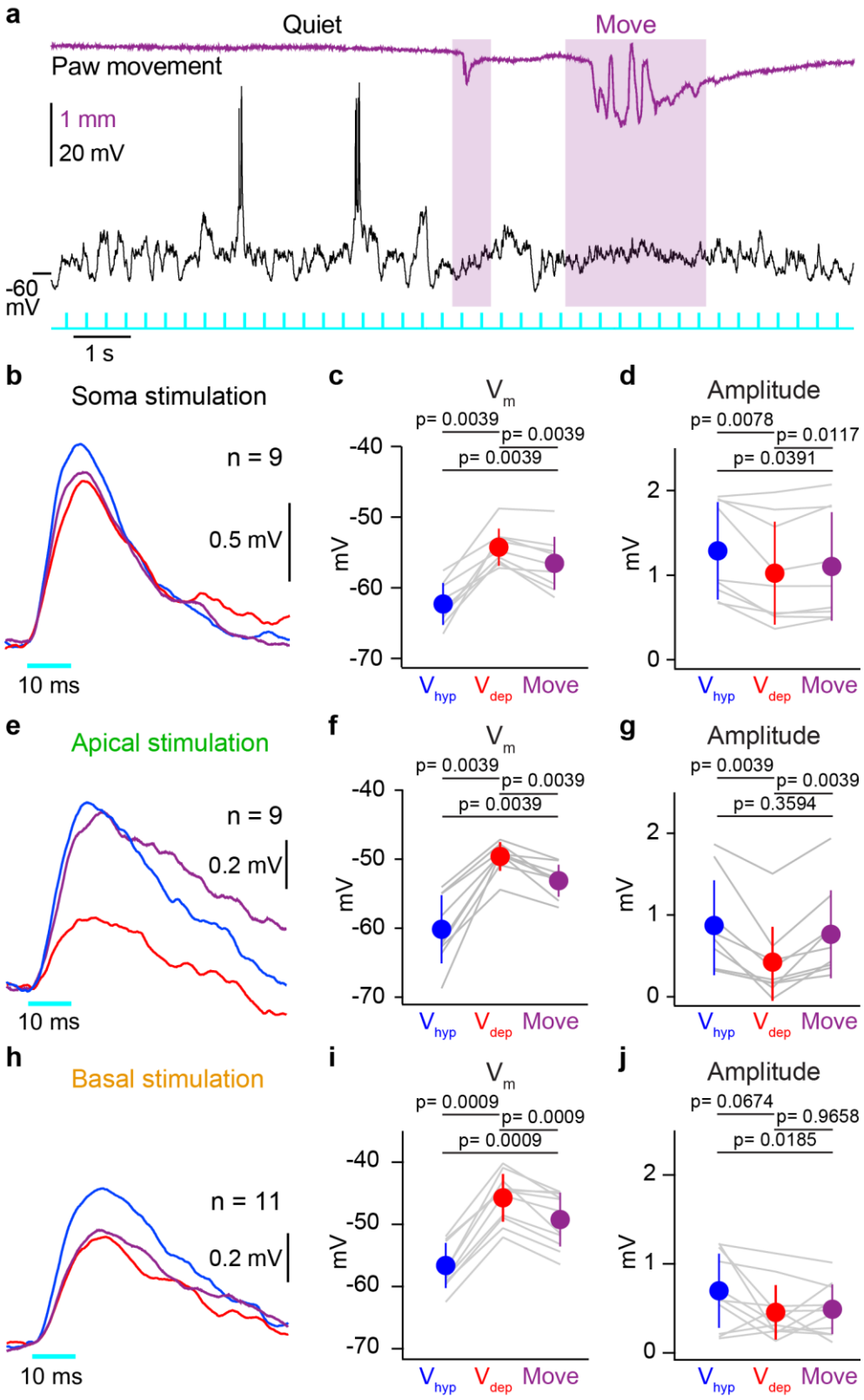

Figure 28. **Optogenetic stimulation during desynchronized active Move state.**
a. Example whole-cell recording of a layer 2/3 cortical neuron in an awake mouse during slow cortical oscillations with epochs of V_{hyp} and V_{dep} in quiet periods compared with paw movement periods (Move, purple trace) showing faster and smaller amplitude V_m oscillations along with a depolarized V_m (purple areas). Cyan ticks show time points of optogenetic stimulations. **b**. Overlay of averaged $_{soma}$OPs during quiet phases, split into V_{hyp} (blue) and V_{dep} (red) (same data as Figure

25 c right) and Move (purple) responses. **c**. V_m difference between V_{hyp} and V_{dep} phases of resting periods (from Figure 25 d) and Move desynchronized phases; the V_m during Move phases lay in between and was significantly different from both quiet phases. **d**. $_{Soma}$OP V_{dep} amplitude was significantly smaller than during V_{hyp} (from Figure 25 e) as was the case for the Move amplitude, which was not different from V_{dep}. **e**. Same as (**b**) but for $_{apical}$OPs; V_{hyp} and V_{dep} (from Figure 26 b right). **f**. Same as (**c**) but for $_{apical}$OPs; V_{hyp}, V_{dep} (from Figure 26 c) and Move are all different. **g**. Same as (**d**) but for $_{apical}$OPs; V_{hyp}, V_{dep} (from Figure 26 d); $_{apical}$OPs during Move were larger than during V_{dep} and undistinguishable from those of V_{hyp}. **h**. Same as (**b**) but for $_{basal}$OPs; V_{hyp} and V_{dep} (from Figure 26 f right). **i**. Same as (**c**) but for $_{basal}$OPs; V_{hyp}, V_{dep} (from Figure 26 g) and Move are all different. **g**. Same as (**d**) but for $_{basal}$OPs; V_{hyp}, V_{dep} (from Figure 26 h). In basal dendrite and soma stimulations, Move periods amplitude were modulated to be different from V_{hyp} and undistinguishable from V_{dep}.

Overall, optogenetic stimulations during awake recordings seem to reproduce the compartment-specific, state-dependent modulations that inputs undergo when the stimuli are applied and recorded in anesthetized mice (Paragraphs 3.5, 3.6.1 and 3.6.2). This lends confidence to the assertion that such state-dependent modulations are not an artifact of anesthesia and additionally suggests that these modulations have a function in the synaptic input integration during the processing of information. Moreover, awake moving periods provided an opportunity to test the effect of an active desynchronized brain state on the process of input integration, shedding light on yet another interesting effect that appears to be confined to the apical compartment.

Nevertheless, because of the relatively small dataset that could be obtained during experiments on awake animals due to the intrinsic difficulty in extracting meaningful signals that rise above the highly variable V_m oscillation that occurs during awake recordings, future studies will be required to enlarge this dataset and examine this surprising finding in more detail.

3.9 Postsynaptic mechanisms of state-dependent changes in synaptic integration

What postsynaptic mechanisms could account for the state-dependent gain modulation of basal inputs during slow network oscillations? Considering that somatic stimulations elicit a flow of current directly at the recording site, I first investigated whether the $_{soma}$OP was influenced by differences in the mean V_m

3.9.1 Somatic modulation can be mimicked by depolarizing current injection

Through the injection of a positive current, the Downstate V_m can be depolarized to the level of an Upstate. This Upstate 'Isopotential' will preserve the low input and V_m variability of Downstate, permitting a discrimination between the relative effects of the Upstate components on the ways OPs are modulated (Figure 29 a).

There are significant differences between the averaged $_{soma}$OPs triggered in Downstates and Isopotential (Iso) based on the pre-stimulus V_m (Down -66.25 ± 2.21 mV vs. Iso -50.06 ± 5.23 mV, n = 10, p = 0.0019), but not between Upstates and Isopotential (Up -50.41 ± 2.5 mV vs. Iso -50.06 ± 5.23 mV, n = 10, p = 0.7695). This makes the Isopotential a good simulator of Upstate V_m (Figure 29 b, e).

$_{Soma}$OP response amplitudes are significantly smaller in the Isopotential compared to Downstate (Down 2.61 ± 0.97 mV vs. Iso 2.16 ± 0.76 mV, n = 10, p = 0.0019) but do not significantly differ from the Upstate (Up 1.98 ± 0.71 mV vs. Iso 2.16 ± 0.76 mV, n = 10, p = 0.0644; Figure 29 c, d, f). In the same way, the half widths of $_{soma}$OP Isopotentials are significantly longer than those of Downstates (Down 20.91 ± 3.46 ms vs. Iso 30.85 ± 6.75 mV, n = 10, p = 0.0019) but similar to those of Upstates (Up 29.38 ± 6.49 ms vs. Iso 30.85 ± 6.75 mV, n = 10, p = 0.4922; Figure 29 c, d, g).

Both $_{soma}$OP amplitudes and state-dependent modulations of half widths can be replicated by simulating the Upstate V_m alone, suggesting that the depolarized mean V_m during network activity is mainly responsible for state-dependent modulations, at least at the soma. Moreover, since V_m variability and synaptic inputs increase in Upstates but are the same during the Downstate and Isopotential, this indicates that these variables have negligible effects on the modulation of somatic inputs.

Since the depolarized V_m is the factor mainly responsible for the reduction of $_{soma}$OP amplitude, the variation can be explained by the difference in the driving force between the two V_m levels.

Like other unspecific cationic channels, which are physiologically responsible for EPSPs in pyramidal neurons such as AMPA and NMDA, the ChR2 variant used here (T159C) has a V_{rev} at around 0 mV (Berndt et al., 2011). This means that activating these channels at different negative V_m values will produce a depolarization whose amplitude will be proportional to the difference between this V_m and 0 mV. The expected Upstate amplitude predicted by the described formula (Paragraph 2.8.8, Equation 1) is very similar to that

actually measured in Upstates (Up 1.98 ± 0.71 mV vs. Exp 1.99 ± 0.73 mV, n = 10, p = 0.6953).

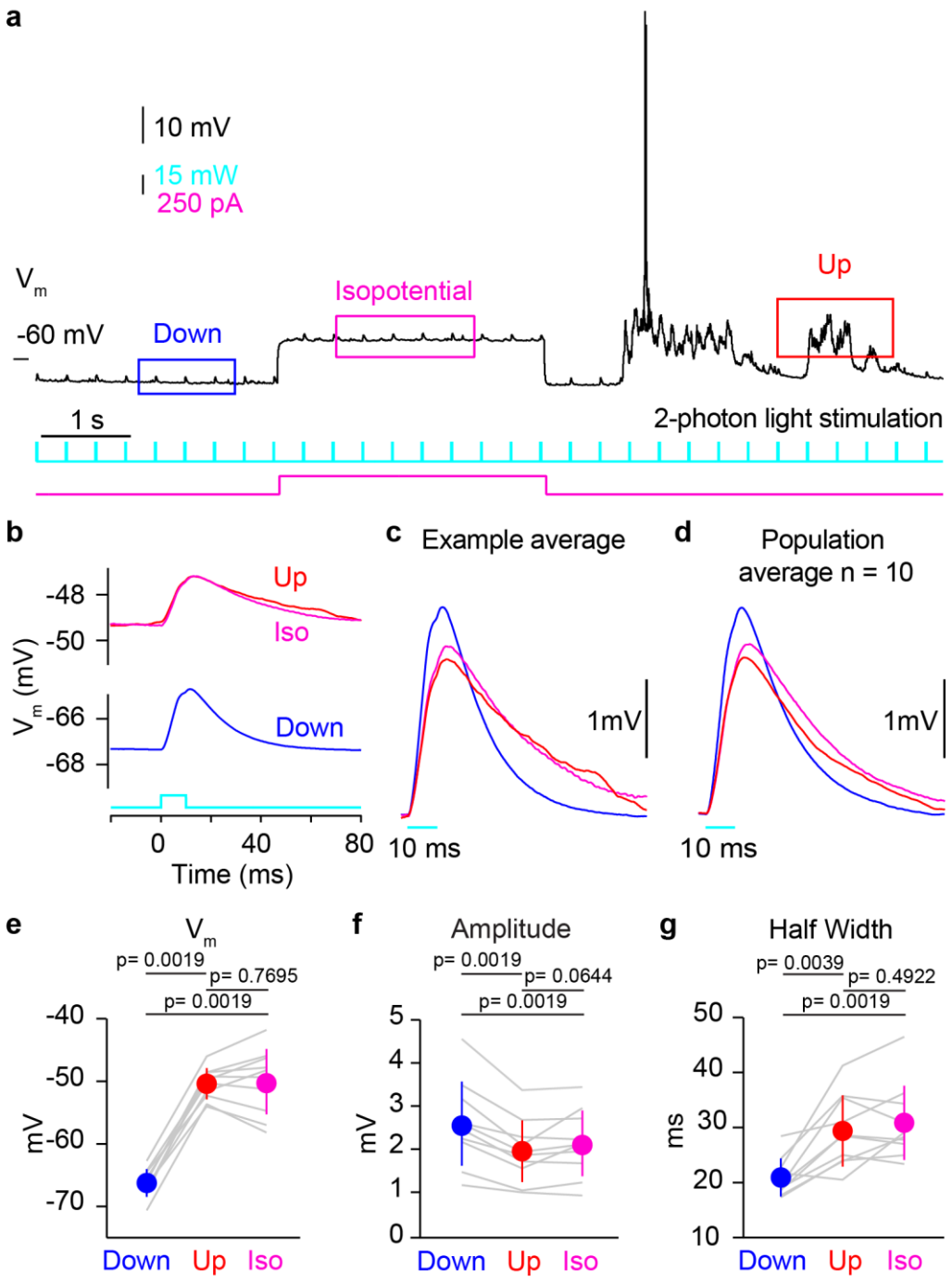

Figure 29. **Somatic Downstate current injection causes a reduction in $_{soma}$OP amplitude as observed during Upstates.**

a. Membrane potential recording of an example neuron during Downstate (blue box), Upstate (red box) and current injection during Downstate depolarizing the V_m to the same level of Upstates (Isopotential, magenta box), with time points of optogenetic stimulation below (cyan). **b**. Mean responses during Down (blue), Up (red) and Isopotential (magenta), highlighting the similarity of the mean V_m in Upstate and Isopotential. **c**. Same example traces as in (**b**) but overlaid to highlight differences in amplitude and half width. **d**. Overlay of the population averages of $_{soma}$OP during

Downstate, Upstate and Isopotential. **e**. Mean resting V_m during Down, Up and Isopotential. This displays the lack of difference between Upstate and Isopotential V_m. **f**. Amplitude of $_{soma}$OP is reduced in Upstates and during somatic current injections as compared to Downstates. **g**. Half width of the $_{soma}$OP is increased in Upstates and during injections of current in Isopotential trials compared to responses during Downstates. Grey lines show data from individual cells; the filled circles with bars show the mean ± S.D..

These results are in line with a model in which the driving force plays a major role in amplitude attenuation, at least in the somatic compartment. This cannot, however, explain the unexpected increase in half width.

3.9.2 The influence of network activity on somatic input resistance

While the reduction in somatic responses observed in the experiments can be predicted based on the increase in baseline V_m, this cannot explain how small basal responses are amplified in depolarized states. One clue might lie in the increase in the half widths of $_{basal}$OPs, which may indicate a change in the cellular input resistance during different states.

The average depolarized V_m during the active cortical Upstate is determined by a sudden increase in synaptic inputs throughout the whole cell body and branches. There is an increase in both excitatory and inhibitory input from synapses; however, since the overall result is a mean V_m depolarization, Upstates are considered periods of increased excitation. During these phases, the V_m is closer to the threshold at which an action potential is generated, and spikes are more likely to occur than in Downstates. Another effect of the intensification of synaptic input in Upstates is an overall increase in the conductance of the cell membrane that in turn changes the conductive properties of dendrites (Destexhe et al., 2003; Spruston, 2009). This means that during Upstates, an input arriving at a synaptic site will encounter a number of open channels that will affect its propagation to the soma by leaking its current (Spruston, 2009). This eventually results in a shortening of the membrane time constant and subsequently the input potential kinetics, and hence in a reduction of the total charge that is transmitted to the soma.

Upstates are thus considered states of high conductance characterized by a lower input resistance (IR) in comparison to the silent Downstate (Williams, 2004). While this may be the case for other neurons in the brain (Destexhe et al., 2003; Destexhe and Paré, 1999), layer 2/3 pyramidal cells have been found to reverse this pattern (Mateo et al., 2011; Waters and Helmchen, 2006). In fact, the recordings of layer 2/3 cortical neurons presented here

reveal an increase in somatic input resistance and the decay time constant, despite an increase in synaptic activity during activated states (Figure 30 and Figure 32 a - d).

Upon injecting brief (80 ms), hyperpolarizing current pulses (-100 pA), while recording the change in V_m during spontaneous state fluctuation, I found a significant increase in IR during Upstates (Down IR, 44.8 ± 7.3 MΩ vs. Up 59.1 ± 10.1 MΩ, n = 7, p = 0.0156) (Figure 30 b, e, h (0 pA)) and a prolongation of the time constant (Tau) (Down tau 7.3 ± 1.7 ms vs. Up 9.4 ± 1.7 ms, p = 0.0156) (Figure 30 e, i (0 pA)). This despite the increase in V_m (Down V_m -63.9 ± 2.8 mV vs. Up -52.2 ± 3.5 mV, p = 0.0156) (Figure 30 b, e, g (0 pA)).

To test whether this input resistance increase is dependent on the depolarized V_m in Upstate, I applied the same steps of hyperpolarizing current while holding the V_m resting potential to a depolarized state by constantly injecting 200 pA. The depolarized-Down V_m was different from the Downstate V_m (Down V_m -63.9 ± 2.8 mV vs. Down+200 -49.1 ± 5.0 mV, p = 0.0156) but not from an Upstate V_m (Down+200 V_m -49.1 ± 5.0 mV vs. Up -52.2 ± 3.5 mV, p = 0.0156) (Figure 30 a, d, g). This resulted in an increase in input resistance (Down IR, 44.8 ± 7.3 MΩ vs. Down+200 75.6 ± 16.8 MΩ, p = 0.0156) (Figure 30 d, h) and time constant with V_m depolarization (Down tau 7.3 ± 1.7 ms vs. Down+200 14.4 ± 5.1 ms, p = 0.0156) (Figure 30 d, i).

In contrast, holding the potential to a more hyperpolarized V_m by constantly injecting -200 pA (Down V_m -63.9 ± 2.8 mV vs. Down-200 -72.3 ± 1.4 mV, p = 0.0156) (Figure 30 c, f, g) led to a decrease in input resistance (Down IR, 44.8 ± 7.3 MΩ vs. Down-200 36.8 ± 9.8 MΩ, p = 0.0156) (Figure 30 f, h) and time constant (Down tau 7.3 ± 1.7 ms vs. Down-200 3.6 ± 0.6 ms, p = 0.0156) (Figure 30 f, i).

This implies that in L2/3 pyramidal neurons the V_m directly influences input resistance, counteracting its trend toward decrease due to channel openings which occur in active states. Additionally, this effect seems to reach a plateau for hyperpolarized potentials, where despite the difference in V_m in Down- and Upstates (Down-200 V_m -72.3 ± 1.4 mV vs. Up-200 -63.1 ± 2.2, p = 0.0156) (Figure 30 c, f, g -200), there is no difference in input resistance (Down -200 IR 36.8 ± 9.8 MΩ vs. Up- 200 40.6 ± 9.7 MΩ, p = 0.2812) (Figure 30 f, h -200) or time constant (Down- 200 tau 3.6 ± 0.6 ms vs. Up-200 4.6 ± 1.4, p = 0.1562) (Figure 30 f, i -200).

This effect can be related to anomalous rectification (Waters and Helmchen, 2006) and might be explained by the action of a voltage-dependent channel which has a dynamic range of activation at V_m between Up- and Downstates that causes it to act differently during the state change. Voltage-dependent channels responsible for a persistent inward sodium current

(Na_P) have an activation threshold of ~ -55 mV (French et al., 1990). Moreover sodium currents have been linked to the increase of IR in Upstate in L2/3 neurons (Sutor and Zieglgänsberger, 1987) thus the activation of Na_P might be responsible for this anomalous rectification.

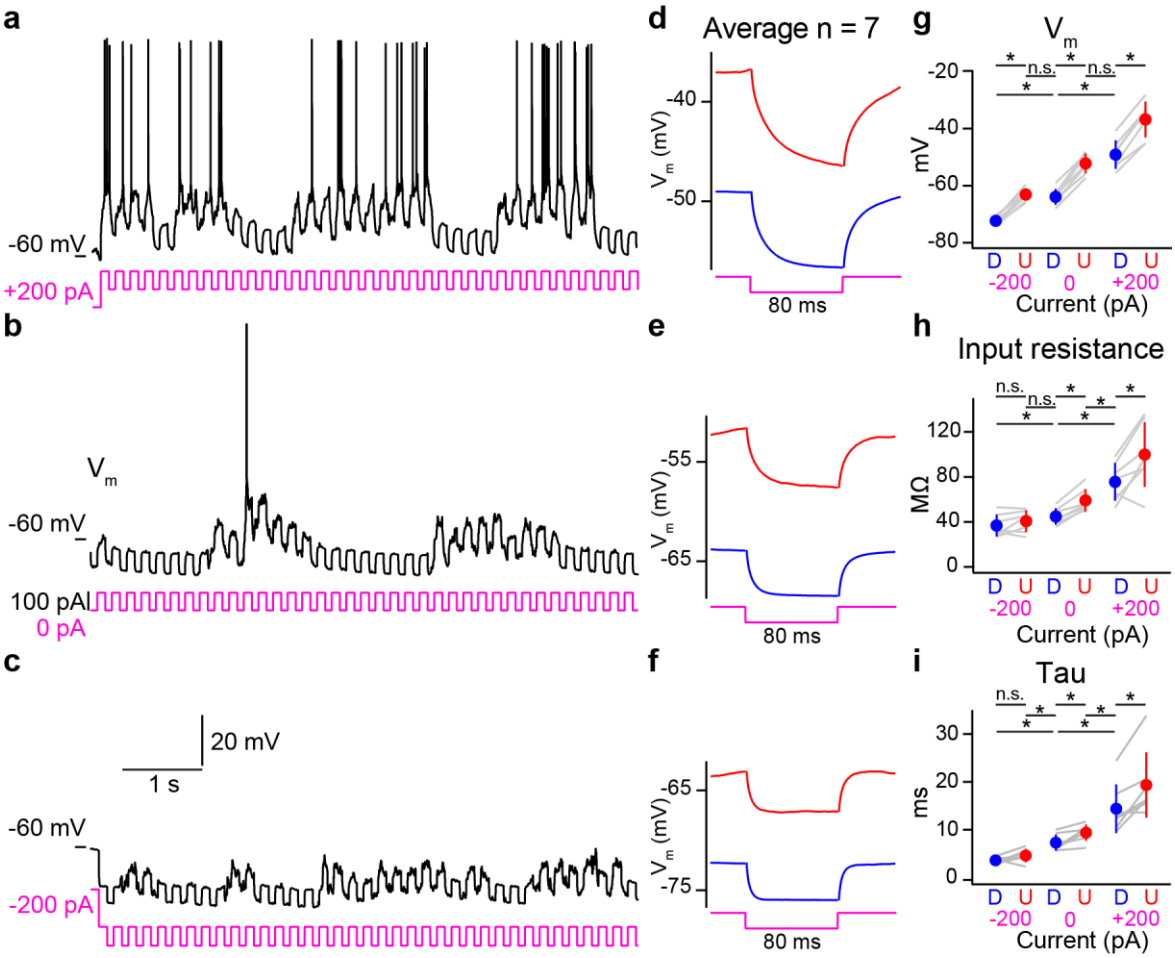

Figure 30. **Input resistance increase in Upstates is determined by change in V_m.**
a. Example whole-cell recording showing the negative current injection pulses (-100 pA, 80 ms, magenta trace) that were used to measure somatic input resistance on top of a tonic depolarization obtained with positive current injection of +200 pA. **b**. The same cell but without the holding potential. **c**. Again the same cell, but with tonic hyperpolarizing -200 pA current injection. **d**. Population average membrane potential (V_m) response to hyperpolarizing current injection pulses during Downstate (blue) and Upstate (red) from depolarizing holding potentials (+200 pA) (**a**). **e**. Same as (**d**) but without the holding potential (0 pA) (**b**). **f**. Same as (**d**) but for hyperpolarizing holding potentials (-200 pA) (**c**). **g**. Mean V_m during Down- (D) and Upstates (U) during the injection of -200, 0 and 200 pA holding potential currents. **h**. Input resistance and **i**. Tau increase with V_m depolarization. Grey lines show data from individual cells; filled circles with bars show the mean ± S.D.; * = $p < 0.05$; n.s. = not significant.

3.9.3 Combined effect of driving force and input resistance on the total transmitted charge

As neurons oscillate between a hyperpolarized Downstate and a depolarized Upstate, the driving force and input resistance seem to have opposing effects on OPs. While the driving force reduces amplitude of OPs, input resistance increases them, causing a prolongation of the kinetics in Upstates.

If a sum is made of the amplitude that is transmitted through the entire kinetics of the depolarized potential, the result is a measure of the total charge delivered by a single OP. Since is the spatial and temporal summation of EPSPs and IPSPs that determines whether the action potential threshold can be reached, the total charge represents the impact that a given input has on the subthreshold signal integration of the neuron. The total charge is represented by the area under the depolarization curve, from onset to decay time on the temporal axis and from pre-stimulus V_m up to the peak amplitude value on the V_m axis. Thus, the total charge can be calculated with an integral.

$_{Soma}$OPs in anesthetized recordings show no difference in the total charge that is transmitted, in comparisons of Down- and Upstate averaged integrals (somatic Down integral 39.8 ± 31.4 mV × ms vs. Up 43.9 ± 37.6 mV × ms, n = 16, p = 0.2978) (Figure 31 a). This implies that the decrease in amplitude and increase in half width (Figure 17 d, f, g) compensate for each other and normalize the total charge between the states. On the contrary, for $_{apical}$OPs, the constant half width (Paragraph 3.6.1, Figure 20 b, e) does not suffice to compensate for the large reduction of amplitude (Figure 20 b, d), also leading to a total charge reduction in Upstates (Apical Down integral 9.9 ± 6.2 mV × ms vs. Up 6.8 ± 5.8 mV × ms, n = 30, p = 0.0047) (Figure 31 b). On the other hand, $_{basal}$OPs showed no overall change in amplitude in comparisons of Up- and Downstates but rather a prolongation of the kinetics (Figure 20 g, i, j), therefore achieving a larger total charge in Upstates (Basal Down integral 8.4 ± 5.7 mV × ms vs. Up 11.5 ± 8.9 mV × ms, n = 48, p = 0.0036) (Figure 31 c).

Additionally, plotting the Up:Down integral ratio of $_{basal}$OPs as a function of the integral in the Downstate reveals an enhancement of the gain modulation observed for the amplitudes (Figure 21 h), with a significant correlation (Up:Down integral vs. lg Down integral, r = -0.48, p = 0.0006) (Figure 31 d). Up:Down ratios show an increase of up to 15 fold for smaller inputs, meaning that the total charge dramatically increases the impact of the gain modulation on dendritic integration.

In awake recordings as well, the total charge of somatic stimulation is normalized across the two quiet states and the moving period (Somatic V_{hyp} integral 27.6 ± 15.0 mV × ms vs. V_{dep} 30.4 ± 28.8 mV × ms, n = 9, p = 1; V_{hyp} vs. Move 24.1 ± 15.0 mV × ms, p = 0.3594; V_{dep} vs. Move, p = 1) (Figure 31 e). For awake $_{apical}$OP averaged integrals, V_{dep} is smaller than V_{hyp} and Move periods, however Move $_{apical}$OPs are larger than V_{hyp} although the difference is not significant (Apical V_{hyp} integral 20.7 ± 17.6 mV × ms vs. V_{dep} 12.0 ± 19.8 mV × ms, n = 9, p = 0.0273; V_{hyp} vs. Move 29.1 ± 24.8 mV × ms, p = 0.0976; V_{dep} vs. Move, p = 0.0039) (Figure 31 f).

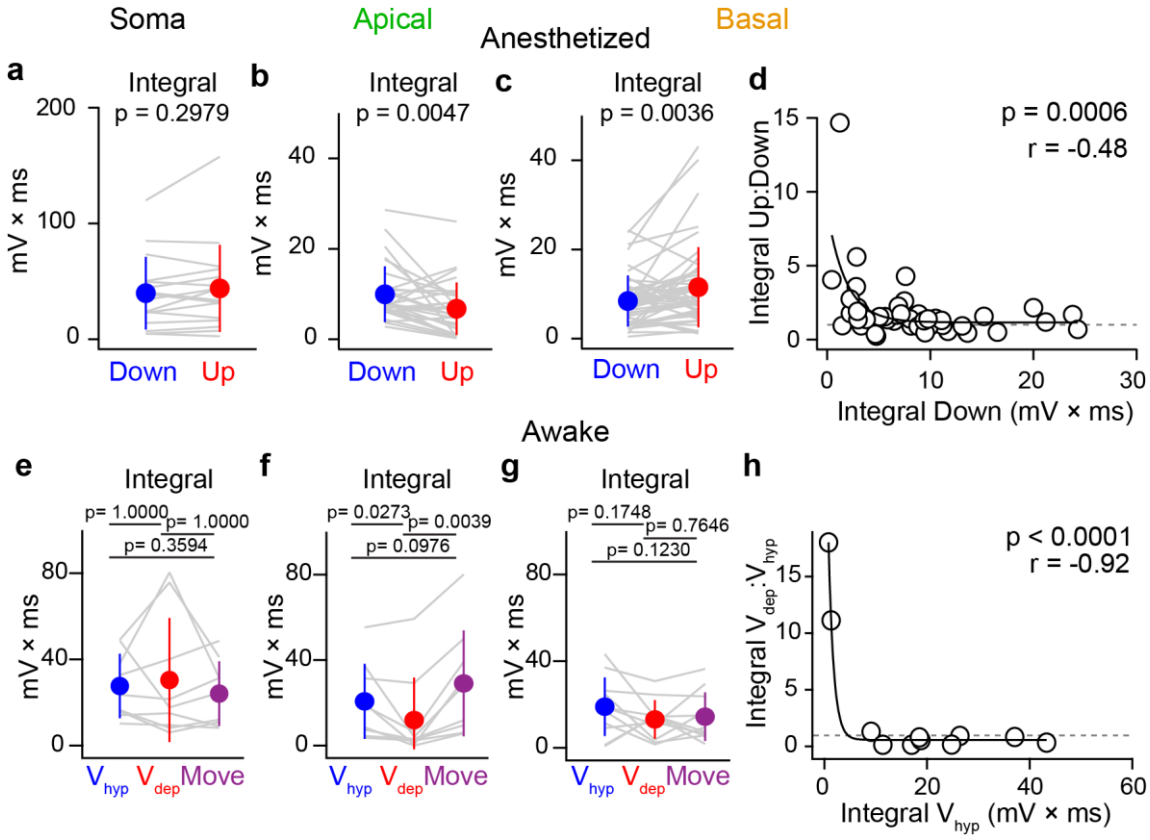

Figure 31. **Influence of network activity on the total charge of OPs in recordings from anesthetized and awake mice.**
a. Averaged $_{soma}$OP integral in anesthetized mice. No difference in the Up- and Downstate total charge. **b**. Input reduction in the Upstate is also observed for the $_{apical}$OP total charge. **c**. Overall increase of the $_{basal}$OP total charge during Upstates. **d**. Significant correlation of Up:Down $_{basal}$OP integral ratio and Downstate $_{basal}$OP lg integral. The gain modulation of the integral is enhanced in comparison to the amplitude (Figure 21 h). **e**. Averaged $_{soma}$OP integral in awake mice. Averaged total charges in V_{dep}, V_{hyp} and Move periods are normalized. **f**. In apical dendrites, the V_{dep} total charge is reduced in comparison with V_{hyp} and Move, and Move is enhanced in comparison to V_{hyp}, though not significantly. **g**. No overall difference among total charges in basal dendrites. **h**. Significant correlation of V_{dep}:V_{hyp} $_{basal}$OP integral ratio and V_{hyp} $_{basal}$OP lg integral. Gain modulation of integral is enhanced in comparison to the amplitude (Figure 27 c).

This increase in Move versus V_{hyp} does not appear as a change in amplitudes (Paragraph 3.8.4, Figure 28 e, g), implying that the impact of movement on $_{apical}$OPs might be greater in enhancing the summation and propagation of inputs. On the contrary, on basal dendrites I found no difference across the three oscillation periods in influencing the averaged $_{basal}$OP integrals (Basal V_{hyp} integral 19.0 ± 13.4 mV × ms vs. V_{dep} 13.1 ± 8.9 mV × ms, n = 11, p = 0.1748; V_{hyp} vs. Move 14.4 ± 11.2 mV × ms, p = 0.1230; V_{dep} vs. Move, p = 0.7646) (Figure 31 f). This result in basal dendrites of awake mice is different from the same observed in anesthetized ones (Figure 31 c). However, because there is a gain modulation depending on the distribution of input in Downstate (or V_{hyp}), for which in awake recordings the dataset is limited for small inputs (compare Figure 21 i to Figure 27 d), a comparable distribution would probably produce the same result also in awake. Indeed, awake gain modulation of $_{basal}$OP integrals, as in anesthetized, is enhanced in comparison to gain modulation of amplitudes (Figure 27 c), with a significant correlation (V_{dep}:V_{hyp} integral vs. lg V_{hyp} integral, r = -0.92, p < 0.0001) (Figure 31 h).

Therefore, the analysis of the total charge provides a means of understanding the ways different state-dependent modulations act on the amplitude and kinetics of inputs and to estimate the impact that specific inputs have on their subthreshold integration. In summary, the total change in Up- and Downstates is normalized for somatic inputs, reduced for those arriving from apical dendrites and enhanced for basal inputs. In awake Move periods, integrals are larger in apical dendrites. Finally, the gain modulation from stimuli arriving via basal dendrites is dramatically enhanced in relation to the total charge.

3.9.4 Synaptic gain modulation of basal inputs is blocked by intracellular applications of voltage-dependent sodium channels using QX-314

What channels might be responsible for the different types of modulations which occur during network activity? Sodium persistent Na_P channels have been reported to influence the integration of EPSPs by affecting both amplitude and kinetics (González-Burgos and Barrionuevo, 2001; Stuart and Sakmann, 1995) and sodium currents have been linked to the input resistance increase with depolarization, responsible for anomalous rectification in L2/3 pyramidal neurons (Sutor and Zieglgänsberger, 1987). A prior study showed that increases in somatic input resistance can be blocked by intracellular applications of QX-314, a voltage-gated sodium channel (Na_V) antagonist (Waters and Helmchen, 2006). Therefore I next

administered 1 mM QX-314 (QX) into the intracellular solution and, after waiting > 5 minutes for it to perfuse, I stimulated basal dendrites in Down- and Upstates.

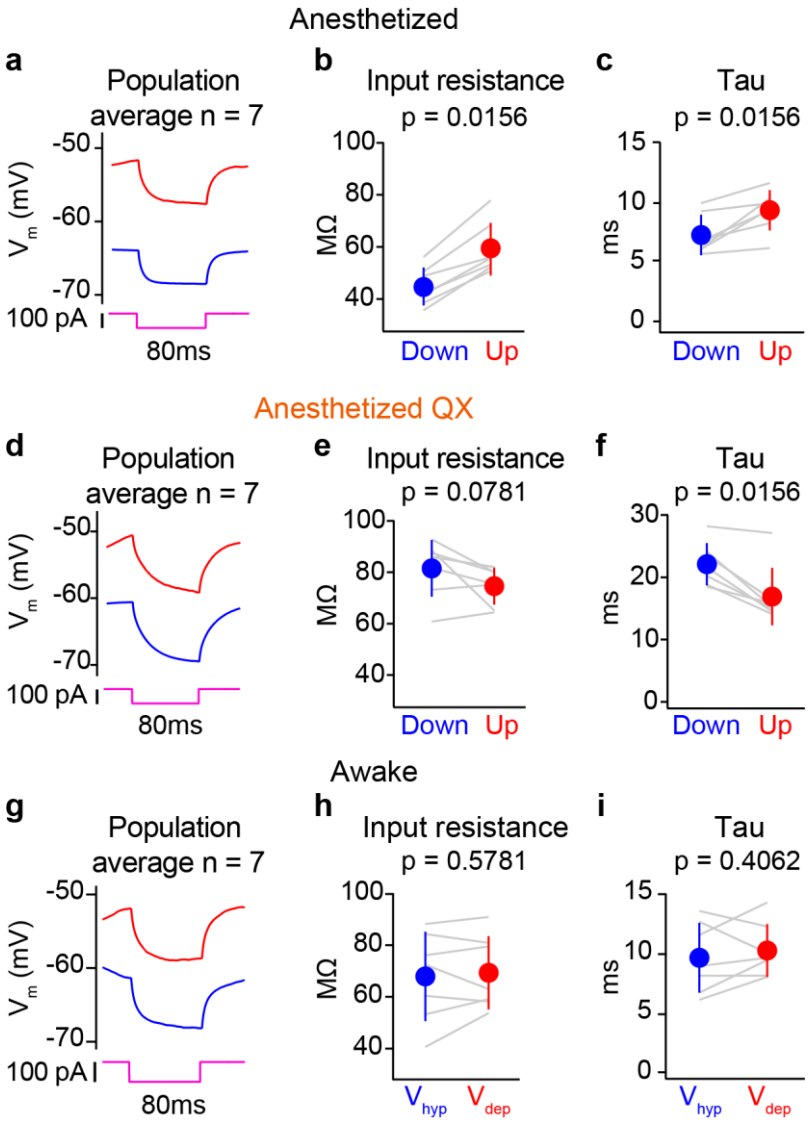

Figure 32. **The increase in input resistance during Upstates is blocked by the intracellular application of QX-314.**
a. Population average membrane potential (V_m) response to hyperpolarizing current injection pulses during Downstate (blue) and Upstate (red). **b**. Input resistance and **c**. Tau increase in Upstates. Grey lines show data from individual cells; filled circles with bars show the mean ± S.D.. **d**. - **f**. Same as (**a** - **c**) but with 1 mM QX-314 in the intracellular solution. Note the reduction (not significant) of input resistance (**e**) and time constant (Tau) (**f**) in comparison of Down- to Upstates. **g**. - **i**. Same as (**a** - **c**) but from awake resting mice during slow network activity split by pre-stimulus V_m.

The application of QX blocked the generation of action potentials, but neurons maintained a normal resting V_m (-60.64 ± 4.57 mV, n = 18) and subthreshold activity. Compared to control Downstate responses, there were increases in both the QX-Downstate input

resistance (Control-Down 44.8 ± 7.3 MΩ vs. QX-Down 81.5 ± 11.0 MΩ, n = 7, p = 0.0156) and QX-Downstate time constant (Control-down 7.3 ± 1.7 ms vs. QX-down 22.1 ± 3.4 ms, n = 7, P = 0.0156). Moreover, during QX-Upstates the input resistance showed no significant change (QX-Down 81.5 ± 11.0 MΩ vs. QX-Up 74.6 ± 7.2 MΩ, n = 7, P = 0.0781), but the time constant decreased (QX-Down 22.1 ± 3.4 ms vs. QX-Up 16.9 ± 4.6 ms, n = 7, p = 0.0156) (Figure 32 d, e, f).

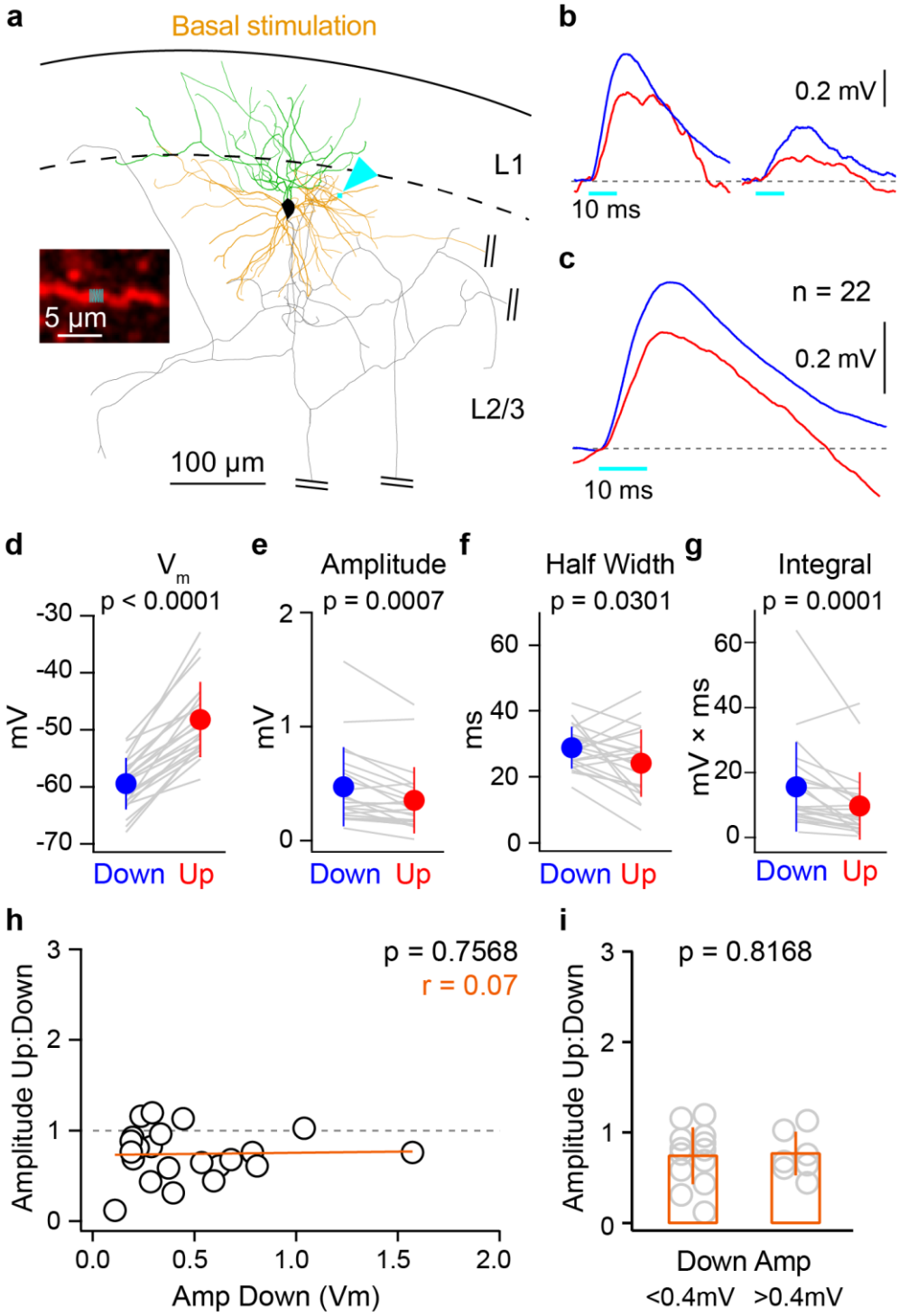

Figure 33. **Gain modulation of basal inputs is blocked by intracellular applications of QX-314**.
a. Biocytin reconstruction of example cell in an optogenetic stimulation experiment targeting a basal dendrite, showing the apical (green) and basal (orange) dendrite, the axon (grey, truncated) and the location of optogenetic stimulation (cyan arrow). Inset shows *in vivo* image of an Alexa-594 filled dendrite in red and the optogenetic stimulation site in cyan. **b**. Mean representative $_{basal}$OPs of both large and small amplitudes show a reduction in amplitude from Down- (blue) to Upstates (red) during whole-cell recordings with 1 mM QX-314 added to the intracellular solution. **c**. The mean $_{basal}$OP of the population is reduced during the intracellular application of QX-314 in Upstates. **d**. V_m increases as neurons go from Down- to Upstates during experiments using intracellular QX-314. Grey lines show data from individual cells; filled circles with bars represent the mean ± S.D.. **e**. A significant reduction of $_{basal}$OP amplitude in Up- compared to Downstates. **f**. Half width is significantly smaller in Upstates than in Downstates. **g**. The total charge reduction is highly significant and more pronounced than the amplitude. **h**. No correlation between the state modulation of $_{basal}$OP amplitude and the lg of Downstate $_{basal}$OP amplitude. Open circles represent mean responses from a single cell; orange line shows the linear fit. **i**. No significant difference in the same data as in (**h**) but divided into two groups of amplitude based on Downstate $_{basal}$OP amplitude.

The application of QX-314 caused a reduction in the amplitude of $_{basal}$OPs during Upstates (QX-Down amplitude 0.47 ± 0.35 mV vs. QX-Up 0.35 ± 0.29 mV, n = 22, p = 0.0007) (Figure 33 a - e); they also exhibited a reduction similar to that expected from the reduction in driving force (QX-314-Up 0.35 ± 0.29 mV vs. QX-Expected 0.37 ± 0.27, n = 22, p = 0.3053) (Equation 1). Moreover, QX-314 led to a reduction in half width during Upstates (Down half width 28.77 ± 6.34 ms vs. Up 24.10 ± 10.15 ms, n = 22, p = 0.0301) (Figure 33 c, f), in contrast to the increase observed in control OPs (Figure 20 g, j). Overall this produced a dramatic reduction of the total charge that was transmitted (Down integral 15.5 ± 13.8 mV × ms vs. Up 9.7 ± 10.3 mV × ms, n = 18, p < 0.0001) (Figure 33 g).

This indicates that QX-314 blocked the state-dependent increase in amplitude that otherwise occurred with small $_{basal}$OPs in Upstates (for basal amplitudes < 0.4 mV, control Upstate amplitude 0.32 ± 0.14 mV, n = 30 vs. QX-Upstate amplitude 0.19 ± 0.09 mV, n = 13, p = 0.0024). Additionally, no significant correlation was detected when plotting the ratio of Up:Down $_{basal}$OP amplitude as a function of the Downstate amplitude during applications of QX-314 (Figure 33 h).

Applications of QX-314 resulted in a reduction of the $_{basal}$OP Up:Down amplitude ratio (for inputs < 0.4 mV) (Figure 33 i) to level similar to that observed in inputs from apical dendrites (inputs < 0.4 mV, Apical Up:Down OP amplitude 0.65 ± 0.34, n = 16 vs. Basal QX Up:Down OP amplitude 0.74 ± 0.31, n = 13, p = 0.5026) (Figure 34).

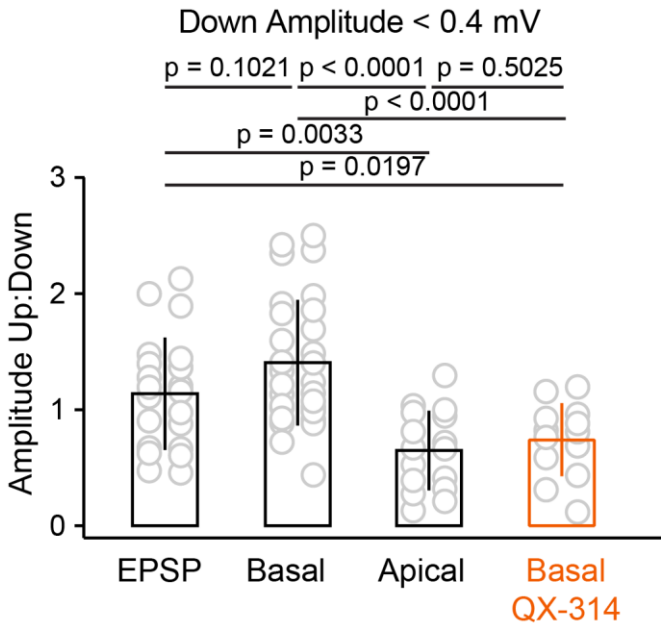

Figure 34. **Small basal input approximates to apical input under QX-314.**
The ratios of the Up:Down amplitude for small amplitude (< 0.4 mV) $_{u}$EPSPs and $_{basal}$OPs are significantly larger than for $_{apical}$OPs and $_{basal}$OPs during intracellular QX-314 application. Grey open circles show data from single cells, bars show mean ± S.D..

In summary, QX-314 has a dual effect on the state-dependent modulations reported in this study: it blocks anomalous rectification, which is responsible for the increase of IR during Upstates, and it abolishes the gain modulation of inputs from basal dendrites. Since QX-314 mainly blocks sodium Na_V channels (Strichartz, 1973), and the persistent sodium Na_P currents have been reported to influence synaptic input integration by modulating amplitude and kinetics of EPSPs (González-Burgos and Barrionuevo, 2001; Stuart and Sakmann, 1995), this suggests that Na_P channels may be involved in the gain modulation of basal dendritic inputs.

This indicates that the gain modulation of basal dendritic inputs reported here for $_{basal}$OP (Paragraph 3.6.2) and $_{u}$EPSPs (Paragraph 3.7.2) may be dependent on postsynaptic, cell-intrinsic mechanisms, which influence the integration of inputs to a network level, as shown by the modulation of VPM connections (Paragraph 3.7.1).

4 DISCUSSION

In recent years, developments in electrophysiological, optical, molecular and behavioral methods have dramatically advanced the study of the living brain. New *in vivo* experiments are shedding light on how network activity changes and shapes information processing, sensory perception and cellular interactions (Barth and Poulet, 2012; Buzsáki, 2006; Destexhe et al., 2003; Grienberger et al., 2015; Lee and Dan, 2012; Petersen and Crochet, 2013; Steriade, 2001; Stuart and Spruston, 2015). The goal of my thesis was to examine the impact of network activity on synaptic integration in cortical pyramidal neurons *in vivo*.

I studied the integration of single excitatory synaptic inputs in L2/3 pyramidal neurons of the primary somatosensory cortex of the mouse in the context of network activity. Because these neurons display a functional and anatomical separation of their dendritic arbors (DeFelipe and Fariñas, 1992; Larkum, 2013; Shipp, 2007), I hypothesized that synaptic integration in active networks may depended on the input site. To test this hypothesis I applied optogenetic stimulation to apical or basal compartments and measured how network activity influenced synaptic integration.

Past *in vivo* studies have produced conflicting data on the ways network activity might influence single EPSP integration in distinct neocortical neurons. Some of these studies relied on sensory (Chadderton et al., 2014; Crochet et al., 2011; Longordo et al., 2013), electrical (Reig et al., 2015; Sachdev et al., 2004) or optogenetic stimulation (Mateo et al., 2011), but they did not resolve the exact locations of synaptic inputs. *In vitro* studies carried out on pyramidal neurons have shown that this factor plays a role in the outcomes of synaptic integration (Larkum and Nevian, 2008; Magee and Johnston, 2005; Major et al., 2013). Since *in vitro* studies take place in the absence of natural brain activity, only inferences could be made regarding the way network oscillations might transform the integration of input.

To study this question *in vivo* required solving technical problems. Two-photon glutamate uncaging permits a location-specific control of synaptic inputs *in vitro*, but its use in studying active networks *in vivo* is limited because of the uncaging compound directly modulating GABA channels (Maier et al., 2005). Another powerful method that could be applied to studies of monosynaptic $_{u}$EPSP integration during network activity would be paired

recordings *in vivo*. While this is probably the most physiological technique for doing so, there are challenges to its actual use: it is technically difficult, and the low connectivity rate of pyramidal neurons (~ 10%) result in a very low throughput (Jouhanneau et al., 2015). Moreover, in the absence of high-resolution methods to discern very fine anatomical structures, this technique does not normally resolve the specific locations of synaptic connections.

Since my question could really only be approached in a living brain, the solution I found was to combine genetic and optical approaches. I turned to Channelrhodopsin-2 (ChR2) as an alternative to glutamate uncaging. This protein can be expressed in genetically defined cell-types, thus avoiding a non-specific activation of inhibitory inputs, and can be rapidly activated by two-photon light stimulation (Nikolenko et al., 2007; Packer et al., 2012; Prakash et al., 2012). I established ChR2-expressing pyramidal neurons in mice and performed somatic whole-cell recordings of their activity *in vivo*. I used subcellular two-photon laser stimulation in a controlled, spatio-temporal manner to activate ChR2 in carefully selected regions of the cell (soma, apical and basal dendrites). Stimulation elicited depolarizing optogenetic potentials (OPs) that closely resembled $_{u}$EPSPs. I then repeated the measurements in mice during different brain states. I performed measurements in urethane anesthetized animals, during the spontaneous occurrence of Up- and Downstates, and in awake mice during periods of quite wakefulness or active forepaw movements.

Combining these experimental components in a new experimental method allowed me to study how brain states affect neuronal dendritic-specific integration of single inputs. I found that input from basal dendrites are normalized in amplitude during network activity, while input from apical dendrites are decreased in amplitude leading to a compartmentalization of synaptic processing in apical dendrites. My findings will ultimately contribute to our understanding of how neurons perform synaptic integration *in vivo*.

In the following discussion, I will focus first on the development of the technique, followed by a discussion of each set of results reported in the previous section. Finally I will draw my findings into a plausible hypothesis that serves not only as an interpretation, but also to suggest a number of interesting experimental and analytical directions for pursuing this work in the future.

4.1 *In vivo* ChR2 two-photon subcellular stimulation development

The discovery of ChR2 and its development as a tool for stimulating or inhibiting genetically identified neurons *in vivo* with millisecond precision has revolutionized neuroscience (Deisseroth, 2015). Together with the development of genetically expressing voltage and calcium sensitive indicators, it has originated a new sub-field of "optogenetics".

Recent developments have shown that two-photon microscopy can be used to perform a spatially confined stimulation with a precision down to micrometer resolution (Packer et al., 2012; Rickgauer and Tank, 2009; Vaziri and Emiliani, 2012; Zipfel et al., 2003). Moreover, thanks to the two-photon effect (Paragraph 1.5.2), regions between the objective and the target pose only small interference, thus optimizing light scattering and making the method suitable for the stimulation of internal brain structures *in vivo*. I took advantage of these findings to develop a method to stimulate single dendritic branches *in vivo* and mimic unitary synaptic inputs.

4.1.1 ChR2 expression *in vivo*

The first goal was to obtain a robust expression of ChR2 in pyramidal neurons of the superficial layers 2/3 in the primary somatosensory cortex (Paragraph 3.1.2). I initially employed a lentivirus as a viral vector, carrying the H134R variant (HR) of ChR2 fused to GFP while using CamKII$_\alpha$ as transcription promoter to limit expression exclusively to excitatory neurons (Jones et al., 1994; Liu and Jones, 1996). Lentiviral vectors produce a set of cells which express the transfected molecule that are confined to the immediate surroundings of the infection site (Figure 11 b); typically within this area, the majority of cells express the protein reporters. AAV vectors have some advantages: they can be obtained in titers of orders of magnitude higher than lentiviruses. The smaller size of the *virions* generally allow AAV infections to spread more homogenously and to a much larger area (Figure 11 d) (Aschauer et al., 2013). Thanks to the virtually absent immune reaction to these viruses, mouse brains can be subjected to billions of AAV particles without tissue health issues (Nathwani et al., 2011). AAVs allowed me to use stereotactic coordinates to target roughly the somatosensory cortex during viral injection, which ensured that neurons in the final primary somatosensory cortex (S1) target area would exhibit high levels of proteins. In addition, the higher number of viral particles per volume injected resulted in a higher, more rapid protein expression in the cells. During the move to AAVs, I also changed the reporter

protein to the enhanced version of GFP: the brighter, yellowish EYFP. Despite these improvements, the packed arrangement of pyramidal neurons in the neocortex and their profusely branching projections made it very difficult to target and patch the somata of expressing neurons and to identify dendrites belonging to one cell (Figure 11 a).

These issues can be overcome by the *in vivo* two-photon targeted electroporation of single cells (Paragraph 3.1.1). While this technique leads to high labeling specificity, it is technically challenging. Unfortunately, I was unable to obtain the expression levels achievable with AAVs, and even though the DNA concentration I was using was at the limit of its solubility in water, consistent OPs were obtained only from somatic or perisomatic areas. In addition, the high plasmid concentration often generated an overexpression of the fusion membrane protein that formed visible clusters along the dendrites, probably interfering with the physiological propagation of dendritic synaptic input and compromising the goal of the experiment. Additionally, brain tissue reaction issues (Paragraph 3.1.1), which were almost unavoidable after the first step of electroporation and during the expression period, made durectomy very difficult or sometimes impossible to achieve. Two-photon visibility was often blurred and the neurons that were recorded were frequently unhealthy. This increased the time required for the durectomy and shadowpatch to the point that only isoflurane anesthetics could be feasibly used. Isoflurane administration can be sustained for hours but it generates higher blood pressure than urethane, causing pulsations in the brain, which interfere with the stability of the recordings. Even though the electroporation throughput of about 75 % was in accordance with figures from the literature (Judkewitz et al., 2009), the combination of problems led to a total number of successfully patched and optically stimulated healthy neurons (~ 10 %) too low to obtain a dataset large enough for the purposes of my study. Moreover, due to the low expression, only perisomatic dendrites responded with OPs large enough after stimulation.

To try solve the problem of the protein clusters forming blebs on the dendrites of expressing neurons, I first tried a non-fused version of ChR2-EYFP that exploits the ribosome shipping site p2A (Gradinaru et al., 2010; Osborn et al., 2005; Prakash et al., 2012) which separately releases ChR2 as a membrane protein and EYFP in its original cytosolic version. This completely solved the issue of cluster formation, which had likely been due to the fact that the cell was expressing high quantities of large proteins, or perhaps to protein-protein interactions triggered by the fused version. Another advantage of using the split version of the ChR2-p2A-EYFP protein is that the EYFP reporter is soluble in the cytosol, which leads to higher accumulations of fluorophore in cellular regions where the surface-

volume ratio is low. This made somata brighter than the low volume of projections surrounding them (Prakash et al., 2012) (Figure 11 a, c). As a result, the p2A versions were highly suitable for viral infections, permitting the visualization and patching of cell soma even in areas with high numbers of EYFP-expressing cells.

At this point I moved back to AAV as the transfection method for ChR2, using an improved version of ChR2 called E123T/T159C (ET-TC) (Berndt et al., 2011) and the AAV serotype 2/9, which is more suitable for cortical infections (Aschauer et al., 2013). This increased the success rates from roughly 1 - 2 good recordings per 10 experiments to one or more per experiment. Additionally, thanks to the improved visibility and higher number of possible targets, I could return to urethane as the anesthesia and even perform experiments while the animals were awake. I used the red intracellular dye (Alexa-594) to target the dendrites of ChR2 expressing neurons. This technique worked but took 5 to 10 minutes for the dye to diffuse to the most distal dendrites and become visible in the red channel. In the future sparser viral infections may improve dendrite visibility and obviate the need for using intracellular dyes.

Using an AAV and this ChR2 variant, I managed to obtain more data of a higher quality in less time. Additionally, it was possible to elicit smaller OPs from dendritic spots of up to 40–50 µm from the soma. To increase the dendritic distance of responsiveness to light stimulation and OP amplitudes I tried to raise expressions levels by injecting more virus, up to 1 µl of viral solution and by prolonging expression times, up to 6 weeks. This effectively increased protein expression but unfortunately also resulted in a positive correlation between expression levels and the depolarization of neurons' resting potential. This in turn narrowed the window of usable neurons that had high enough expression levels of ChR2 to obtain distal dendritic OPs but not too high to produce a constant membrane depolarization at non-physiological levels (Figure 12). Attempting to widen the window of usability, I tried another ChR2 variant, T159C (TC), which ought to deliver more photocurrent. To my positive surprise, this variant had no effect on resting potential depolarization despite increased expression levels. Infections with AAV2/9 carrying ChR2(TC)-p2A-EYFP delivered very reliable and strong protein expression without affecting the health of the neurons even after 6 weeks. After 3 to 6 weeks of infection, it was possible to obtain robust and large OPs following stimulation < 30 mW on dendrites up to 150 µm from the soma.

Around 90% of the dataset reported here was obtained with the TC variant and the rest with ET-TC. The TC variant of ChR2 is known to deliver more photocurrent than the ET-TC but the responses are weakly voltage dependent (Berndt et al., 2011). However, from

somatic OP responses I obtained at different baseline membrane potential (V_m) values, I noticed no difference in the impact on the Up:Down response amplitude between the two variants (Figure 18). Moreover, the normalization of basal input amplitude was present using multiple techniques (paired recordings, thalamic stimulation). Together I therefore conclude that the intrinsic voltage dependence of the TC did not significantly influenced my results.

4.1.2 Two-photon scanned stimulation *in vivo*

As explained above (Paragraphs 1.5.2, 3.2 and Figure 14) the two-photon beam can deliver laser light with high intensity to a very spatially defined area (Denk et al., 1990; Zipfel et al., 2003). In control experiments on agar, the highest intensity of a stationary two-photon laser beam can be confined on less than a single micrometer on the focal plane. From this central point the intensity decreases quadratically in any direction. Axially the specificity is less confined and can be up to 5 to 10-fold lower. In a non-homogeneous, organic tissue such as the brain, light power delivery is heterogeneous at the focal plane and scattering may interfere with spatial specificity. But for short distances of penetration (< 200 μm) this effect is minimal (Packer et al., 2012; Rickgauer and Tank, 2009; Zipfel et al., 2003).

Nonetheless, this high spatial specificity is counterproductive in stimulating a single cell or subcellular spot (Andrasfalvy et al., 2010; Nikolenko et al., 2007). A stationary beam will activate only a small portion of the ChR2 proteins expressed on the membrane, thus delivering only a fraction of the potential photocurrent. Moreover, even a few milliseconds of exposure to a high-intensity, focused, steady two-photon laser may be enough to damage the stimulated cell. Some two-photon stimulation systems overcome this issue using temporal focusing (Andrasfalvy et al., 2010) or light sculpting (Papagiakoumou et al., 2010) that enlarges the beam's spatial alignment and reduces the power delivered per micrometer squared. I employed a fast scanning mode (Paragraph 2.5) (Packer et al., 2012) that moves the light beam to stimulate sequentially nearby spots on the cell surface, achieving a quasi-simultaneous activation of ChR2 in the area and avoiding overexposure to single focused points.

Ultimately, the method of subcellular two-photon stimulation proved to be reliable, reproducible and specific, generating a dataset of optogenetic potentials closely resembling real EPSPs. ChR2 expression was also reliable and strong, without major side effects. This should not imply that the method cannot be further improved: improved photosensitive

opsins with faster opening kinetics can be implemented and better stimulation parameters may be chosen to even more closely imitate the kinetics of EPSPs.

4.2 Spontaneous spiking and subthreshold activity in neocortex

Sub- and suprathreshold activities are interdependent modes by which neurons compute information. Excitatory and inhibitory inputs drive subthreshold activity, which consists of a continuous spatio-temporal summation, subtraction and integration of even the smallest perturbation of the V_m. Once the threshold is reached, all this analogical continuous fluctuation is commuted into discrete, all-or-none action potentials (AP), which are the expression of the neuronal output (Purves, 2008). During the suprathreshold mode, large Na^+ currents completely overtake V_m dynamics, leading to depolarizations that are rapid and large, while input resistance and driving force undergo a dramatic decrease (Destexhe et al., 2003; Waters and Helmchen, 2006).

$_U$EPSPs between pyramidal neurons are small amplitude depolarizing potentials (about 0.5 mV as measured at the soma), which means that usually several inputs are thought to be required to create a sum which reaches the AP threshold. Single action potentials have been reported to perturb the network's spontaneous firing activity to the point that a single extra spike of a neuron can increase the firing rate of its postsynaptic targets (London et al., 2010). Such a single action potential will produce an $_u$EPSPs in one or more postsynaptic cells, implying that each EPSP in turn may influence a neuron's firing rate (Häusser et al., 2000).

Both the subthreshold membrane potential fluctuations and firing rate output of the neuron can be influenced by different network activity states. During an active state, whether it is an Upstate under anesthesia or a depolarized V_m (V_{dep}) phase, or a movement (Move) period in the awake brain, the average V_m is more depolarized than in a Downstate or in hyperpolarized (V_{hyp}) phases, putting it closer to the AP threshold. Consequently, spontaneous cell firing and synaptic transmission between local pyramidal neurons happens exclusively during these depolarized phases (Destexhe et al., 2003; Steriade, 2001).

The data here comprises anesthetized and awake recordings, somatic and dendritic stimulations during different types of network activity. I have found no evidence of a significant impact of an OP on the spontaneous neuronal firing rate of a pyramidal neuron throughout my dataset (Paragraph 3.3, Figure 16). This suggests that neurons require a synchronous, perhaps clustered excitatory input to change their output behavior (Larkum and Nevian, 2008; Takahashi et al., 2012). Nevertheless, studying how a single isolated

excitatory potential is integrated during subthreshold activity is of pivotal importance in understanding the way neurons compute the multiple simultaneous inputs to which they are normally subjected, and which are ultimately responsible for their suprathreshold activity. I therefore decided to focus this study exclusively on subthreshold activity.

4.3 Cortical states in anesthetized and awake mice

The first part of this study, which represents the majority of the dataset, was conducted under urethane anesthesia. This anesthetic exerts a depressive function on neuronal brain activity by facilitating inhibitory and modulatory inputs through the potentiation of $GABA_A$, Glycine and nicotinic acetylcholine receptors and by inhibiting excitatory input interfering with AMPA and NMDA receptors activation (Hara and Harris, 2002). However, urethane has been reported to cause only a minimal disruption of signal transmission in the neocortex (Sceniak, 2006). In animals, anesthesia induces unconsciousness and an absence of pain and it can replicate natural brain activities such as slow wave sleep. Urethane triggers a state that is closer to natural sleep cycles than other anesthetics (Clement et al., 2008). Under anesthesia, cortical neurons' V_m undergo a bimodal distribution that can be divided in synaptically active, depolarized Up- and synaptically quiescent, hyperpolarized Downstates (Destexhe et al., 2003; Waters and Helmchen, 2006) (Paragraph 2.8.4, Figure 7). Comparing how the information flow in the brain is influenced by these two modes of network activity can help unravel the impact of synaptic activity on neurons and, ultimately, contribute to our understanding of the functions of cortical states in the brain.

During Downstates, neurons receive virtually no spontaneous synaptic input, thus a postsynaptic potential elicited during such a silent state is not subject to synaptic noise. In this scenario, Downstate potentials can be taken as reference points in which the input amplitude and kinetics are smooth and unaltered. Moreover, Downstate responses can be related to *in vitro* datasets in which neurons are constantly at rest (Figure 5 a, b). Additionally, the same Downstate responses can be directly compared to the alternating Upstate periods, in which the active network influences synaptic input. Since *in vitro* studies have provided an extensive description of the types of computations that dendrites can potentially perform, comparisons between *in vivo* Down- and Upstates can help determine which of the many forms of synaptic integration described *in vitro* are employed by the brain under more natural conditions (Stuart and Spruston, 2015).

A subset of mice was trained so that awake recordings could be made while their heads were restrained. All such recordings were performed on the forepaw S1 cortex while monitoring spontaneous movements of the contralateral forepaw (Paragraph 2.6). During quiet wakefulness, neuronal V_m exhibited slow, large fluctuations of amplitude (Crochet and Petersen, 2006; Poulet and Petersen, 2008). While these V_m oscillations were faster than those which occurred during anesthesia, they can nonetheless be cleanly divided into periods of hyperpolarized V_m (V_{hyp}) that are comparable to Downstates, and depolarized periods (V_{dep}) resembling Upstates (Figure 5 b, c, and Figure 25 b). During paw movements, large fluctuations in neuronal V_m ceased, showing an average depolarized V_m that lay somewhere between V_{hyp} and V_{dep} (Figure 5 b and Figure 28 a). These periods of movement (Move) were analyzed separately and compared to the other two resting periods (Figure 28).

Findings from the optogenetic stimulation dataset under anesthesia were partially replicated by those found in awake mice (Paragraph 3.8). Awake single cell recordings are more difficult to obtain, so here I used them to validate the larger anesthetized dataset and exclude the possibility that state-dependent modulations were an artifact of anesthesia. Moreover, comparing the resting and movement periods, I obtained insights into the effects of an active brain state on synaptic integration.

4.4 Somatic optogenetic stimulation

Two-photon optogenetic stimulations were delivered to the soma ($_{soma}$OP) using a scanning spiral path as described (Paragraphs 2.5, 3.5, Figure 17 a - c). Pyramidal neurons do not receive excitatory input directly to their soma (DeFelipe and Fariñas, 1992) but dendritic input to branches very close to the soma (< 5 µm) could be strongly influenced by the somatic V_m (Williams, 2004) and might be functionally considered as somatic input. Somatic stimulation served to carry out two functions: to establish the degree of responsiveness that recorded ChR2-expressing neurons exhibited to light, and to provide a baseline for the state-dependent modulation of OPs. Moreover, because recording and stimulation sites were extremely close, it was possible to measure carefully the relationship between $_{soma}$OP amplitude and the V_m by clamping the somatic V_m with current injections while applying somatic light stimulations (Paragraph 3.9.1). Somatic stimulations reliably triggered depolarizing $_{soma}$OPs whose onset latency was fast (~ 0.5 ms), indicating that these were direct responses to the optical stimulation, and their kinetics were similar to those evoked by excitatory synaptic input.

Since every neuron of the dataset was recorded by somatic whole-cell patch clamp, the OPs evoked on the soma are the nearest to the neuronal V_m recording site. Therefore, amplitude and kinetics of $_{soma}$OP are strictly dependent on the kinetics of ChR2 activation and the response properties of the neuronal membrane. By analyzing the state-dependent modulation of $_{soma}$OPs, it is possible to define the basic voltage-dependent features of a given depolarizing potential.

Measurements of single dendritic stimulations also took place at the soma, rather than at the position in the dendrite where they originated. The cable properties of dendrites are clearly very different to that at the soma (Cuntz et al., 2014; Rall, 1967; Rall and Rinzel, 1973), however it is technically currently not possible to measure the optogenetic potential at its dendritic origin *in vivo*, before it undergoes transformations and integration that occur along the dendritic path toward the soma. Here data from *in vitro* studies can provide some insights on the amplitude of input strength. Simultaneous somatic and dendritic recordings have shown that dendritic potentials caused by EPSPs can be an order of magnitude higher in amplitude than when recorded at the soma (Nevian et al., 2007; Spruston, 2008; Williams and Stuart, 2002). To imitate this level, I produced $_{soma}$OPs up to ~ 4 mV in amplitude (Figure 17 d, f and Figure 21 b) as an attempt to cover the range of possible dendritic potentials and determine whether large depolarizations are modulated differently than smaller ones. Overall, somatic stimulation provided a tool to measure the impact of changing V_m on the activation of ChR2.

4.5 Dendritically evoked optogenetic potentials

As explained above (Paragraphs 1.5.2, 3.6) ChR2 is not a natural physiological channel found in mammalian neurons. However, the depolarization it produces has features that are similar to the activation of glutamatergic channels at synaptic connections (Jouhanneau et al., 2015). By tuning the power and exposure time of the two-photon light for dendritic stimulation, I produced excitatory depolarizing OPs whose amplitude and kinetics were similar to those of $_{u}$EPSPs (compare Figure 20 to Figure 24). In an attempt to reproduce the wide distribution of physiological excitatory synaptic inputs in L2/3 pyramidal neurons (DeFelipe and Fariñas, 1992; Feldmeyer et al., 2006, 2002), I targeted non-perisomatic, spiny dendritic branches at distances ranging from 15 to 140 µm from the soma, in both apical and basal dendrites (Figure 19 and Figure 22).

Dendritic two-photon stimulations were delivered in a scanned squared zigzag pattern centered on the dendritic shaft (Paragraph 2.5). In pyramidal neurons, synaptic excitatory input arrives predominantly, but not exclusively on dendritic spines that emerge from this shaft (DeFelipe and Fariñas, 1992). Ultimately the EPSP is the result of the activation of thousands of glutamatergic channels (AMPA and NMDA) present on the spines and on the shaft (Feldmeyer et al., 2006). On spines, the depolarizing potential is gathered, integrated and delivered to the shaft through the spine's neck. Within the shaft, a single potential evoked by a synaptic input is added to, and integrated with those flowing in from activated synapses on other spines and on the shaft itself. Each unitary, single axon evoked, EPSP ($_{u}$EPSP) – the potential produced by the activity of a single presynaptic excitatory neuron – is thus a combined input determined by the activation of at least one synapse, or multiple synapses which may lie near each other or not (DeFelipe and Fariñas, 1992; Feldmeyer et al., 2006; Markram et al., 1997). The $_{u}$EPSP is therefore determined by the spatiotemporal sum in a shaft segment, comprising the contribution of each neighboring synapse and on the soma as the sum of non-neighboring synapses.

Synaptic connections between two pyramidal neurons typically have ~ 4 synaptic contact points (Feldmeyer et al., 2006) that are distributed around different basal dendrites. However some researchers suggest that pyramidal neurons receive clusters of inputs, which arrive at single dendritic segments from their presynaptic terminals, likely to be caused by the synchronous firing of the same assembly of multiple presynaptic neurons (Takahashi et al., 2012). This produces an EPSP which is combined locally at the spatially defined dendritic shaft segment where they arrive. Studies of thalamo-cortical connectivity, however have shown that afferent sensory inputs carrying specific types of somatosensory (Jia et al., 2010; Varga et al., 2011) or auditory (Chen et al., 2011) information may be widely dispersed over a dendritic tree and do not converge on single dendrites.

Here I have simulated a $_{u}$EPSPs arising from a single synaptic input or cluster of inputs, by optically eliciting potentials in a single, confined dendritic segment, consisting of both shaft and spines. It will be necessary to study how such single $_{u}$EPSPs are handled and integrated before one can consider expanding this work in a future study, which would be more complicated. Ultimately, we would like to know how the cell integrates and computes input arriving from multiple shafts simultaneously, even in different regions of the neuron. That would not be possible without first understanding the contributions of single shafts. In the future progress in optical two-photon stimulation may allow fast simultaneous patterned stimulation of different dendritic segments (Emiliani et al., 2015).

4.5.1 Influence of distance from the soma on dendritic OP kinetics

The distance of a synaptic input from the soma has an effect on somatic response kinetics; here I discuss what my data reveals about this influence of distance from the soma on integration properties of apical and basal inputs in the Downstate.

Despite minor differences in stimulation power and expression of the ChR2, there was no correlation between the somatic amplitude of dendritically elicited OPs and the distance of stimulation from the soma across the entire dataset (Paragraph 3.6, Figure 19 a, b).

In pyramidal neurons dendritic recordings have shown that inputs more distal from the soma are larger in amplitude than more proximal ones (Nevian et al., 2007; Williams and Stuart, 2002). In hippocampal neurons this acts to normalize the somatic impact of a dendritic input so that inputs have similar amplitude (Magee and Cook, 2000), in contrast a somatic normalization is not present in cortical neurons (Williams and Stuart, 2002).

Even if synapses at widely different distances within the dendritic arbor were to produce the same level of local potential, a distant-dependent reduction of the somatic potential would occur due to intrinsic cable properties because more distant synapses are located on thinner dendritic branches – whose diameter shrinks toward the outer terminal. This increases the surface-volume ratio and with its electric impedance, which creates a boosting effect on the local potential amplitude (Cuntz et al., 2014; Jaffe and Carnevale, 1999; Nicholson et al., 2006; Rall, 1967; Rall and Rinzel, 1973; Spruston, 2009, 2008). This means that at dendritic locations further from the soma, the local potential amplitude is boosted relative to sites closer to the soma, provided the level of input is identical. As they propagate toward the soma, these large amplitude potentials face the increasing diameter of the shaft and thus a constant decrease of impedance, which also experiences sudden drops at each node at which the dendrites bifurcates (Rall and Rinzel, 1973). Additionally, the charge constantly leaks due to the conductance of the membrane; the farther the distance of the synaptic input from the soma, the more charge will be leaked (Spruston, 2009). Thus, this filtering produces a distant-dependent reduction of the somatically recorded EPSP amplitudes (Nevian et al., 2007; Williams and Stuart, 2002). Direct recordings from basal dendrites of L5 pyramidal neurons showed that at medium-short distances (30–150 μm), the opposing effects caused by high dendritic impedance and its decrease toward the soma compensate equally each other. The dendritic amplitudes are therefore normalized in a location dependent manner, resulting in a somatic amplitude that is homogeneous across

such medium-short distances (Nevian et al., 2007). This is in line with the basal dendritic stimulations data reported here (Paragraph 3.6, Figure 19 a, b).

The latencies of OP responses exhibited a linear correlation to the distance from the soma. I calculated the average OP propagation velocity by subtracting somatic response latencies from the dendritic latencies and dividing the distances of stimulations by these values (Paragraph 3.6, Figure 19 c, d). The resulting velocities are in the normal range of EPSP propagation velocities for the dendrites of mammalian neurons (tens to hundreds of millimeters per second) (Agmon-Snir and Segev, 1993). In L5 pyramidal neurons Nevian et al., 2007 found velocities five times faster than those presented here. This discrepancy may be due to fact that dendrites in L2/3 cells are smaller. The average propagation velocity attained when apical dendrites were stimulated was slightly faster than that of basal OPs, presumably because apical dendrites tend to have a larger average diameter than basal dendrites and therefore lower axial impedance. These dendritic-specific differences have also been reported for L5 neurons (Nevian et al., 2007; Williams and Stuart, 2002). Nonetheless, propagation velocities are not constant along the dendrites; they are slowed by higher transmembrane conductance and axial impedance. This means that the potentials on distant dendrites start slow and accelerate toward the soma, where they encounter less axial impedance (Agmon-Snir and Segev, 1993; Nevian et al., 2007).

The kinetics parameters of dendritic OPs (rise, peak, decay times and half width) were all significantly longer as the distance of generation from the soma increases, in both apical and basal dendrites (Figure 19 e - l). Distant dendrites tend to have smaller diameters with a higher input resistance and longer time constants. Thus, the smaller the dendrite, the larger and longer the local potential (Jaffe and Carnevale, 1999; Rall, 1967; Spruston, 2009, 2008; Williams, 2004). Moreover, the filtering that takes place while propagating toward the soma – due to decreasing axial impedance – mainly decreases the amplitude of the potential while the time constant is only minimally affected (Spruston, 2009). Because somatic time course of $_{u}$EPSPs has been demonstrated to be an accurate predictor of synapse location (Redman and Walmsley, 1983), prolonged kinetics can be seen as a footprint of large local potentials, which are generated in distant dendrites (Williams and Stuart, 2002).

While, the range and distance dependency of amplitudes in Downstate OPs resemble data of spontaneous EPSPs and dendritic current injection to mimic EPSPs in cortical slice studies (Larkum et al., 2007; Nevian et al., 2007; Williams and Stuart, 2002), the kinetics of OPs were slightly longer than $_{u}$EPSPs in the Downstate, with an average peak time around 14 ms in comparison to 9 ms for glutamatergic inputs (compare Paragraph 3.6, Figure 20 b,

g to Figure 24 c) (Jouhanneau et al., 2015). Nevertheless, because the potentials in this study were generated with relatively low frequencies (3 Hz) and I did not investigate how OPs are directly integrated using multiple simultaneous stimuli, the slightly longer values for the kinetics should not interfere with the interpretation of the data.

4.6 State-dependent modulation of somatic OPs

I applied two-photon stimulations until enough OPs were collected to compare Up- and Downstates (Paragraph 3.5). A subset of the recordings were made while mice were awake, this allowed me to compare Up- and Downstates from anesthesia with periods of V_{dep}, V_{hyp} during quiet wakefulness and with periods of movement (Paragraph 3.8.1). When comparing somatic responses to Up- and Downstate with V_{dep} and V_{hyp} in awake, I consistently found a reduction of the amplitude and a prolongation of the half width and decay time of the $_{soma}$OP with membrane V_m depolarization (Figure 17 and Figure 25). Regardless of the Downstate or V_{dep} amplitude, the ratio of the Up:Down or V_{dep}:V_{hyp} amplitude was always decreased by the same amount (~ 0.8) (Figure 21 a - c). This reduction was directly related to the depolarization in Upstate or V_{dep}. Given the reduction in driving force that occurs while depolarizing towards the ChR2(TC) reversal (~ 0 mV (Berndt et al., 2011)), and calculating the expected amplitude at Upstate or V_{dep} V_m values for any given Downstate or V_{hyp} $_{soma}$OP (Equation 1), this meant that there was no difference between the expected and measured amplitude of Upstate or V_{dep} $_{soma}$OP. Furthermore, by holding the Downstate V_m at Upstate values (Isopotential) with somatic current injections, and generating $_{soma}$OPs during Down, Upstate and Isopotential, I did not find any difference between the expected Upstate and Isopotential and measured Upstate OP amplitude values (Paragraph 3.9.1, Figure 29). This means that the reduction of $_{soma}$OP amplitudes in Upstates is mainly caused by a reduction of the driving force in the Upstate. Additionally, the driving force effect seems to remain constant throughout the wide range of distribution in amplitudes of the somatic stimulations (0.2 to 4 mV). It appears to have no detectable, additional effects on large depolarizations, where the OP itself might be large enough to induce a saturation effect in the driving force.

In the same way as for the amplitude reduction, the prolongation of $_{soma}$OP kinetics during Upstate are directly linked to the V_m difference between the states. The half width is identical in the Upstate and Isopotential, both of which are longer than the Downstate somatic response. Synaptic input intensifies during active depolarized states and this leads to an

increase of the total leakage conductance in most neurons. However, L2/3 pyramidal neurons of the somatosensory cortex have been reported to show the opposite behavior, in which the input resistance increases during Upstates (Mateo et al., 2011; Waters and Helmchen, 2006). This means that the increase in synaptic input is counteracted and completely reversed due to the effects of other ionic channels on total membrane conductance. This effect is probably due to anomalous rectification (Waters and Helmchen, 2006) and can be clearly seen in the data reported here (Paragraph 3.9.2, Figure 30). Therefore slower kinetics during Upstates are likely due to an increase in somatic input resistance.

The combination of driving force reduction and the increase in input resistance during depolarized Upstates seems to have a compensatory effect on the total charge transmitted by OPs. Calculating the area under the $_{soma}$OP curves shows that there is no difference in total charge between Down- and Upstate and during awake V_{hyp} and V_{dep} (Paragraph 3.9.3, Figure 31 a, e). The reasons why other cortical cells do not show this compensatory effect are not yet clear (Cossart et al., 2003; Haider, 2006; Hasenstaub et al., 2007) but would be important to investigate in future experiments.

4.7 State-dependent modulation of dendritic OPs

In this study the discrimination between the Up- and Downstate is obtained from the values of the somatic V_m. Although, somatic V_m values do not strictly represent their dendritic counterparts, oscillations in dendritic and somatic V_m are thought to be synchronized (Waters and Helmchen, 2004). To decrease as much as possible the likelihood of mismatches between V_m states in the soma and dendrites, I considered only periods in which the somatic Down- or Upstate appeared to have been completely established, excluding transition periods in which they rose, fell, or became unstable (Paragraph 2.8.4, Figure 7 a - c). Here the maximum distance of dendritic stimulation was 140 µm from the soma and somatic latencies were never > 3 ms (Figure 19 c, d) (values a thousand times faster than the V_m state oscillations). Therefore, it is probably safe to assume that an Upstate in the soma is correlated with an Upstate in the dendrite. However, it will be necessary to conduct recordings directly from dendrites and soma during network activity to confirm this hypothesis.

The membranes of the soma and dendrites have different passive and active properties (Cuntz et al., 2014; Rall, 1967). Thinner dendrites have a higher impedance and lower capacitance than the large somatic compartment that may differentially modulate the amplitude of synaptic inputs. Moreover, the expression of voltage-dependent currents is not

homogenous across the dendritic tree and this shapes the magnitude and kinetics of synaptic potentials (Larkum and Nevian, 2008; Spruston, 2009, 2008). Additionally, during different states, dendritic OPs will be affected by other excitatory, inhibitory and modulatory inputs that arrive along their dendritic path toward the soma (Lee and Dan, 2012). Thus, the effect of Upstates on OPs may be different in dendrites than in the soma. Nevertheless, the features of somatic responses will participate in the modulation of dendritic-elicited OPs at the somatic level, where they are integrated with all the other synaptic inputs the neuron is receiving and ultimately participate in the firing output.

As described above, somatic stimulations were modulated by the Upstate in a coherent and amplitude-independent manner across the dataset, allowing me to isolate two main factors that influence the shape of response: the decreasing driving force that reduces amplitude and the increasing input resistance that prolongs kinetics during depolarized Upstates. The driving force also plays a role at the dendritic stimulation site because, even at different magnitudes, the dendritic V_m can be considered mostly correlated to the soma. Thus, the amplitude of local potentials in Upstates should also be decreased by the same somatic ratio for amplitudes up to 4–5 mV. This effect could be amplified by the magnitude of the response potential itself, which in distal dendrites may reach 20–30 mV (Jaffe and Carnevale, 1999; Nicholson et al., 2006; Spruston, 2008). This causes a saturation effect for the driving force in Upstates that could contribute to increases in the Up:Down amplitude ratio. Because somatic stimulations did not reveal that this effect was dependent on amplitude, I do not have direct indication that this happens in dendrites.

Any given potential change across the membrane is, in principle, instantaneous across the whole membrane (in electrical terms) and thus the driving force, input resistance and other characteristics will be active at any given location. The changes that are imposed on the waveform are dependent on the axial diameter and the expression of channels along the dendrite, which produce different waveform distortions at the point of measurement. Therefore, both the driving force and the input resistance will shape the kinetics of the response along the whole cell body. While the driving force strictly depends on the conductive properties of the channel that is activated and on the V_m at the stimulation site, input resistance depends on membrane properties – particularly the composition of open conductances expressed along the length of the dendrite.

Despite the fact that conductance in L2/3 pyramidal neurons is quite homogeneous over the short range in dendrites (Larkum et al., 2007), input resistance in these cells is dominated by an anomalous rectification effect that counteracts the open conductances and increases

resistance in Upstates (Mateo et al., 2011; Waters and Helmchen, 2006). Several voltage-dependent ion channels may contribute to anomalous rectification. Typically, inward-rectifying K^+ currents (K_{ir}) are responsible at hyperpolarized voltages (Nisenbaum and Wilson, 1995; Sutor and Zieglgänsberger, 1987) while in the depolarizing direction, inward Na^+ and Ca^{2+} currents have also been implicated (Stafstrom et al., 1985; Sutor and Zieglgänsberger, 1987). Here I have used QX-314 to block anomalous rectification, potentially affecting any of these channels. Since, I do not know the distribution of the putative channel responsible for the effects, the increase of input resistance in the Upstate that is registered at the soma might be completely unrepresentative of conditions in the dendritic shaft. In spite of this, the OP elicited in dendrites is also affected by somatic response features, and an increase in somatic input resistance will influence its kinetics at the soma.

As detailed above, dendritic responses upon optical stimulation were compared in two main subcellular compartments: apical and basal dendrites. I first address the responses of apical dendrites.

4.7.1 Modulation of input to apical dendrites

The mean amplitude of an OP evoked by apical stimulation was smaller in Upstates than Downstates. The reduction in amplitude was proportionally greater than the reduction at the soma, and was stronger than expected compared to calculations of the reduction of the driving force for the Up:Downstate V_m difference registered at the soma (measured ratio 0.6, expected ratio 0.8) (Paragraph 3.6.1, Figure 20 a - e). Moreover, this apical reduction of the amplitude in Upstates increased linearly in proportion to the distance of the point of stimulation from the soma (Paragraph 3.6.3, Figure 22 a).

In contrast, dendritic OP kinetics (averaged half width) did not differ between Up- and Downstates (Figure 20 b, e). This also diverges from the constant increase of the averaged half width of Upstates registered in somatic $_{soma}$OP. Despite the fact that during Upstates, the half width of OPs generated in apical dendrites ($_{apical}$OP) is more reduced than in those generated in somata, the reduction was proportionally related to that of the amplitude, and thus the reduction in Upstates is mainly a result of a reduction in amplitude and was not present in normalized $_{apical}$OPs (Paragraph 3.6.3).

In recordings made in awake mice during quiet periods, $_{apical}$OPs as well as $_{soma}$OPs underwent a modulation during V_{dep} compared to V_{hyp} that was similar to the difference

between Up- versus Downstates in anesthetized animals. However, V_{dep}:V_{hyp} $_{apical}$OP amplitude ratio showed a greater reduction than expected, beyond the effects of the driving force (Paragraph 3.8.2, Figure 26 a - d). Moreover, there was a stronger attenuation of V_{dep}:V_{hyp} amplitude compared to Up:Down ratio.

Unexpectedly the amplitude of $_{apical}$OPs was increased during movement (Move) compared to V_{dep}. Indeed, the averaged apical response during Move phases differed significantly from the V_{dep}, reaching levels that were indistinguishable from the amplitudes of V_{hyp} OPs (Paragraph 3.8.4, Figure 28 e - g). Moreover, the kinetics were prolonged further during the Move phase, even in comparison to the V_{hyp} response, resulting in a significant increase of the total charge (Paragraph 3.9.3, Figure 31 f).

What could account for the differences between Upstate modulations in apical dendrites?

4.7.1.1 Mechanisms mediating the state-dependent modulation of synaptic input to apical dendrites

Here I will outline mechanisms that might be responsible for the modulations, which specifically appear in apical dendrites during Upstates and cause a distance-dependent decrease in amplitudes without affecting the kinetics of a response.

Assuming that V_m is correlated between the cell body and dendrites during Up- and Downstates (Waters and Helmchen, 2004) the Up:Downstate ratio of the driving force is expected to be similar on the soma and across the dendritic tree. In pyramidal neurons, however, the somatic amplitude has been reported to be location independent (Magee, 1999), due to a distance-dependent increase of local potential amplitudes (Larkum et al., 2007; Nevian et al., 2007; Nicholson et al., 2006; Spruston, 2008; Williams and Stuart, 2002). In apical dendrites of hippocampal neurons, the cause of this effect has been shown to involve not only the passive properties of dendrites but also a distance-dependent increase of synaptic strength along the dendrite (Magee and Cook, 2000; Nicholson et al., 2006). This increase of local synaptic currents in distal apical dendrites may produce a saturation of the local driving force during Upstates, which might explain why amplitudes fall in proportion to distance. However, additional factors may contribute to distance-dependent decreasing of amplitude, including an even distribution of leaking conductances along the apical dendritic tree, perhaps due to a K_{ir} channel, which opens during depolarized V_m (Sanders et al., 2013).

Multicellular mechanisms might also be involved; inhibitory synapses along dendrites could produce a shunting inhibition during Upstates. During Upstates and V_{dep}, pyramidal

neurons receive a high number synaptic inputs along the dendrites and the soma from inhibitory GABAergic interneurons (Jiang et al., 2013; Petersen and Crochet, 2013). These inputs are mediated by the opening of $GABA_A$ chloride channels, which result in IPSPs, negative potentials that hyperpolarize the V_m. An IPSP produces both a shunting effect, that has a divisive inhibitory outcome on the charge of EPSPs and a negative potential that has a subtractive effect (Blomfield, 1974). The $GABA_A$ reversal potential is very close to the resting potential of pyramidal neurons (-65 – -70 mV), so in Downstates or V_{hyp} the opening of such Cl^- currents has a purely shunting effect on EPSPs. In Upstates and V_{dep} (at $V_{rest} \sim$ -55 – -45 mV), however, it will produce a hyperpolarizing potential whose effects on EPSPs are also subtractive. So during an Upstate, the opening of Cl^- channels along the OP's path to the soma will produce both a local reduction in input resistance (shunting) that shortens the kinetics, and a subtraction of potential (IPSP) that decreases the amplitude.

While the inhibitory synapses of most interneurons link to pyramidal cells in axo-somatic regions, a subpopulation of somatostatin interneurons (SST) called Martinotti cells, found in upper cortical layers, exhibit a particular pattern of projection and innervate the apical dendritic tufts of L5 and L2/3 pyramidal neurons (Jiang et al., 2013; McGarry, 2010; Murayama et al., 2009; Wang et al., 2004). This means that Martinotti cells could play a role in modulating the way OPs in apical dendrites are integrated in different ways in different states. Moreover during movement when most of the excitatory and inhibitory neurons increase their firing rates, the Layer 2/3 somatostatin interneurons go from relatively high rates during quiet periods to a low rate during movement (Gentet et al., 2012; Muñoz et al., 2017). By increasing their inhibitory action along apical dendrites during V_{dep} periods, Martinotti cells could have a divisive or subtractive effect on the total charge transmitted by $_{apical}$OPs, and this might enhance the compartmentalization of the apical tuft during depolarized states. On the other hand, during active movements, the silencing of these SST interneurons would reduce the inhibition on the apical compartment, and boost the amplitude of inputs arriving at the soma. Nevertheless, the firing rate of SST neurons is relatively low under anesthesia even during network activity (Pala and Petersen, 2015). So it is unclear whether this mechanism could fully explain the reduction of apical amplitudes during Upstates. Future experiments using selective SST optogenetic manipulation and recordings will help resolve this issue.

In summary, a voltage-dependent leakage of current combined with a distance-dependent saturation of the driving force might account for the attenuation of $_{apical}$OPs in Upstates. This

reduction might be enhanced during awake V_{dep} periods by an increase in the activity of SST neurons.

4.7.2 Gain modulation of synaptic input to basal dendrites

A central result of this study is the gain modulation of basal inputs caused by the amplification and broadening of small-amplitude basally elicited OPs ($_{basal}$OP) and a reduction of larger $_{basal}$OPs during Upstates (Paragraph 3.6.2, Figure 21 g - i). This effect was also observed for glutamatergic inputs from VPM (Paragraph 3.7.1, Figure 23 b, f) and monosynaptic $_{u}$EPSP from neighboring pyramidal neurons (Paragraph 3.7.2, Figure 24 b, f), both of which are thought to target the basal dendrites of layer 2/3 neurons.

In contrast to the effects of stimulations on apical dendrites and the soma, the averaged amplitude response of OPs generated in the basal compartment exhibited no significant differences between Upstates and Downstates (Paragraph 3.6.1, Figure 20 g, i). On the other hand, the kinetics of $_{basal}$OPs were significantly prolonged in Upstates compared to $_{soma}$OPs (Figure 20 j). While the average total charge of $_{soma}$OPs (integral) did not differ between the states, Upstates $_{basal}$OPs exhibited a larger integral than in Downstates (Paragraph 3.9.3, Figure 31 c). However, there was a high variance in $_{basal}$OP Up:Down amplitude ratios across the dataset (spanning from ~ 0.4 to 2.5) (Figure 21 h), higher than that observed for $_{soma}$OPs, which was quite constant (~ 0.8) (Figure 21 b). This was also higher than the variance seen in $_{apical}$OP (from ~ 0.01 to 1.2) (Figure 21 e). The variance of modulation was not significantly correlated with the distances of stimulations from the soma. In opposition to $_{apical}$OP, however, $_{basal}$OP Upstate tended to be increased as the distance of their generation from the soma increased (Paragraph 3.6.3, Figure 22 b).

Plotting the amplitude of responses in Downstate versus Upstate revealed that smaller Downstate $_{basal}$OPs were increased in Upstate while larger amplitudes were decreased. The point at which a significant linear regression crossed the Up:Down amplitude ratio unity (ratio = 1) gave a Downstate amplitude value of 0.4 mV. I used this value as a way to divide "large" > 0.4 mV from "small" < 0.4 mV responses. Plots of Up:Down as a function of the Downstate amplitudes showed significant correlation, for which the best fit was a single exponential curve (Paragraph 3.6.2, Figure 21 h). This corresponded to a significant linear correlation between the logarithm of Downstate amplitudes and the Up:Down ratios (Figure 21 h inset). Additionally, directly comparing the Up:Down amplitude ratios of large and

small inputs groups showed a significant difference (Figure 21 i). This effect may be considered as a gain modulation of synaptic input during Upstates.

The average total charge of $_{basal}$OPs in Upstates was larger than in Downstates. Additionally, plotting the integral of response ratios as a function of Downstate integrals led to an exponential correlation that was stronger than the correlation for Up:Down amplitudes. Indeed, the smallest inputs were increased in the Upstate to a level where, the charge that was ultimately transmitted was up to 15 times larger than when the same light stimulus was administered in Downstate (Paragraph 3.9.3, Figure 31 d). This magnitude-dependent gain modulation was also observed in awake recordings, comparing V_{dep} or Move phases to V_{hyp} periods (Figure 31 h). This suggests that such a gain modulation contributes to the integration of inputs during physiological signal computation in awake animals.

The basal dendritic compartment of L2/3 pyramidal neurons in the somatosensory cortex is targeted by excitatory synapses from neighboring pyramidal neurons sitting in the same layer (Feldmeyer et al., 2006), from spiny stellate cells in L4 (Feldmeyer et al., 2002) and from L5 pyramidal cells (Lefort et al., 2009); it also receives direct and indirect feedforward input from the thalamic VPM nucleus (Oberlaender et al., 2012). Connectivity data from other two projects in our laboratory permitted me to compare the $_{basal}$OPs with real $_{u}$EPSPs and thalamic input. One project concerned local pyramid-to-pyramid single synaptic connections (Jouhanneau et al., 2015). The other involved optogenetic stimulation of the VPM, during recordings of L2/3 pyramid cells (Jouhanneau et al., 2014).There were striking similarities between the $_{basal}$OPs with real $_{u}$EPSPs from local pyramid connectivity. While in the two datasets the responses exhibited minor differences in kinetics, the range of the amplitudes and the variability in Up:Down amplitude ratios were similar (compare Figure 20 b, g and Figure 21 h to Figure 24 b, c and f). Plots of $_{u}$EPSPs Up:Down ratios as a function of the Downstate amplitudes showed a similar correlation, for which the best fit was also a single exponential curve (Paragraph 3.7.2, Figure 24 f). This corresponded to a significant linear correlation between the logarithm of Downstate amplitudes and the Up:Down ratios. Additionally, splitting the dataset into large and small responses in Downstates, and comparing the Up:Down response ratios, revealed a significant differences between the two groups, also for $_{u}$EPSPs.

Several conclusions can be drawn between these correlations between OPs and $_{u}$EPSPs. First, they confirm that the use of two-photon ChR2 dendritic stimulation is a reliable and coherent method to mimic EPSPs effectively in a controlled spatiotemporal manner. Secondly, the technique permits an isolation of the contribution of postsynaptic mechanisms

from possible presynaptic and di-synaptic contributions that are involved in $_{u}$EPSPs or VPM input and might participate in state-dependent modulations. The fact that there is an impressive similarity in the distribution of ratios for magnitude-dependent amplitudes between OPs and $_{u}$EPSPs suggests that state-dependent normalization is achieved through an entirely post-synaptic mechanism.

With regard to the VPM stimulations, it is much harder to define the mechanism underlying state depend input modulation. Optically stimulating ChR2-expressing neurons in the VPM nucleus or directly stimulating their projections into L2/3 activates an entire network. Generally, we should assume that sensory input in the brain is probably achieved through the activation of a network of neurons that deliver EPSPs to the postsynaptic cell, rather than through single excitatory synapses. The synapses of VPM cortical excitatory projections connect mostly with cells in L4 and to a lesser extent in L3 (Oberlaender et al., 2012). In turn, L4 spiny stellate cells mostly extend excitatory projections into L2/3 but not L1 (Feldmeyer et al., 2002). This means that the VPM network activation probably affects a L2/3 pyramidal neuron mostly through its basal dendrites. This activation produces a wave of EPSPs which appear on the soma as a single depolarizing potential; during Upstates it is followed by an inhibitory wave of IPSPs, because same excitatory network recruits inhibitory interneurons (Jouhanneau et al., 2014). This allows us to consider the extent to which our findings about the brain state modulation of single $_{u}$EPSP amplitudes can be extended to clusters of EPSPs, at least up to the late phase of the response. In fact, we found that excitatory thalamic inputs into L2/3 neurons also exhibit a normalization during Upstates, whereby there is a reduction in amplitude of large inputs and an increase of small inputs (Paragraph 3.7.1, Figure 23 b, f). Thus, the input from a network of neurons carrying somatosensory information to the cortex and to the basal compartment of L2/3 pyramidal neurons also undergoes a normalization of inputs during Upstates. The location of the divide in amplitude magnitudes seems to be different: for $_{u}$EPSPs and OPs it was around 0.3–0.4 mV, while for multiple VPM connections it may be around 1 mV, however further data is needed. Other features including differences in number of synaptic inputs and a magnitude-dependent recruitment of inhibitory networks (Reig et al., 2015) may play a role in the amplification of VPM inputs. However based on similar findings in EPSPs and OPs, I hypothesize that similar postsynaptic mechanisms account for the normalization of VPM thalamic and basal cortical inputs during network activity.

4.7.2.1 Postsynaptic mechanisms mediating the state-dependent gain modulation of synaptic input to basal dendrites

Various active properties of dendrites may be involved in the way the state-dependent modulation affects the integration of stimuli by the basal dendrites of L2/3 neurons (Larkum and Nevian, 2008; Spruston, 2009). At more depolarized potentials an increase in basal OP amplitude and the broadening of the half width, resembles the voltage dependency seen in evoked and dendritically simulated EPSPs in cortical slice experiments during somatic depolarization (Andreasen and Lambert, 1999; Deisz et al., 1991; Markram et al., 1997; Stuart and Sakmann, 1995). Since the main intracellular difference between the states is the mean V_m, voltage-dependent channels may be involved.

A surprising feature of L2/3 neurons is the counterintuitive decrease in conductance during Upstates linked to anomalous rectification, which is dependent on voltage-dependent currents. Applying the intracellular drug QX-314 (QX) abolishes this effect (Waters and Helmchen, 2006). Mechanistically, QX mainly blocks voltage-gated channels selective for sodium (Strichartz, 1973), but it also affects potassium (Perkins and Wong, 1995) and calcium channels (Talbot and Sayer, 1996). This blockage of active properties of neural membranes makes them behave more like passive cables.

Anomalous rectification has been linked to voltage-gated sodium channel that produces an inward current during depolarization (Stafstrom et al., 1985; Sutor and Zieglgänsberger, 1987). Injecting a constant negative or positive current during the spontaneous alternation of the states shows that the V_m affects input resistance more than other features of the Upstate (Paragraph 3.9.2, Figure 30). Applying QX to the intracellular solution abolished the increase of input resistance (IR) in depolarized states (Paragraph 3.9.4, Figure 32 d - f). Nonetheless, a comparison of the IR of cells in control and with QX clearly shows that the drug predominantly affects the Downstate, whose average IR values double under QX (compare Figure 32 b, c to e, f). As a result, rather than stating that QX-314 abolishes the increase of input resistance in Upstates, it is more correct to say that it blocks the decrease of IR in Downstates.

The modulation of basal inputs was different in QX-filled cells. Upstate responses were decreased in amplitude compared to Downstates, to a degree that reflected the difference between the driving forces of the two states (Figure 33 b, c, e). Moreover, the distribution of amplitude ratios displayed less variation, resembling somatic or apical responses in non-QX recordings (Figure 33 h). Additionally, the amplitude showed no magnitude-dependent

modulation, and the subgroup of small Downstate inputs (< 0.4 mV) responded differently than the same basal subgroup in non-treated cells, in a way that resembled small apical inputs (Figure 33 h, i and Figure 34). In Upstates the kinetics were not prolonged, with a half width significantly shorter than in Downstates. Nevertheless, the drug prolongs the average half width in Downstates (~ 30 ms) compared to the control in basal dendrites (~ 20 ms), while the Upstates kinetics remain unaltered (~ 25 ms) (Figure 33 c, f)). As was the case for the IR, QX affects the Downstate phase more, suggesting that the increase in IR in the Upstate is responsible for the prolongation of kinetics. Overall, during QX application the $_{basal}$OP response resembles a scaled-down version of the Downstate, with the driving force reduction leading to a reduction in amplitudes, and shortened kinetics, suggesting that QX-314 linearizes dendritic computations by blocking voltage-gated currents.

An anomalous rectifying potassium K_{ir} channel has been proposed to be responsible for the increase in input resistance in Upstates by closing at more depolarizing potentials (Waters and Helmchen, 2006). However while the K_{ir} can explain how IR modulation affects kinetics, it cannot be responsible for the gain modulation of amplitude, because the amplitudes of short transients such as OPs or $_{u}$EPSPs are only minimally affected by changes in conductance. Nevertheless, the primary mechanism underlying the activity of QX-314 is its blockage of voltage gated sodium channels (Na_V). Na_V currents are mainly responsible for the generation of APs and their propagation in the axon. There the expression of the channel is very high, producing the regenerative large currents that reach the axon terminals. In dendrites Na_V are expressed at much lower densities, but the channels can generate local sodium spikes when the membrane is sufficiently depolarized by clustered inputs, and this produces voltage-dependent non-linear signaling in dendrites (Larkum and Nevian, 2008).

Small depolarizations can open different types of Na^+ channel (French et al., 1990), or activate Na_V slowly to produce a persistent inward current (Na_P) (Carter et al., 2012). When the V_m reaches threshold depolarization values (~ -55 mV) that lie just between Up- and Downstates, such Na^+ conductances open (French et al., 1990) and influence the integration of EPSPs by increasing both amplitude and kinetics (González-Burgos and Barrionuevo, 2001; Stuart and Sakmann, 1995). Ultimately, this amplifies the total charge transmitted to the soma (Figure 35). The activation of Na_P may be responsible for the increase of IR in Upstate (Sutor and Zieglgänsberger, 1987). Although when the channel opens it increases the conductance of the membrane, any V_m change that lies within its dynamic range will enhance a fluctuation in V_m, which means that Na_P actively contributes to increases in input resistance. Since, Na_P has been reported to influence the amplitude of EPSPs in a voltage-

dependent manner (Deisz et al., 1991; González-Burgos and Barrionuevo, 2001; Stuart and Sakmann, 1995), I hypothesis that it could be involved in the gain modulation of $_{basal}$OPs and real $_{u}$EPSPs.

Why aren't larger amplitude inputs amplified? In the model I propose, Na_P are constantly active during depolarized phases such as Upstates, V_{dep} and Move during which the mean V_m is near or above -55 mV. Thus basally generated OPs and $_{u}$EPSPs are all increased by Na^+ currents during these periods, regardless the magnitude of the input (Figure 35 a, b left). But taking in consideration the large impedance of thin basal dendrites and the filtering of the potential toward the soma, we know that local potential amplitudes are 5 to 20 times higher in magnitude than those recorded in the soma (Nicholson et al., 2006; Spruston, 2008) (Figure 35 a, b center compare to right). This implies that inputs at large amplitudes (> 0.4 mV) may correspond to > 4 – 8 mV at the point of dendritic generation, potentially triggering depolarizations that also reach -55 mV of V_m during Downstates. This in turn could trigger Na_P to increase large inputs as well. Moreover, a large input during a Downstate would retain its advantage in terms of the driving force effect over Upstates, and as a result would be larger on the soma (Figure 35 b). Small inputs in Downstates, on the other hand, would not depolarize the V_m enough to reach -55 mV. This means they would not be increased by the Na_P and thus have lower values than their Upstate counterparts (Figure 35 a). Ultimately, the nonlinear activation profile of these voltage-gated sodium currents would cause a larger relative amplification of smaller inputs in the depolarized Upstate.

What prevents Na_P from increasing somatic OPs in Upstates? I hypothesis that this is the result of features of the recruitment of Na_P currents: at the site of stimulation, whether soma or dendrite, the driving force of a transient potential exerts a local domination over the Na^+ currents (Figure 35 a center). Along the length of the dendrite the recruitment of Na_P currents becomes additive and on the soma their contribution overtakes differences in the initial driving force (Figure 35 a right).

In collaboration with Dr. M. Remme in the laboratory of Prof. S. Schreiber we constructed a mathematical model in a neuron's simulator (Neuron), using the data I collected as validation (Figure 35). We simulated a homogeneous distribution of Na_P channels along the basal dendrites of a reconstructed neuron from the OP dataset. When imposing the activation parameters of Na_P channels (French et al., 1990), the dendritic Up- and Downstate V_{rev} (Williams, 2004), the putative dendritic synaptic potentials (Spruston, 2008) and applied the range of distribution of recorded somatic amplitude responses to basal OPs, the model recapitulated the basal dendritic input gain modulation (Figure 35 d).

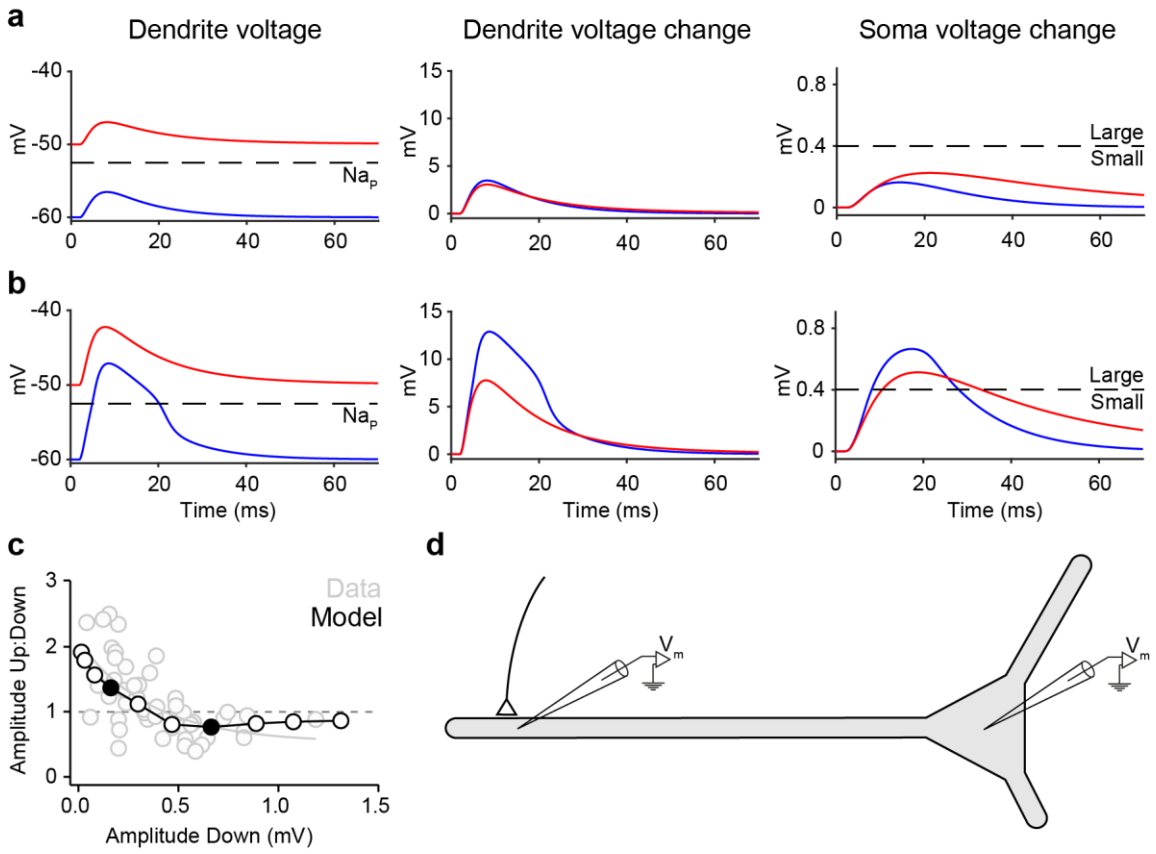

Figure 35. **Neuron model employing a dendritic distribution of sodium currents to recapitulate the gain modulation of basal input.**
The model constructed on Neuron exploits the anatomy of a reconstructed cell from the basal dendritic stimulations dataset. A homogeneous dendritic distribution of Na_P, whose dynamic range of activation lies in between of Up- and Downstate, is differentially activated by small and large dendritic inputs. **a**. Simulation of a small dendritic input and dendritic voltage recording; (left) the Upstate V_{rev} is above the threshold of Na_P activation, while the Downstate V_{rev} and peak are below; (center) the overlaid Up and Down responses show that the local Downstate potential is larger; (right) the corresponding somatic potential highlights the somatic filtering that accounts for a reduction of ~ 15 folds in amplitude and shows how the additive effect of Na_P along the dendrite reverses the Up:Down ratio for input < 0.4 mV. **b**. Same as (**a**) but for a large dendritic input; (left) the peak Downstate amplitude crosses the Na_P activation threshold; (center) the Downstate local response is boosted by the activation of Na_P; (right) on the soma the Downstate response results larger for input > 0.4 mV. **c**. Distribution of Up:Down amplitude ratios as a function of Downstate amplitude for the basal dendritic anesthetized dataset (grey) (from Figure 21 h); the superimposed Neuron model based on Na_P expression, recapitulates the gain modulation (black). Filled black circles represent the relative position in the distribution of the two examples showed in (**a**) and (**b**); empty black circles represent the other tested input parameters not showed here. **d**. Cartoon representing the simulated experiment layout with a pipette recording the dendritic V_m close to a synaptic input and another pipette recording the same input from the soma.

Another consideration is that at V_m above -55 mV, the membrane time constant is always prolonged due to the active contributions of Na_P to input resistance. Therefore, whenever potentials are elicited in Upstates, their kinetics are always longer in Upstates (Figure 35 a,

b right). When Na_P are blocked by QX-314, the time constant of the membrane becomes linear across different V_m and none of the inputs will be increased, regardless the amplitude, the brain state or V_m value, and the gain of modulation effect is abolished.

This hypothesis is one of the simplest potential explanations for the data since it involves the effect of a single type of channel, evenly distributed along the basal dendrites. But other factors cannot be ruled out, including contributions from more complex interactions of voltage-dependent currents along the dendrites, which might be disrupted by unspecific direct or indirect effects of QX-314. Testing the hypothesis would require *in vivo* dendritic patch-clamp recordings to measure the baseline V_m and OP amplitude directly at the stimulation site as well as new drugs to block specific currents intracellularly.

4.8 Functional consequences of dendrite-specific modulations of synaptic input

Considerable work has been devoted to the impact of cortical network activity on sensory-evoked synaptic input. Synaptic responses to brief whisker (Petersen et al., 2003; Sachdev et al., 2004), forepaw (Zhao et al., 2016) and auditory (Zhou et al., 2014) stimuli undergo reductions in amplitude in depolarized phases of slow activity compared to hyperpolarized phases. An increase in the amplitude of synaptic inputs has also been observed in visual stimuli of longer duration (Polack et al., 2013). Intriguingly, a gain modulation of synaptic inputs has been detected in recent work using different amplitude auditory stimulation (Reig et al., 2015).

The aim of this work was to establish whether the network activity of different brain states modulates the integration of similar inputs arriving from either the apical or basal compartments of L2/3 pyramidal neurons in different ways. Here, I reported that apical input is attenuated in a distance-dependent manner during Upstates and V_{dep} periods, and is disinhibited or even amplified during active movement. In the basal compartment, inputs experience a gain modulation during increased network activity. Only smaller inputs are increased over similar inputs that arrive during Downstate and V_{hyp} periods.

What function could such a distinct state-dependent modulation strategy fulfill in a single cell? A theory of pyramidal cell function suggests that these neurons integrate external, sensory, “feedforward” input that arrives via basal dendrites with internal “feedback” information from apical dendrites (Larkum, 2013) (Paragraph 1.1.3, Figure 3). In the whisker system, for example, a L2/3 pyramidal neuron of the somatosensory barrel cortex

corresponding to the C2 whisker predominantly receives direct and indirect input from deflections of the C2 whisker. This feedforward sensory input passes through the VPM specific thalamic nucleus and reaches mainly L4 and then spreads to L5 and L2/3 along the same barrel columns, expanding laterally to neighboring columns. The many cells it reaches in L5 and L2/3 trigger a process of reciprocal local communication through which the sensory information is integrated and decoded. Such feedforward direct and indirect inputs are mainly gathered by the basal dendritic compartment (Feldmeyer et al., 2006, 2002; Oberlaender et al., 2012). At the same time, the same neurons receive higher-order, top-down feedback input predominantly in L1 from the posteromedial (POm) higher order thalamic complex (Shipp, 2007; Wimmer et al., 2010). This delivers information related to the activity of all of the other whiskers. L1 in the sensory cortex is also the target of projections from M1 and other cortical regions (Veinante and Deschênes, 2003). Thus while the pyramidal neuron decodes specific information during a whisker deflection, it is receiving another layer of input, whose proposed function is to trigger a supralinear enhancement of the neuronal output. The simultaneous combination of the two streams may result in sustained firing and possibly a change in the mode of firing to bursts (Larkum, 2013) (Figure 3).

This model of signal integration is based on the activation of Ca^{2+}-spiking via a backpropagation of action potentials (BAC) in L5 pyramidal neurons (Larkum et al., 1999). But a synaptic activation of Ca^{2+} waves has also been reported for apical dendrites of L2/3 cells (Larkum et al., 2003). Moreover, in the pyramidal neurons of these layers, a pairing of APs and EPSPs evokes supralinear Ca^{2+} influx (Larkum et al., 2007; Waters et al., 2003). This type of coupling has been shown to be enhanced by blocking GABAergic transmission (Larkum et al., 2007). The activity-dependent calcium influx has been shown to be enhanced in a population of apical dendrites of L5 cells but to be reduced in L2/3 cells *in vivo* (Murayama and Larkum, 2009). This does not, however, rule out the possibility that single layer 2/3 cells exploit such a coupling mechanism to change their firing behavior. In fact, in contrast to L5, while populations of L2/3 pyramidal neurons reduce their mean firing rate during desynchronized (Move) states (Poulet and Petersen, 2008; Zhao et al., 2016) an enhancement of activity is seen in a small subset of cells (Barth and Poulet, 2012), suggesting that L2/3 and L5 have distinct sensory coding strategies. This means that L2/3 neurons might employ a coupling strategy similar to that of L5 neurons, but only in response to a combination of stimuli carrying specific sensory information, and not as a whole population (Andermann and Moore, 2006; Bathellier et al., 2012; O'Connor et al., 2010; Ohki et al.,

2006, 2005; Rothschild et al., 2010). The overall reduction of activity in 2/3, together with sparse firing (Barth and Poulet, 2012) may work to enhance the extraction of behaviorally relevant synaptic inputs against a backdrop of noisy brain activity (Sakata and Harris, 2012).

The postsynaptic state-dependent gain modulation reported here for basal dendrites may be part of a tuning system that normalizes the impact of input along the basal arbor. Here it is interesting to note that a minority of synaptic inputs to cortical neurons are > 1 mV; the vast majority are < 0.5 mV (Jouhanneau et al., 2015). Selectively amplifying lower synaptic input could increase the relative contributions they make to cortical coding in active networks, giving them a more important role than has been assumed. In keeping with this idea, an intrinsic system that normalizes the location dependency of dendritic synaptic input has been already reported for CA1 pyramidal neurons (Magee, 1999). Synaptic normalization may therefore be a common functional property that neurons employ to counteract the effects of dendritic morphology and background activity.

The passive cable properties of thin dendrites may completely filter small, distant inputs during the turbulent V_m fluctuations in Upstate and make small, distal synapses almost completely irrelevant with regard to their contributions to somatic integration and AP outputs (Nevian et al., 2007). The intrinsically active system for basal dendrites proposed here would enhance the impact of smaller synaptic inputs that would otherwise be filtered, without boosting those that are already large. This would, effectively homogenize the strengths of sensory feedforward synaptic inputs that arrive at L2/3 cells. A gain modulation of basal inputs may, therefore, provide a cell-intrinsic mechanism that enhances the cortical representation of weak sensory inputs (Chance et al., 2002). Such gain modulations are seen at many levels of signal processing, from postsynaptic-elicited OPs to the stimulation of a large sensory area such as the VPM, as well as across other sensory systems (Reig et al., 2015). I hypothesize that these types of gain modulations are a core feature of the information processing of sensory perception.

Counterbalancing this, a state-dependent reduction of apical input might function as a gate control to prevent coincidental detection events until salient moments. L2/3 pyramidal neurons exhibit particularly sparse and low rates of firing, whose function has been linked to a selective responsiveness to particular features of sensory stimulation (Barth and Poulet, 2012; Petersen and Crochet, 2013; Sakata and Harris, 2012). Nonetheless, strong inputs to the apical compartment can elicit calcium events that in turn enhance the probability of firing (Larkum et al., 2007; Waters et al., 2003). Here I suggest that during active movement, this inhibition is removed. I hypothesize that this is dependent on a sudden reduction in the firing

output of layer 2/3 SST Martinotti interneurons (Gentet et al., 2012), which selectively target apical dendrites in L1 with inhibitory synapses (Jiang et al., 2013; McGarry, 2010). If this were the case, then Martinotti cells would function as the gate for coincident detection in pyramidal neurons. When no feedback input arrives, SSTs constantly inhibit the whole apical compartment of L2/3 cells, which may suppress the somatic impact of top-down information and help maintain their low firing pattern. On the other hand, when a strong signal from other brain areas is transmitted to L1, SST neurons release their inhibition and pyramidal neurons now receive strong input from both their compartments, which may increase firing rate. Their output will then be transmitted both locally and to other cortical areas as a signal of the detection of coincident input (Larkum, 2013).

Nevertheless, while SSTs have high firing rates during V_{dep} phases in resting awake animals (Gentet et al., 2012), this is less prominent during Upstates under anesthesia (Pala and Petersen, 2015). Thus it is not clear whether SSTs can mediate the distance-dependent shunting that occurs in Upstates in apical dendrites reported here. Other factors, including perhaps a cell-intrinsic mechanism involving a driving force saturation effect in distal dendrites, may be mainly responsible for this apical compartmentalization. Martinotti cells may enhance this apical compartmentalization with a shunting effect during resting periods and release the inhibition during movement. Ultimately, this intrinsic compartmentalization or shunting mechanism in the apical compartment may play a role in the reduction of apical dendritic calcium responses in the L2/3 population (Murayama and Larkum, 2009), low firing rates (Zhao et al., 2016) and sparse firing (Barth and Poulet, 2012). These features may enhance the selectivity of sensory responses and tune the top-down control of sensory processing, which may also play an important role in experience-dependent modifications of sensory representation (Sakata and Harris, 2012).

4.9 Outlook and future experiments

A number of further experiments will be needed to examine the cellular mechanisms of state dependent modulation of input amplitude in more detail.

Intracellular blocking via QX-314 suggested that the gain modulation of basal synaptic inputs is a postsynaptic specific effect dependent on Na_P channels. However, the unspecific nature of QX-314 may block other ion channels (Perkins and Wong, 1995; Strichartz, 1973; Talbot and Sayer, 1996). A logical consequence is to apply more selective intracellular drugs such as the NMDA selective blocker MK-801 (Palmer, 2014; Wong et al., 1986), or D-890

a voltage gated calcium blocker (Deisz and Prince, 1987; Grienberger et al., 2014). Such experiments may help clarify or exclude the role of other voltage-gated channels in the mechanisms of modulation. I have already collected a partial dataset of basal dendritic stimulation under MK-801.

A drug which specifically targets Na_V is Tetrodotoxin (TTX) (Narahashi et al., 1964); unfortunately, it produces its effects by binding to an external site of the sodium channel and does not work intracellularly (Kao, 1986). Due to its high affinity for Na_V, *in vivo* applications of TTX completely block the generation and propagation of APs, and thus may well entirely disrupt the spontaneous network activity that is the source of the modulation itself. A second glass pipette connected to a iontophoresis device could permit a very focused application of TTX close to the dendritic spot to be stimulated, or along the course of the basal dendrite (Müller et al., 2012), and the results might be helpful. Alternatively, using TTX in an *in vitro* slice model of Upstates (Gerkin et al., 2010) would also permit an examination of the mechanism in greater detail.

Alternative modeling approaches based on different distributions of Na_P, K_{ir} and calcium channels along the dendritic branches and soma may also be helpful in elucidating the mechanisms underlying synaptic input modulation.

Apart from the complete unraveling of the intracellular mechanism, it would be interesting to test more generally the extent to which such gain modulation is present during sensory processing. Similar gain modulations have been reported in the auditory system (Reig et al., 2015), and it would be interesting to confirm whether it is also present with different intensities of whisker deflection.

The POm thalamic nucleus delivers feedback information on the activity of the whole barrel field to L1 of the somatosensory whisker cortex (Jouhanneau et al., 2014; Shipp, 2007; Wimmer et al., 2010). It would therefore be interesting to test whether the neurons projecting to the apical compartment in layer 1 are attenuated during Upstates, as for apical direct stimulation, or if such input would undergo a gain modulation, as for basal inputs and VPM activation. A partial dataset has already been collected by my colleague Dr. Jouhanneau which exploits my POm viral infections of ChR2.

Finally, it would be important to confirm the role of SST interneurons in the motor activity-dependent gating of apical inputs to L2/3 neurons. SST neurons are known to fire during quiet wakefulness (Gentet et al., 2012; Muñoz et al., 2017) and inhibit apical dendrites (Jiang et al., 2013; McGarry, 2010; Murayama et al., 2009; Wang et al., 2004). A difficult yet compelling experiment would involve the selective inhibition of SST neurons,

in combination with ChR2 subcellular stimulation, during quiet and moving periods. The design of such an experiment could involve the use of a transgenic mouse line expressing the CRE recombinase in SST neurons (Taniguchi et al., 2011), in combination with cortical AAV infections delivering a CRE-dependent, red-shifted inhibitory opsin such as the cruxhalorhodopsin Jaws. Jaws is a chloride-selective inhibitory channel sensible to red light (Chuong et al., 2014), with an activation spectrum that only partially overlaps that of ChR2(TC). This would permit an activation of the two opsins in the same sample using two distinct wavelengths of light. A coinfection of the CRE-dependent Jaws, which would be expressed only in SST cells, and CamKII-ChR2(TC) expressed mostly in pyramidal neurons, can be obtained in the superficial cortical layers of the somatosensory cortex. During the recording of a ChR2 expressing pyramidal neuron and two-photon stimulation of an apical dendritic target area, a red diffused light can be applied to the superficial L1, blocking only SST neurons.

I have already determined that ChR2(TC)-expressing neurons are completely nonresponsive to a diffuse red light. While it cannot be excluded that the two-photon activation of apical dendrites at 920 nm might affect Jaws-expressing SST neurons as well, the interference would probably be marginal. My prediction would be that a suppression of SST neuron firing during movement would prevent the attenuation of apical inputs.

Conclusions

This work represents the first attempt to exploit subcellular two-photon stimulations *in vivo* to study the brain state-dependent modulation of synaptic input. I have shown that optically generated potentials can resemble basic cellular features of glutamatergic synaptic input in Downstates. Moreover, the data collected with this method showed how such OPs undergo state-dependent modulations very similar to those observed in real EPSPs. This makes two-photon dendritic stimulations of ChR2 a robust method to reproduce and study synaptic input *in vivo* for future studies even in awake animals. The dendrite-specific, state-dependent modulations observed here should help unravel the influence that brain states have on the subthreshold integration of sensory inputs. Moreover, it brings up to light some of the multicellular and cell-intrinsic mechanisms that evolved in L2/3 pyramidal neurons and are employed in the management of their functions as integrative elements for information processing in the neocortex.

BIBLIOGRAPHY

Abella, I.D., 1962. Optical Double-Photon Absorption in Cesium Vapor. Phys. Rev. Lett.

Agmon-Snir, H., Segev, I., 1993. Signal delay and input synchronization in passive dendritic structures. J. Neurophysiol. 70, 2066–2085.

Albertson, A.J., Williams, S.B., Hablitz, J.J., 2013. Regulation of epileptiform discharges in rat neocortex by HCN channels. J. Neurophysiol. 110, 1733–1743. doi:10.1152/jn.00955.2012

Andermann, M.L., Moore, C.I., 2006. A somatotopic map of vibrissa motion direction within a barrel column. Nat. Neurosci. 9, 543–551. doi:10.1038/nn1671

Andrasfalvy, B.K., Zemelman, B.V., Tang, J., Vaziri, A., 2010. Two-photon single-cell optogenetic control of neuronal activity by sculpted light. Proc. Natl. Acad. Sci. U. S. A. 107, 11981–11986. doi:10.1073/pnas.1006620107

Andreasen, M., Lambert, J.D., 1999. Somatic amplification of distally generated subthreshold EPSPs in rat hippocampal pyramidal neurones. J. Physiol. 519, 85–100.

Aschauer, D.F., Kreuz, S., Rumpel, S., 2013. Analysis of Transduction Efficiency, Tropism and Axonal Transport of AAV Serotypes 1, 2, 5, 6, 8 and 9 in the Mouse Brain. PLoS ONE 8, e76310. doi:10.1371/journal.pone.0076310

Auger, C., Marty, A., 2000. Quantal currents at single-site central synapses. J. Physiol. 526, 3–11.

Azevedo, F.A.C., Carvalho, L.R.B., Grinberg, L.T., Farfel, J.M., Ferretti, R.E.L., Leite, R.E.P., Jacob Filho, W., Lent, R., Herculano-Houzel, S., 2009. Equal numbers of neuronal and nonneuronal cells make the human brain an isometrically scaled-up primate brain. J. Comp. Neurol. 513, 532–541. doi:10.1002/cne.21974

Barth, A.L., 2004. Alteration of Neuronal Firing Properties after In Vivo Experience in a FosGFP Transgenic Mouse. J. Neurosci. 24, 6466–6475. doi:10.1523/JNEUROSCI.4737-03.2004

Barth, A.L., Poulet, J.F.A., 2012. Experimental evidence for sparse firing in the neocortex. Trends Neurosci. 35, 345–355. doi:10.1016/j.tins.2012.03.008

Bathellier, B., Ushakova, L., Rumpel, S., 2012. Discrete neocortical dynamics predict behavioral categorization of sounds. Neuron 76, 435–449. doi:10.1016/j.neuron.2012.07.008

Beltramo, R., D'Urso, G., Dal Maschio, M., Farisello, P., Bovetti, S., Clovis, Y., Lassi, G., Tucci, V., De Pietri Tonelli, D., Fellin, T., 2013. Layer-specific excitatory circuits differentially control recurrent network dynamics in the neocortex. Nat. Neurosci. 16, 227–234. doi:10.1038/nn.3306

Berger, H., 1929. Über das Elektrenkephalogramm des Menschen. Arch. Für Psychiatr. Nervenkrankh. 87, 527–570. doi:10.1007/BF01797193

Berger, T., Larkum, M.E., Lüscher, H.R., 2001. High I(h) channel density in the distal apical dendrite of layer V pyramidal cells increases bidirectional attenuation of EPSPs. J. Neurophysiol. 85, 855–868.

Bernander, O., Douglas, R.J., Martin, K.A.C., Koch, C., 1991. Synaptic background activity influences spatiotemporal integration in single pyramidal cells. Proc. Natl. Acad. Sci. 88, 11569–11573.

Berndt, A., Schoenenberger, P., Mattis, J., Tye, K.M., Deisseroth, K., Hegemann, P., Oertner, T.G., 2011. High-efficiency channelrhodopsins for fast neuronal stimulation at low light levels. Proc. Natl. Acad. Sci. 108, 7595–7600. doi:10.1073/pnas.1017210108

Binzegger, T., 2004. A Quantitative Map of the Circuit of Cat Primary Visual Cortex. J. Neurosci. 24, 8441–8453. doi:10.1523/JNEUROSCI.1400-04.2004

Blomfield, S., 1974. Arithmetical operations performed by nerve cells. Brain Res. 69, 115–124. doi:10.1016/0006-8993(74)90375-8

Boyden, E.S., Zhang, F., Bamberg, E., Nagel, G., Deisseroth, K., 2005. Millisecond-timescale, genetically targeted optical control of neural activity. Nat. Neurosci. 8, 1263–1268. doi:10.1038/nn1525

Branco, T., Clark, B.A., Häusser, M., 2010. Dendritic discrimination of temporal input sequences in cortical neurons. Science 329, 1671–1675. doi:10.1126/science.1189664

Brock, L.G., Coombs, J.S., Eccles, J.C., 1952. The recording of potentials from motoneurones with an intracellular electrode. J. Physiol. 117, 431–460.

Brown, T.G., 1911. The Intrinsic Factors in the Act of Progression in the Mammal. Proc. R. Soc. Lond. B Biol. Sci. 84, 308–319. doi:10.1098/rspb.1911.0077

Buzsáki, G., 2006. Rhythms of the brain. Oxford University Press, Oxford ; New York.

Carter, B.C., Giessel, A.J., Sabatini, B.L., Bean, B.P., 2012. Transient Sodium Current at Subthreshold Voltages: Activation by EPSP Waveforms. Neuron 75, 1081–1093. doi:10.1016/j.neuron.2012.08.033

Chadderton, P., Schaefer, A.T., Williams, S.R., Margrie, T.W., 2014. Sensory-evoked synaptic integration in cerebellar and cerebral cortical neurons. Nat. Rev. Neurosci. 15, 71–83. doi:10.1038/nrn3648

Chance, F.S., Abbott, L.F., Reyes, A.D., 2002. Gain modulation from background synaptic input. Neuron 35, 773–782.

Chen, X., Leischner, U., Rochefort, N.L., Nelken, I., Konnerth, A., 2011. Functional mapping of single spines in cortical neurons in vivo. Nature 475, 501–505. doi:10.1038/nature10193

Chuong, A.S., Miri, M.L., Busskamp, V., Matthews, G.A.C., Acker, L.C., Sørensen, A.T., Young, A., Klapoetke, N.C., Henninger, M.A., Kodandaramaiah, S.B., Ogawa, M., Ramanlal, S.B., Bandler, R.C., Allen, B.D., Forest, C.R., Chow, B.Y., Han, X., Lin, Y., Tye, K.M., Roska, B., Cardin, J.A., Boyden, E.S., 2014. Noninvasive optical inhibition with a red-shifted microbial rhodopsin. Nat. Neurosci. 17, 1123–1129. doi:10.1038/nn.3752

Clark, S.L., 1946. The electroencephalogram in concussion in cats. Anat. Rec. 94, 454.

Clement, E.A., Richard, A., Thwaites, M., Ailon, J., Peters, S., Dickson, C.T., 2008. Cyclic and Sleep-Like Spontaneous Alternations of Brain State Under Urethane Anaesthesia. PLoS ONE 3, e2004. doi:10.1371/journal.pone.0002004

Colonnier, M., 1968. Synaptic patterns on different cell types in the different laminae of the cat visual cortex. An electron microscope study. Brain Res. 9, 268275–273287.

Constantinople, C.M., Bruno, R.M., 2013. Deep cortical layers are activated directly by thalamus. Science 340, 1591–1594.

Cossart, R., Aronov, D., Yuste, R., 2003. Attractor dynamics of network UP states in the neocortex. Nature 423, 283–288.

Crochet, S., Chauvette, S., Boucetta, S., Timofeev, I., 2005. Modulation of synaptic transmission in neocortex by network activities. Eur. J. Neurosci. 21, 1030–1044. doi:10.1111/j.1460-9568.2005.03932.x

Crochet, S., Petersen, C.C.H., 2006. Correlating whisker behavior with membrane potential in barrel cortex of awake mice. Nat. Neurosci. 9, 608–610. doi:10.1038/nn1690

Crochet, S., Poulet, J.F.A., Kremer, Y., Petersen, C.C.H., 2011. Synaptic mechanisms underlying sparse coding of active touch. Neuron 69, 1160–1175. doi:10.1016/j.neuron.2011.02.022

Cuntz, H., Remme, M.W.H., Torben-Nielsen, B. (Eds.), 2014. The Computing Dendrite, Springer Series in Computational Neuroscience. Springer New York, New York, NY. doi:10.1007/978-1-4614-8094-5

DeFelipe, J., Fariñas, I., 1992. The pyramidal neuron of the cerebral cortex: Morphological and chemical characteristics of the synaptic inputs. Prog. Neurobiol. 39, 563–607. doi:10.1016/0301-0082(92)90015-7

Deisseroth, K., 2015. Optogenetics: 10 years of microbial opsins in neuroscience. Nat. Neurosci. 18, 1213–1225. doi:10.1038/nn.4091

Deisz, R.A., Fortin, G., Zieglgansberger, W., 1991. Voltage dependence of excitatory postsynaptic potentials of rat neocortical neurons. J. Neurophysiol. 65, 371–382.

Deisz, R.A., Prince, D.A., 1987. Effect of D890 on membrane properties of neocortical neurons. Brain Res. 422, 63–73.

Demos, J.N., 2005. Getting Started with Neurofeedback, 61144th edition. ed. W. W. Norton & Company, New York.

Denk, W., Strickler, J.H., Webb, W.W., 1990. Two-photon laser scanning fluorescence microscopy. Science.

Destexhe, A., Paré, D., 1999. Impact of network activity on the integrative properties of neocortical pyramidal neurons in vivo. J. Neurophysiol. 81, 1531–1547.

Destexhe, A., Rudolph, M., Paré, D., 2003. The high-conductance state of neocortical neurons in vivo. Nat. Rev. Neurosci. 4, 739–751. doi:10.1038/nrn1198

Douglas, R.J., Martin, K.A.C., 2004. NEURONAL CIRCUITS OF THE NEOCORTEX. Annu. Rev. Neurosci. 27, 419–451. doi:10.1146/annurev.neuro.27.070203.144152

Elston, G.N., 2003. Cortex, Cognition and the Cell: New Insights into the Pyramidal Neuron and Prefrontal Function. Cereb. Cortex 13, 1124–1138. doi:10.1093/cercor/bhg093

Emiliani, V., Cohen, A.E., Deisseroth, K., Hausser, M., 2015. All-Optical Interrogation of Neural Circuits. J. Neurosci. 35, 13917–13926. doi:10.1523/JNEUROSCI.2916-15.2015

Feldmeyer, D., Lubke, J., Sakmann, B., 2006. Efficacy and connectivity of intracolumnar pairs of layer 2/3 pyramidal cells in the barrel cortex of juvenile rats. J. Physiol. 575, 583–602. doi:10.1113/jphysiol.2006.105106

Feldmeyer, D., Lübke, J., Silver, R.A., Sakmann, B., 2002. Synaptic connections between layer 4 spiny neurone-layer 2/3 pyramidal cell pairs in juvenile rat barrel cortex: physiology and anatomy of interlaminar signalling within a cortical column. J. Physiol. 538, 803–822.

French, C.R., Sah, P., Buckett, K.J., Gage, P.W., 1990. A voltage-dependent persistent sodium current in mammalian hippocampal neurons. J. Gen. Physiol. 95, 1139–1157.

Froemke, R.C., Poo, M., Dan, Y., 2005. Spike-timing-dependent synaptic plasticity depends on dendritic location. Nature 434, 221–225. doi:10.1038/nature03366

Gambino, F., Pagès, S., Kehayas, V., Baptista, D., Tatti, R., Carleton, A., Holtmaat, A., 2014. Sensory-evoked LTP driven by dendritic plateau potentials in vivo. Nature 515, 116–119. doi:10.1038/nature13664

Gentet, L.J., Kremer, Y., Taniguchi, H., Huang, Z.J., Staiger, J.F., Petersen, C.C.H., 2012. Unique functional properties of somatostatin-expressing GABAergic neurons in mouse barrel cortex. Nat. Neurosci. 15, 607–612. doi:10.1038/nn.3051

George, M.S., Abbott, L.F., Siegelbaum, S.A., 2009. HCN hyperpolarization-activated cation channels inhibit EPSPs by interactions with M-type K+ channels. Nat. Neurosci. 12, 577–584. doi:10.1038/nn.2307

Gerkin, R.C., Clem, R.L., Shruti, S., Kass, R.E., Barth, A.L., 2010. Cortical Up State Activity Is Enhanced After Seizures: A Quantitative Analysis: J. Clin. Neurophysiol. 27, 425–432. doi:10.1097/WNP.0b013e3181fdf8bd

Giugliano, M., Darbon, P., Arsiero, M., Luscher, H.-R., Streit, J., 2004. Single-Neuron Discharge Properties and Network Activity in Dissociated Cultures of Neocortex. J. Neurophysiol. 92, 977–996. doi:10.1152/jn.00067.2004

Goebbels, S., Bormuth, I., Bode, U., Hermanson, O., Schwab, M.H., Nave, K.-A., 2006. Genetic targeting of principal neurons in neocortex and hippocampus of NEX-Cre mice. Genes. N. Y. N 2000 44, 611–621. doi:10.1002/dvg.20256

Golgi, C., 1873. Sulla struttura della sostanza grigia del cervello. Gazzetta Medica Ital. Lomb. 33, 244–246.

González-Burgos, G., Barrionuevo, G., 2001. Voltage-gated sodium channels shape subthreshold EPSPs in layer 5 pyramidal neurons from rat prefrontal cortex. J. Neurophysiol. 86, 1671–1684.

Gordon, U., Polsky, A., Schiller, J., 2006. Plasticity Compartments in Basal Dendrites of Neocortical Pyramidal Neurons. J. Neurosci. 26, 12717–12726. doi:10.1523/JNEUROSCI.3502-06.2006

Gradinaru, V., Zhang, F., Ramakrishnan, C., Mattis, J., Prakash, R., Diester, I., Goshen, I., Thompson, K.R., Deisseroth, K., 2010. Molecular and cellular approaches for diversifying and extending optogenetics. Cell 141, 154–165. doi:10.1016/j.cell.2010.02.037

Grienberger, C., Chen, X., Konnerth, A., 2015. Dendritic function in vivo. Trends Neurosci. 38, 45–54. doi:10.1016/j.tins.2014.11.002

Grienberger, C., Chen, X., Konnerth, A., 2014. NMDA Receptor-Dependent Multidendrite Ca2+ Spikes Required for Hippocampal Burst Firing In Vivo. Neuron 81, 1274–1281. doi:10.1016/j.neuron.2014.01.014

Haider, B., 2006. Neocortical Network Activity In Vivo Is Generated through a Dynamic Balance of Excitation and Inhibition. J. Neurosci. 26, 4535–4545. doi:10.1523/JNEUROSCI.5297-05.2006

Hara, K., Harris, R.A., 2002. The anesthetic mechanism of urethane: the effects on neurotransmitter-gated ion channels. Anesth. Analg. 94, 313–318, table of contents.

Harnett, M.T., Makara, J.K., Spruston, N., Kath, W.L., Magee, J.C., 2012. Synaptic amplification by dendritic spines enhances input cooperativity. Nature 491, 599–602. doi:10.1038/nature11554

Harris, K.D., Shepherd, G.M.G., 2015. The neocortical circuit: themes and variations. Nat. Neurosci. 18, 170–181. doi:10.1038/nn.3917

Hasenstaub, A., Sachdev, R.N.S., McCormick, D.A., 2007. State Changes Rapidly Modulate Cortical Neuronal Responsiveness. J. Neurosci. 27, 9607–9622. doi:10.1523/JNEUROSCI.2184-07.2007

Häusser, M., Spruston, N., Stuart, G.J., 2000. Diversity and dynamics of dendritic signaling. Science 290, 739–744.

Helmchen, F., Denk, W., 2005. Deep tissue two-photon microscopy. Nat. Methods 2, 932–940. doi:10.1038/nmeth818

Herzog, R.W., 2007. Immune Responses to AAV Capsid: Are Mice Not Humans After All? Mol. Ther. 15, 649–650. doi:10.1038/sj.mt.6300123

Hirsch, J.A., Gilbert, C.D., 1991. Synaptic physiology of horizontal connections in the cat's visual cortex. J. Neurosci. 11, 1800–1809.

Hô, N., Destexhe, A., 2000. Synaptic background activity enhances the responsiveness of neocortical pyramidal neurons. J. Neurophysiol. 84, 1488–1496.

Hromádka, T., Deweese, M.R., Zador, A.M., 2008. Sparse representation of sounds in the unanesthetized auditory cortex. PLoS Biol. 6, e16. doi:10.1371/journal.pbio.0060016

Jaffe, D.B., Carnevale, N.T., 1999. Passive Normalization of Synaptic Integration Influenced by Dendritic Architecture. J. Neurophysiol. 82, 3268–3285.

Jia, H., Rochefort, N.L., Chen, X., Konnerth, A., 2010. Dendritic organization of sensory input to cortical neurons in vivo. Nature 464, 1307–1312. doi:10.1038/nature08947

Jiang, X., Wang, G., Lee, A.J., Stornetta, R.L., Zhu, J.J., 2013. The organization of two new cortical interneuronal circuits. Nat. Neurosci. 16, 210–218. doi:10.1038/nn.3305

Jones, E.G., Huntley, G.W., Benson, D.L., 1994. Alpha calcium/calmodulin-dependent protein kinase II selectively expressed in a subpopulation of excitatory neurons in monkey sensory-motor cortex: comparison with GAD-67 expression. J. Neurosci. 14, 611–629.

Jouhanneau, J.-S., Ferrarese, L., Estebanez, L., Audette, N.J., Brecht, M., Barth, A.L., Poulet, J.F.A., 2014. Cortical fosGFP Expression Reveals Broad Receptive Field Excitatory Neurons Targeted by POm. Neuron 84, 1065–1078. doi:10.1016/j.neuron.2014.10.014

Jouhanneau, J.-S., Kremkow, J., Dorrn, A.L., Poulet, J.F.A., 2015. In Vivo Monosynaptic Excitatory Transmission between Layer 2 Cortical Pyramidal Neurons. Cell Rep. 13, 2098–2106. doi:10.1016/j.celrep.2015.11.011

Judkewitz, B., Rizzi, M., Kitamura, K., Häusser, M., 2009. Targeted single-cell electroporation of mammalian neurons in vivo. Nat. Protoc. 4, 862–869. doi:10.1038/nprot.2009.56

Kao, C.Y., 1986. Structure-activity relations of tetrodotoxin, saxitoxin, and analogues. Ann. N. Y. Acad. Sci. 479, 52–67.

Kitamura, K., Judkewitz, B., Kano, M., Denk, W., Häusser, M., 2008. Targeted patch-clamp recordings and single-cell electroporation of unlabeled neurons in vivo. Nat. Methods 5, 61–67. doi:10.1038/nmeth1150

Klapoetke, N.C., Murata, Y., Kim, S.S., Pulver, S.R., Birdsey-Benson, A., Cho, Y.K., Morimoto, T.K., Chuong, A.S., Carpenter, E.J., Tian, Z., Wang, J., Xie, Y., Yan, Z., Zhang, Y., Chow, B.Y., Surek, B., Melkonian, M., Jayaraman, V., Constantine-Paton, M., Wong, G.K.-S., Boyden, E.S., 2014. Independent optical excitation of distinct neural populations. Nat. Methods 11, 338–346. doi:10.1038/nmeth.2836

Kobayashi, T., Himwich, H.E., 1962. An electrocorticographic study of changes in mouse brain with age. Life Sci. 1962 1, 343–345.

Larkman, A.U., 1991. Dendritic morphology of pyramidal neurones of the visual cortex of the rat: III. Spine distributions. J. Comp. Neurol. 306, 332–343.

Larkum, M., 2013. A cellular mechanism for cortical associations: an organizing principle for the cerebral cortex. Trends Neurosci. 36, 141–151. doi:10.1016/j.tins.2012.11.006

Larkum, M.E., Nevian, T., 2008. Synaptic clustering by dendritic signalling mechanisms. Curr. Opin. Neurobiol. 18, 321–331. doi:10.1016/j.conb.2008.08.013

Larkum, M.E., Nevian, T., Sandler, M., Polsky, A., Schiller, J., 2009. Synaptic Integration in Tuft Dendrites of Layer 5 Pyramidal Neurons: A New Unifying Principle. Science 325, 756–760. doi:10.1126/science.1171958

Larkum, M.E., Watanabe, S., Nakamura, T., Lasser-Ross, N., Ross, W.N., 2003. Synaptically Activated Ca $^{2+}$ Waves in Layer 2/3 and Layer 5 Rat Neocortical Pyramidal Neurons. J. Physiol. 549, 471–488. doi:10.1113/jphysiol.2002.037614

Larkum, M.E., Waters, J., Sakmann, B., Helmchen, F., 2007. Dendritic Spikes in Apical Dendrites of Neocortical Layer 2/3 Pyramidal Neurons. J. Neurosci. 27, 8999–9008. doi:10.1523/JNEUROSCI.1717-07.2007

Larkum, M.E., Zhu, J.J., Sakmann, B., 1999. A new cellular mechanism for coupling inputs arriving at different cortical layers. Nature 398, 338–341.

Lee, S., Hjerling-Leffler, J., Zagha, E., Fishell, G., Rudy, B., 2010. The Largest Group of Superficial Neocortical GABAergic Interneurons Expresses Ionotropic Serotonin Receptors. J. Neurosci. 30, 16796–16808. doi:10.1523/JNEUROSCI.1869-10.2010

Lee, S.-H., Dan, Y., 2012. Neuromodulation of Brain States. Neuron 76, 209–222. doi:10.1016/j.neuron.2012.09.012

Lefort, S., Tomm, C., Floyd Sarria, J.-C., Petersen, C.C.H., 2009. The excitatory neuronal network of the C2 barrel column in mouse primary somatosensory cortex. Neuron 61, 301–316. doi:10.1016/j.neuron.2008.12.020

Lin, J.Y., 2012. Optogenetic excitation of neurons with channelrhodopsins: light instrumentation, expression systems, and channelrhodopsin variants. Prog. Brain Res. 196, 29–47. doi:10.1016/B978-0-444-59426-6.00002-1

Liu, X.-B., Jones, E.G., 1996. Localization of alpha type II calcium calmodulin-dependent protein kinase at glutamatergic but not gamma-aminobutyric acid (GABAergic) synapses in thalamus and cerebral cortex. Proc. Natl. Acad. Sci. 93, 7332–7336.

London, M., Roth, A., Beeren, L., Häusser, M., Latham, P.E., 2010. Sensitivity to perturbations in vivo implies high noise and suggests rate coding in cortex. Nature 466, 123–127. doi:10.1038/nature09086

Longordo, F., To, M.-S., Ikeda, K., Stuart, G.J., 2013. Sublinear integration underlies binocular processing in primary visual cortex. Nat. Neurosci. 16, 714–723. doi:10.1038/nn.3394

Losonczy, A., Makara, J.K., Magee, J.C., 2008. Compartmentalized dendritic plasticity and input feature storage in neurons. Nature 452, 436–441. doi:10.1038/nature06725

Madisen, L., Zwingman, T.A., Sunkin, S.M., Oh, S.W., Zariwala, H.A., Gu, H., Ng, L.L., Palmiter, R.D., Hawrylycz, M.J., Jones, A.R., Lein, E.S., Zeng, H., 2010. A robust and high-throughput Cre reporting and characterization system for the whole mouse brain. Nat. Neurosci. 13, 133–140. doi:10.1038/nn.2467

Magee, J.C., 1999. Dendritic Ih normalizes temporal summation in hippocampal CA1 neurons. Nat. Neurosci. 2, 508–514.

Magee, J.C., Cook, E.P., 2000. Somatic EPSP amplitude is independent of synapse location in hippocampal pyramidal neurons. Nat. Neurosci. 3, 895–903. doi:10.1038/78800

Magee, J.C., Johnston, D., 2005. Plasticity of dendritic function. Curr. Opin. Neurobiol. 15, 334–342. doi:10.1016/j.conb.2005.05.013

Maier, W., Corrie, J.E.T., Papageorgiou, G., Laube, B., Grewer, C., 2005. Comparative analysis of inhibitory effects of caged ligands for the NMDA receptor. J. Neurosci. Methods 142, 1–9. doi:10.1016/j.jneumeth.2004.07.006

Major, G., Larkum, M.E., Schiller, J., 2013. Active Properties of Neocortical Pyramidal Neuron Dendrites. Annu. Rev. Neurosci. 36, 1–24. doi:10.1146/annurev-neuro-062111-150343

Major, G., Polsky, A., Denk, W., Schiller, J., Tank, D.W., 2008. Spatiotemporally Graded NMDA Spike/Plateau Potentials in Basal Dendrites of Neocortical Pyramidal Neurons. J. Neurophysiol. 99, 2584–2601. doi:10.1152/jn.00011.2008

Marder, E., Calabrese, R.L., 1996. Principles of rhythmic motor pattern generation. Physiol. Rev. 76, 687–717.

Markram, H., Lübke, J., Frotscher, M., Roth, A., Sakmann, B., 1997. Physiology and anatomy of synaptic connections between thick tufted pyramidal neurones in the developing rat neocortex. J. Physiol. 500, 409.

Marshel, J.H., Mori, T., Nielsen, K.J., Callaway, E.M., 2010. Targeting single neuronal networks for gene expression and cell labeling in vivo. Neuron 67, 562–574. doi:10.1016/j.neuron.2010.08.001

Mateo, C., Avermann, M., Gentet, L.J., Zhang, F., Deisseroth, K., Petersen, C.C.H., 2011. In Vivo Optogenetic Stimulation of Neocortical Excitatory Neurons Drives Brain-State-Dependent Inhibition. Curr. Biol. CB. doi:10.1016/j.cub.2011.08.028

McBain, C.J., Mayer, M.L., 1994. N-methyl-D-aspartic acid receptor structure and function. Physiol. Rev. 74, 723–760.

McGarry, 2010. Quantitative classification of somatostatin-positive neocortical interneurons identifies three interneuron subtypes. Front. Neural Circuits. doi:10.3389/fncir.2010.00012

Meunier, D., Lambiotte, R., Bullmore, E.T., 2010. Modular and hierarchically modular organization of brain networks. Front. Neurosci. 4, 200. doi:10.3389/fnins.2010.00200

Migliore, M., Shepherd, G.M., 2002. EMERGING RULES FOR THE DISTRIBUTIONS OF ACTIVE DENDRITIC CONDUCTANCES. Nat. Rev. Neurosci. 3, 362–370. doi:10.1038/nrn810

Milenkovic, N., Zhao, W.-J., Walcher, J., Albert, T., Siemens, J., Lewin, G.R., Poulet, J.F.A., 2014. A somatosensory circuit for cooling perception in mice. Nat. Neurosci. 17, 1560–1566. doi:10.1038/nn.3828

Müller, C., Beck, H., Coulter, D., Remy, S., 2012. Inhibitory Control of Linear and Supralinear Dendritic Excitation in CA1 Pyramidal Neurons. Neuron 75, 851–864. doi:10.1016/j.neuron.2012.06.025

Muñoz, W., Tremblay, R., Levenstein, D., Rudy, B., 2017. Layer-specific modulation of neocortical dendritic inhibition during active wakefulness. Science 355, 954–959.

Murayama, M., Larkum, M.E., 2009. Enhanced dendritic activity in awake rats. Proc. Natl. Acad. Sci. 106, 20482–20486.

Murayama, M., Pérez-Garci, E., Nevian, T., Bock, T., Senn, W., Larkum, M.E., 2009. Dendritic encoding of sensory stimuli controlled by deep cortical interneurons. Nature 457, 1137–1141. doi:10.1038/nature07663

Nagel, G., Ollig, D., Fuhrmann, M., Kateriya, S., Musti, A.M., Bamberg, E., Hegemann, P., 2002. Channelrhodopsin-1: a light-gated proton channel in green algae. Science 296, 2395–2398. doi:10.1126/science.1072068

Nagel, G., Szellas, T., Huhn, W., Kateriya, S., Adeishvili, N., Berthold, P., Ollig, D., Hegemann, P., Bamberg, E., 2003. Channelrhodopsin-2, a directly light-gated cation-selective membrane channel. Proc. Natl. Acad. Sci. 100, 13940–13945.

Naldini, L., Blömer, U., Gage, F.H., Trono, D., Verma, I.M., 1996. Efficient transfer, integration, and sustained long-term expression of the transgene in adult rat brains injected with a lentiviral vector. Proc. Natl. Acad. Sci. 93, 11382–11388.

Narahashi, T., Moore, J.W., Scott, W.R., 1964. Tetrodotoxin Blockage of Sodium Conductance Increase in Lobster Giant Axons. J. Gen. Physiol. 47, 965–974.

Nathwani, A.C., Rosales, C., McIntosh, J., Rastegarlari, G., Nathwani, D., Raj, D., Nawathe, S., Waddington, S.N., Bronson, R., Jackson, S., Donahue, R.E., High, K.A., Mingozzi, F., Ng, C.Y., Zhou, J., Spence, Y., McCarville, M.B., Valentine, M., Allay, J., Coleman, J., Sleep, S., Gray, J.T., Nienhuis, A.W., Davidoff, A.M., 2011. Long-term Safety and Efficacy Following Systemic Administration of a Self-

complementary AAV Vector Encoding Human FIX Pseudotyped With Serotype 5 and 8 Capsid Proteins. Mol. Ther. 19, 876–885. doi:10.1038/mt.2010.274

Nevian, T., Larkum, M.E., Polsky, A., Schiller, J., 2007. Properties of basal dendrites of layer 5 pyramidal neurons: a direct patch-clamp recording study. Nat. Neurosci. 10, 206–214. doi:10.1038/nn1826

Nicholson, D.A., Trana, R., Katz, Y., Kath, W.L., Spruston, N., Geinisman, Y., 2006. Distance-dependent differences in synapse number and AMPA receptor expression in hippocampal CA1 pyramidal neurons. Neuron 50, 431–442. doi:10.1016/j.neuron.2006.03.022

Nieuwenhuys, R., 1994. The neocortex. An overview of its evolutionary development, structural organization and synaptology. Anat. Embryol. (Berl.) 190, 307–337.

Nikolenko, V., Poskanzer, K.E., Yuste, R., 2007. Two-photon photostimulation and imaging of neural circuits. Nat. Methods 4, 943–950. doi:10.1038/nmeth1105

Nikolic, K., Grossman, N., Grubb, M.S., Burrone, J., Toumazou, C., Degenaar, P., 2009. Photocycles of Channelrhodopsin-2. Photochem. Photobiol. 85, 400–411. doi:10.1111/j.1751-1097.2008.00460.x

Nisenbaum, E.S., Wilson, C.J., 1995. Potassium currents responsible for inward and outward rectification in rat neostriatal spiny projection neurons. J. Neurosci. Off. J. Soc. Neurosci. 15, 4449–4463.

Noguchi, J., Nagaoka, A., Watanabe, S., Ellis-Davies, G.C.R., Kitamura, K., Kano, M., Matsuzaki, M., Kasai, H., 2011. In vivo two-photon uncaging of glutamate revealing the structure-function relationships of dendritic spines in the neocortex of adult mice: In vivo two-photon glutamate uncaging. J. Physiol. 589, 2447–2457. doi:10.1113/jphysiol.2011.207100

Nyhus, E., Curran, T., 2010. Functional role of gamma and theta oscillations in episodic memory. Neurosci. Biobehav. Rev. 34, 1023–1035. doi:10.1016/j.neubiorev.2009.12.014

Oberlaender, M., de Kock, C.P.J., Bruno, R.M., Ramirez, A., Meyer, H.S., Dercksen, V.J., Helmstaedter, M., Sakmann, B., 2012. Cell Type-Specific Three-Dimensional Structure of Thalamocortical Circuits in a Column of Rat Vibrissal Cortex. Cereb. Cortex 22, 2375–2391. doi:10.1093/cercor/bhr317

O'Connor, D.H., Peron, S.P., Huber, D., Svoboda, K., 2010. Neural activity in barrel cortex underlying vibrissa-based object localization in mice. Neuron 67, 1048–1061. doi:10.1016/j.neuron.2010.08.026

Ohki, K., Chung, S., Ch'ng, Y.H., Kara, P., Reid, R.C., 2005. Functional imaging with cellular resolution reveals precise micro-architecture in visual cortex. Nature 433, 597–603. doi:10.1038/nature03274

Ohki, K., Chung, S., Kara, P., Hübener, M., Bonhoeffer, T., Reid, R.C., 2006. Highly ordered arrangement of single neurons in orientation pinwheels. Nature 442, 925–928. doi:10.1038/nature05019

Osborn, M., Panoskaltsismortari, A., Mcelmurry, R., Bell, S., Vignali, D., Ryan, M., Wilber, A., Mcivor, R., Tolar, J., Blazar, B., 2005. A picornaviral 2A-like sequence-based tricistronic vector allowing for high-level therapeutic gene expression coupled to a dual-reporter system. Mol. Ther. 12, 569–574. doi:10.1016/j.ymthe.2005.04.013

Packer, A.M., Peterka, D.S., Hirtz, J.J., Prakash, R., Deisseroth, K., Yuste, R., 2012. Two-photon optogenetics of dendritic spines and neural circuits. Nat. Methods 9, 1202–1205. doi:10.1038/nmeth.2249

Packer, A.M., Yuste, R., 2011. Dense, Unspecific Connectivity of Neocortical Parvalbumin-Positive Interneurons: A Canonical Microcircuit for Inhibition? J. Neurosci. 31, 13260–13271. doi:10.1523/JNEUROSCI.3131-11.2011

Pakkenberg, B., Pelvig, D., Marner, L., Bundgaard, M.J., Gundersen, H.J.G., Nyengaard, J.R., Regeur, L., 2003. Aging and the human neocortex. Exp. Gerontol. 38, 95–99.

Pala, A., Petersen, C.C.H., 2015. In Vivo Measurement of Cell-Type-Specific Synaptic Connectivity and Synaptic Transmission in Layer 2/3 Mouse Barrel Cortex. Neuron 85, 68–75. doi:10.1016/j.neuron.2014.11.025

Palmer, L.M., 2014. Dendritic integration in pyramidal neurons during network activity and disease. Brain Res. Bull. 103, 2–10. doi:10.1016/j.brainresbull.2013.09.010

Papagiakoumou, E., Anselmi, F., Bègue, A., de Sars, V., Glückstad, J., Isacoff, E.Y., Emiliani, V., 2010. Scanless two-photon excitation of channelrhodopsin-2. Nat. Methods 7, 848–854. doi:10.1038/nmeth.1505

Pearce, J.M.S., 2009. Marie-Jean-Pierre Flourens (1794–1867) and Cortical Localization. Eur. Neurol. 61, 311–314. doi:10.1159/000206858

Perkins, K.L., Wong, R.K., 1995. Intracellular QX-314 blocks the hyperpolarization-activated inward current Iq in hippocampal CA1 pyramidal cells. J. Neurophysiol. 73, 911–915.

Petersen, C.C.H., Crochet, S., 2013. Synaptic Computation and Sensory Processing in Neocortical Layer 2/3. Neuron 78, 28–48. doi:10.1016/j.neuron.2013.03.020

Petersen, C.C.H., Hahn, T.T.G., Mehta, M., Grinvald, A., Sakmann, B., 2003. Interaction of sensory responses with spontaneous depolarization in layer 2/3 barrel cortex. Proc. Natl. Acad. Sci. U. S. A. 100, 13638–13643. doi:10.1073/pnas.2235811100

Pi, H.-J., Hangya, B., Kvitsiani, D., Sanders, J.I., Huang, Z.J., Kepecs, A., 2013. Cortical interneurons that specialize in disinhibitory control. Nature 503, 521–524. doi:10.1038/nature12676

Pinto, L., Dan, Y., 2015. Cell-Type-Specific Activity in Prefrontal Cortex during Goal-Directed Behavior. Neuron 87, 437–450. doi:10.1016/j.neuron.2015.06.021

Polack, P.-O., Friedman, J., Golshani, P., 2013. Cellular mechanisms of brain state-dependent gain modulation in visual cortex. Nat. Neurosci. 16, 1331–1339.

Poulet, J.F.A., Fernandez, L.M.J., Crochet, S., Petersen, C.C.H., 2012. Thalamic control of cortical states. Nat. Neurosci. 15, 370–372. doi:10.1038/nn.3035

Poulet, J.F.A., Petersen, C.C.H., 2008. Internal brain state regulates membrane potential synchrony in barrel cortex of behaving mice. Nature 454, 881–885. doi:10.1038/nature07150

Prakash, R., Yizhar, O., Grewe, B., Ramakrishnan, C., Wang, N., Goshen, I., Packer, A.M., Peterka, D.S., Yuste, R., Schnitzer, M.J., Deisseroth, K., 2012. Two-photon optogenetic toolbox for fast inhibition, excitation and bistable modulation. Nat. Methods 9, 1171–1179. doi:10.1038/nmeth.2215

Purves, D. (Ed.), 2008. Neuroscience, 4th ed. ed. Sinauer, Sunderland, Mass.

Rall, W., 1967. Distinguishing theoretical synaptic potentials computed for different soma-dendritic distributions of synaptic input. J. Neurophysiol. 30, 1138–1168.

Rall, W., Rinzel, J., 1973. Branch Input Resistance and Steady Attenuation for Input to One Branch of A DENDRITIC NEURON MODEL. Theor. Found. Dendritic Funct. Sel. Pap. Wilfrid Rall Comment. 287.

Ramón y Cajal, S., 1904. Textura del sistema nervioso del hombre y de los vertebrados. Zaragoza Madr.

Ramón y Cajal, S., 1899. Comparative study of the sensory areas of the h...

Redman, S., Walmsley, B., 1983. The time course of synaptic potentials evoked in cat spinal motoneurones at identified group Ia synapses. J. Physiol. 343, 117–133.

Reig, R., Sanchez-Vives, M.V., 2007. Synaptic transmission and plasticity in an active cortical network. PloS One 2, e670. doi:10.1371/journal.pone.0000670

Reig, R., Zerlaut, Y., Vergara, R., Destexhe, A., Sanchez-Vives, M.V., 2015. Gain Modulation of Synaptic Inputs by Network State in Auditory Cortex In Vivo. J. Neurosci. 35, 2689–2702. doi:10.1523/JNEUROSCI.2004-14.2015

Rickgauer, J.P., Tank, D.W., 2009. Two-photon excitation of channelrhodopsin-2 at saturation. Proc. Natl. Acad. Sci. 106, 15025–15030.

Rothschild, G., Nelken, I., Mizrahi, A., 2010. Functional organization and population dynamics in the mouse primary auditory cortex. Nat. Neurosci. 13, 353–360. doi:10.1038/nn.2484

Rudolph, M., Destexhe, A., 2003. A fast-conducting, stochastic integrative mode for neocortical neurons in vivo. J. Neurosci. 23, 2466–2476.

Rudolph, M., Destexhe, A., 2001. Correlation detection and resonance in neural systems with distributed noise sources. Phys. Rev. Lett. 86, 3662–3665. doi:10.1103/PhysRevLett.86.3662

Sachdev, R.N.S., Ebner, F.F., Wilson, C.J., 2004. Effect of subthreshold up and down states on the whisker-evoked response in somatosensory cortex. J. Neurophysiol. 92, 3511–3521. doi:10.1152/jn.00347.2004

Sakata, S., Harris, K.D., 2012. Laminar-dependent effects of cortical state on auditory cortical spontaneous activity. Front. Neural Circuits 6. doi:10.3389/fncir.2012.00109

Sanchez-Vives, M.V., McCormick, D.A., 2000. Cellular and network mechanisms of rhythmic recurrent activity in neocortex. Nat. Neurosci. 3, 1027–1034.

Sanders, H., Berends, M., Major, G., Goldman, M.S., Lisman, J.E., 2013. NMDA and GABAB (KIR) Conductances: The "Perfect Couple" for Bistability. J. Neurosci. 33, 424–429. doi:10.1523/JNEUROSCI.1854-12.2013

Sandler, M., Shulman, Y., Schiller, J., 2016. A Novel Form of Local Plasticity in Tuft Dendrites of Neocortical Somatosensory Layer 5 Pyramidal Neurons. Neuron 90, 1028–1042. doi:10.1016/j.neuron.2016.04.032

Sceniak, M.P., 2006. Cellular Actions of Urethane on Rat Visual Cortical Neurons In Vitro. J. Neurophysiol. 95, 3865–3874. doi:10.1152/jn.01196.2005

Shipp, S., 2007. Structure and function of the cerebral cortex. Curr. Biol. 17, R443–R449. doi:10.1016/j.cub.2007.03.044

Sineshchekov, O.A., Jung, K.-H., Spudich, J.L., 2002. Two rhodopsins mediate phototaxis to low- and high-intensity light in Chlamydomonas reinhardtii. Proc. Natl. Acad. Sci. U. S. A. 99, 8689–8694. doi:10.1073/pnas.122243399

Spruston, N., 2009. Dendritic Signal Integration, in: Squire, L.R. (Ed.), Encyclopedia of Neuroscience. Academic Press, Oxford, pp. 445–452. doi:10.1016/B978-008045046-9.01648-X

Spruston, N., 2008. Pyramidal neurons: dendritic structure and synaptic integration. Nat. Rev. Neurosci. 9, 206–221. doi:10.1038/nrn2286

Stacey, W.C., Durand, D.M., 2001. Synaptic noise improves detection of subthreshold signals in hippocampal CA1 neurons. J. Neurophysiol. 86, 1104–1112.

Stafstrom, C.E., Schwindt, P.C., Chubb, M.C., Crill, W.E., 1985. Properties of persistent sodium conductance and calcium conductance of layer V neurons from cat sensorimotor cortex in vitro. J. Neurophysiol. 53, 153–170.

Staiger, J.F., Masanneck, C., Schleicher, A., Zuschratter, W., 2004. Calbindin-containing interneurons are a target for VIP-immunoreactive synapses in rat primary somatosensory cortex. J. Comp. Neurol. 468, 179–189. doi:10.1002/cne.10953

Steriade, M., 2001. Impact of network activities on neuronal properties in corticothalamic systems. J. Neurophysiol. 86, 1–39.

Steriade, M., Nunez, A., Amzica, F., 1993. Intracellular analysis of relations between the slow (< 1 Hz) neocortical oscillation and other sleep rhythms of the electroencephalogram. J. Neurosci. 13, 3266–3283.

Strichartz, G.R., 1973. The Inhibition of Sodium Currents in Myelinated Nerve by Quaternary Derivatives of Lidocaine. J. Gen. Physiol. 62, 37–57.

Stuart, G.J., Sakmann, B., 1995. Amplification of EPSPs by axosomatic sodium channels in neocortical pyramidal neurons. - PubMed - NCBI. Neuron.

Stuart, G.J., Spruston, N., 2015. Dendritic integration: 60 years of progress. Nat. Neurosci. 18, 1713–1721. doi:10.1038/nn.4157

Sutor, B., Zieglgänsberger, W., 1987. A low-voltage activated, transient calcium current is responsible for the time-dependent depolarizing inward rectification of rat neocortical neurons in vitro. Pflugers Arch. 410, 102–111.

Takahashi, N., Kitamura, K., Matsuo, N., Mayford, M., Kano, M., Matsuki, N., Ikegaya, Y., 2012. Locally synchronized synaptic inputs. Science 335, 353–356. doi:10.1126/science.1210362

Talbot, M.J., Sayer, R.J., 1996. Intracellular QX-314 inhibits calcium currents in hippocampal CA1 pyramidal neurons. J. Neurophysiol. 76, 2120–2124.

Tamamaki, N., Yanagawa, Y., Tomioka, R., Miyazaki, J.-I., Obata, K., Kaneko, T., 2003. Green fluorescent protein expression and colocalization with calretinin, parvalbumin, and somatostatin in the GAD67-GFP knock-in mouse. J. Comp. Neurol. 467, 60–79. doi:10.1002/cne.10905

Taniguchi, H., He, M., Wu, P., Kim, S., Paik, R., Sugino, K., Kvitsani, D., Fu, Y., Lu, J., Lin, Y., Miyoshi, G., Shima, Y., Fishell, G., Nelson, S.B., Huang, Z.J., 2011. A Resource of Cre Driver Lines for Genetic Targeting of GABAergic Neurons in Cerebral Cortex. Neuron 71, 995–1013. doi:10.1016/j.neuron.2011.07.026

Thivierge, J.-P., Marcus, G.F., 2007. The topographic brain: from neural connectivity to cognition. Trends Neurosci. 30, 251–259. doi:10.1016/j.tins.2007.04.004

Thomson, A.M., Girdlestone, D., West, D.C., 1988. Voltage-dependent currents prolong single-axon postsynaptic potentials in layer III pyramidal neurons in rat neocortical slices. J. Neurophysiol. 60, 1896–1907.

Varga, Z., Jia, H., Sakmann, B., Konnerth, A., 2011. Dendritic coding of multiple sensory inputs in single cortical neurons in vivo. Proc. Natl. Acad. Sci. 108, 15420–15425. doi:10.1073/pnas.1112355108

Vaziri, A., Emiliani, V., 2012. Reshaping the optical dimension in optogenetics. Curr. Opin. Neurobiol. 22, 128–137. doi:10.1016/j.conb.2011.11.011

Veinante, P., Deschênes, M., 2003. Single-cell study of motor cortex projections to the barrel field in rats: Motor Cortex Projections to the Barrel Field. J. Comp. Neurol. 464, 98–103. doi:10.1002/cne.10769

Wang, Y., Toledo-Rodriguez, M., Gupta, A., Wu, C., Silberberg, G., Luo, J., Markram, H., 2004. Anatomical, physiological and molecular properties of Martinotti cells in the somatosensory cortex of the juvenile rat: Martinotti cells in somatosensory cortex. J. Physiol. 561, 65–90. doi:10.1113/jphysiol.2004.073353

Waters, J., Helmchen, F., 2006. Background Synaptic Activity Is Sparse in Neocortex. J. Neurosci. 26, 8267–8277. doi:10.1523/JNEUROSCI.2152-06.2006

Waters, J., Helmchen, F., 2004. Boosting of Action Potential Backpropagation by Neocortical Network Activity In Vivo. J. Neurosci. 24, 11127–11136. doi:10.1523/JNEUROSCI.2933-04.2004

Waters, J., Larkum, M., Sakmann, B., Helmchen, F., 2003. Supralinear Ca2+ influx into dendritic tufts of layer 2/3 neocortical pyramidal neurons in vitro and in vivo. J. Neurosci. 23, 8558–8567.

Williams, S.R., 2004. Spatial compartmentalization and functional impact of conductance in pyramidal neurons. Nat. Neurosci. 7, 961–967. doi:10.1038/nn1305

Williams, S.R., Stuart, G.J., 2002. Dependence of EPSP Efficacy on Synapse Location in Neocortical Pyramidal Neurons. Science 295, 1907–1910. doi:10.1126/science.1067903

Williams, S.R., Stuart, G.J., 2000. Site Independence of EPSP Time Course Is Mediated by DendriticI h in Neocortical Pyramidal Neurons. J. Neurophysiol. 83, 3177–3182.

Wilson, D.M., 1961. The Central Nervous Control of Flight in a Locust. J. Exp. Biol. 38, 471–490.

Wimmer, V.C., Bruno, R.M., de Kock, C.P.J., Kuner, T., Sakmann, B., 2010. Dimensions of a Projection Column and Architecture of VPM and POm Axons in Rat Vibrissal Cortex. Cereb. Cortex 20, 2265–2276. doi:10.1093/cercor/bhq068

Wong, E.H., Kemp, J.A., Priestley, T., Knight, A.R., Woodruff, G.N., Iversen, L.L., 1986. The anticonvulsant MK-801 is a potent N-methyl-D-aspartate antagonist. Proc. Natl. Acad. Sci. U. S. A. 83, 7104–7108.

Woolsey, C.N., Chang, H.T., Bard, P., 1947. Distribution of cortical potentials evoked by electrical stimulation of dorsal roots in Macaca mulatta. Fed. Proc. 6, 230.

Yizhar, O., Fenno, L.E., Davidson, T.J., Mogri, M., Deisseroth, K., 2011. Optogenetics in neural systems. Neuron 71, 9–34. doi:10.1016/j.neuron.2011.06.004

Zhang, F., Wang, L.-P., Brauner, M., Liewald, J.F., Kay, K., Watzke, N., Wood, P.G., Bamberg, E., Nagel, G., Gottschalk, A., Deisseroth, K., 2007. Multimodal fast optical interrogation of neural circuitry. Nature 446, 633–639. doi:10.1038/nature05744

Zhao, W.-J., Kremkow, J., Poulet, J.F.A., 2016. Translaminar Cortical Membrane Potential Synchrony in Behaving Mice. Cell Rep. 15, 2387–2399. doi:10.1016/j.celrep.2016.05.026

Zhou, M., Liang, F., Xiong, X.R., Li, L., Li, H., Xiao, Z., Tao, H.W., Zhang, L.I., 2014. Scaling down of balanced excitation and inhibition by active behavioral states in auditory cortex. Nat. Neurosci. 17, 841–850. doi:10.1038/nn.3701

Zimmermann, D., Zhou, A., Kiesel, M., Feldbauer, K., Terpitz, U., Haase, W., Schneider-Hohendorf, T., Bamberg, E., Sukhorukov, V.L., 2008. Effects on capacitance by overexpression of membrane proteins. Biochem. Biophys. Res. Commun. 369, 1022–1026. doi:10.1016/j.bbrc.2008.02.153

Zipfel, W.R., Williams, R.M., Webb, W.W., 2003. Nonlinear magic: multiphoton microscopy in the biosciences. Nat. Biotechnol. 21, 1369–1377. doi:10.1038/nbt899

APPENDIX

Abbreviations

AAV	adeno-associated virus
AMPA	alpha-amino-3-hydroxy-5-methyl-4-isoxazole propionic acid
AP	action potential
$_{Apical}$OP	apical dendritic optogenetic potential
BAC	backpropagation activated calcium channels
bAP	backpropagating action potential
$_{Basal}$OP	basal dendritic optogenetic potential
Ca^{2+}	calcium ion
ChR2	Channelrhodopsin-2
Cl^-	chloride ion
Down	down state
EEG	electroencephalography
EPSP	excitatory postsynaptic potential
EYFP	enhanced yellow fluorescent protein
GABA	γ-aminobutyric acid
GFP	green fluorescent protein
I_h	hyperpolarization-activated current
IPSP	inhibitory postsynaptic potential
IR	input resistance
Iso	upstate iso-potential
K^+	potassium ion
K_{ir}	anomalous rectifying potassium channel
L(n)	layer (n)
lg	logarithm base 10
M1	primary motor cortex
Move	movement phase

Na^+	sodium ion
Na_P	sodium persistent current
Na_V	voltage-dependent sodium current
NMDA	N-methyl-D-aspartate
OP	optogenetic potential
P(n)	post-natal day (n)
PFA	paraformaldehyde
PMT	photomultiplier
POm	posteromedial thalamic nucleus
PSTH	peristimulus time histogram
PV	parvalbumin interneurons
QX	QX-314
S.D.	standard deviation
S1	primary somatosensory cortex
$_{Soma}$OP	somatic optogenetic potential
SST	somatostatin interneurons
Tau	membrane time constant
TTX	Tetrodotoxin
$_U$EPSP	unitary excitatory postsynaptic potential
Up	up state
V_{dep}	depolarized V_m phase
V_{hyp}	hyperpolarized V_m phase
VIP	vasoactive intestinal peptide interneurons
V_m	membrane potential
VPM	ventroposteromedial thalamic nucleus
V_{rev}	reversal potential
WL	wavelength
WT	wild type

Index of Figures

Figure 1. **Definition of excitatory cell types in a barrel column.** 14
Figure 2. **Excitatory synaptic input-output relationships in the somatosensory barrel cortex.** 16
Figure 3. **Conceptual representation of pyramidal neurons functioning as a coincident detector.** 17
Figure 4. **Dendritic attenuation and filtering of an EPSP.** 21
Figure 5. **Intracellular whole-cell recordings during different states of activity.** 25
Figure 6. **Intrinsic optical imaging to identify the somatosensory forepaw cortical area.** 35
Figure 7. **Up- and Downstate selection and analysis.** 41
Figure 8. **Offline access resistance subtraction and input resistance calculation.** 43
Figure 9. **Online access resistance assessment and correction with bridge balance.** 43
Figure 10. ***In vivo* two-photon guided single cell electroporation.** 48
Figure 11. **Cortical viral infections of ChR2-EYFP.** 49
Figure 12. **Channelrhodopsin2 (ET-TC) expression effect on neuronal physiology.** 51
Figure 13. **Two-photon stimulation of ChR2-non expressing neocortical pyramidal neurons *in vivo*.** 53
Figure 14. **Off target two-photon stimulation of ChR2 expressing neurons.** 53
Figure 15. **Two-photon stimulation parameters of ChR2-expressing neocortical pyramidal neurons *in vivo*.** 54
Figure 16. **Two-photon optogenetic stimulation did not trigger action potentials.** 56
Figure 17. **Modulation of somatic two-photon evoked response amplitude in ChR2 expressing layer 2/3 pyramidal neurons.** 58
Figure 18. **Slower kinetics in Upstates in two different ChR2 variants.** 60
Figure 19. **Dendritically evoked OP kinetics during Downstates are correlated to the distance of stimulation site from soma.** 61
Figure 20. **Dendrite-specific modulation of subcellular two-photon evoked response amplitude and kinetics.** 64
Figure 21. **Cortical state-dependent gain modulation of basal dendritic inputs in anesthetized mice.** 66
Figure 22. **OP amplitude Up:Down ratio as a function of the distance of dendritic optogenetic stimulation from the soma.** 67
Figure 23. **Glutamatergic inputs to layer 2/3 neurons from ventral posteromedial thalamic nucleus show state dependent gain modulation.** 69
Figure 24. **Local cortical monosynaptic glutamatergic connections show state dependent gain modulation.** 70

Figure 25. **Somatic optogenetic stimulation during slow cortical activity in awake, resting mice.** 72

Figure 26. **Basal and apical dendrite optogenetic stimulation during slow cortical activity in awake, resting mice.** 74

Figure 27. **Cortical state dependent gain modulation of basal dendritic input in awake mice during quiet or active movement.** 75

Figure 28. **Optogenetic stimulation during desynchronized active Move state.** 78

Figure 29. **Somatic Downstate current injection causes a reduction in $_{soma}$OP amplitude as observed during Upstates.** 81

Figure 30. **Input resistance increase in Upstates is determined by change in V_m.** 84

Figure 31. **Influence of network activity on the total charge of OPs in recordings from anesthetized and awake mice.** 86

Figure 32. **The increase in input resistance during Upstates is blocked by the intracellular application of QX-314.** 88

Figure 33. **Gain modulation of basal inputs is blocked by intracellular applications of QX-314.** 89

Figure 34. **Small basal input approximates to apical input under QX-314.** 91

Figure 35. **Neuron model employing a dendritic distribution of sodium currents to recapitulate the gain modulation of basal input.** 117

Equation 1. **Expected amplitude based on driving force difference due to V_m difference.** 44

PUBLICATIONS

Jouhanneau, J.-S., Ferrarese, L., Estebanez, L., Audette, N.J., Brecht, M., Barth, A.L., Poulet, J.F.A., 2014. Cortical fosGFP Expression Reveals Broad Receptive Field Excitatory Neurons Targeted by POm. Neuron 84, 1065–1078. doi:10.1016/j.neuron.2014.10.014

Frahm, S., Ślimak, M.A., Ferrarese, L., Santos-Torres, J., Antolin-Fontes, B., Auer, S., Filkin, S., Pons, S., Fontaine, J.-F., Tsetlin, V., Maskos, U., Ibañez-Tallon, I., 2011. Aversion to Nicotine Is Regulated by the Balanced Activity of β4 and α5 Nicotinic Receptor Subunits in the Medial Habenula. Neuron 70, 522–535. doi:10.1016/j.neuron.2011.04.013